Yeast model of human betabeta-enolase deficiency disease: Characterization of G157D yeast enolase
Choy, Bonny Shu Fen
ProQuest Dissertations and Theses; 2007; ProQuest
pg. n/a

Yeast Model of Human ββ-Enolase Deficiency Disease: Characterization of G157D Yeast Enolase

Bonny Shu Fen Choy

A Thesis

In

The Department

Of

Chemistry and Biochemistry

Presented in Partial Fulfillment of the Requirements
for the Degree of Master of Science at
Concordia University
Montreal, Quebec, Canada

December 2006

© Bonny Shu Fen Choy, 2006

Reproduced with permission of the copyright owner. Further reproduction prohibited without permission.

Library and Archives Canada

Published Heritage Branch

395 Wellington Street
Ottawa ON K1A 0N4
Canada

Bibliothèque et Archives Canada

Direction du Patrimoine de l'édition

395, rue Wellington
Ottawa ON K1A 0N4
Canada

Your file Votre référence
ISBN: 978-0-494-28878-8
Our file Notre référence
ISBN: 978-0-494-28878-8

NOTICE:
The author has granted a non-exclusive license allowing Library and Archives Canada to reproduce, publish, archive, preserve, conserve, communicate to the public by telecommunication or on the Internet, loan, distribute and sell theses worldwide, for commercial or non-commercial purposes, in microform, paper, electronic and/or any other formats.

The author retains copyright ownership and moral rights in this thesis. Neither the thesis nor substantial extracts from it may be printed or otherwise reproduced without the author's permission.

AVIS:
L'auteur a accordé une licence non exclusive permettant à la Bibliothèque et Archives Canada de reproduire, publier, archiver, sauvegarder, conserver, transmettre au public par télécommunication ou par l'Internet, prêter, distribuer et vendre des thèses partout dans le monde, à des fins commerciales ou autres, sur support microforme, papier, électronique et/ou autres formats.

L'auteur conserve la propriété du droit d'auteur et des droits moraux qui protège cette thèse. Ni la thèse ni des extraits substantiels de celle-ci ne doivent être imprimés ou autrement reproduits sans son autorisation.

In compliance with the Canadian Privacy Act some supporting forms may have been removed from this thesis.

While these forms may be included in the document page count, their removal does not represent any loss of content from the thesis.

Conformément à la loi canadienne sur la protection de la vie privée, quelques formulaires secondaires ont été enlevés de cette thèse.

Bien que ces formulaires aient inclus dans la pagination, il n'y aura aucun contenu manquant.

Canada

Reproduced with permission of the copyright owner. Further reproduction prohibited without permission.

ABSTRACT

Yeast Model of Human ββ-Enolase Deficiency Disease: Characterization of G157D Yeast Enolase

Bonny Shu Fen Choy

Enolase is an essential enzyme in glycolysis and gluconeogenesis. In 2001, the first known case of a human disorder diagnosed as muscle enolase deficiency was found (Comi et al., 2001). The patient carried two heterozygous missense mutations changing glycine 156 to aspartate 156 in one case and glycine 374 to a glutamate 374 in the other. In this study, yeast enolase is used as a model to study the role of G156 (G157 in yeast enolase) and the effects of the G156D mutation in human ββ-enolase. Specifically, site directed mutagenesis was used to change G157 to D in yeast enolase. Spectroscopic studies using fluorescence, circular dichroism, and analytical ultracentrifugation indicated no substantial differences in the conformational foldings of G157D compared to wild-type enolase. The conformational stability of the G157D variant was found to be slightly decreased compared to the wild-type enolase when subjected to chemical or thermal denaturation. The G157D variant is also more susceptible to limited proteolysis by trypsin. The G157D protein exhibits only 0.06% wild-type activity under standard enolase assay conditions. Kinetic studies indicate that the G157D enolase has a higher K_M for Mg^{2+}, no significant differences in K_M for Mn^{2+}, and a slightly increased K_M for its substrate, 2-phospho-D-glycerate, than has the wild-type enzyme. ^2H kinetic isotope effect studies proved that the first step of enolase catalysis, abstraction of the C-2 proton from 2-PGA becomes more rate limiting for the G157D enolase. Ligand binding studies indicate similar K_d for the first Mg^{2+} site for both G157D and wild-type enolase. Isothermal titration calorimetry indicates comparable association constants for the second Mn^{2+}, PhAH, and 2-PGA/PEP.

Reproduced with permission of the copyright owner. Further reproduction prohibited without permission.

To further investigate the effects of size and charge upon replacing a small, non-charged glycine residue by a bulky, charged aspartate, G157A, G157N, and G157L yeast enolase variants were also created. Studies on the latter three proteins illustrate correct folding of the proteins and no substantial stability discrepancies compared to the wild-type enzyme. In spite of this, activity studies show that as the size of the amino acid at this site increases, the enzyme activity decreases. It is possible that the small and non-charged properties of G157 are necessary for proper coordination of active site residues to the metal cofactors and the substrate 2-phospho-D-glycerate.

Reproduced with permission of the copyright owner. Further reproduction prohibited without permission.

Acknowledgments

First and foremost, I would like to express my sincere gratitude to my supervisor, Dr. M. J. Kornblatt, for her endless patience and guidance. Her indispensable advice and supervision have enabled me to gain deeper insights into my research project.

I would like to thank my committee members, Dr. Joyce and Dr. Dewolf, for their valuable time and suggestions for my thesis.

I want to thank Dr. Ulycznyj for kindly running my AUC samples.

I would also like to thank my lab colleagues, Shujun Liu and Song Ping Zhao, along with fellow graduate student, Yu Lei, for their valuable suggestions and companionship.

I would like to give a warm thank you to my family for encouraging and supporting me through these numerous years of studies.

Last, but not least, I would like to sincerely thank Amy Wong, Wally Lee, Viviane Choy, and David Nguyen for their friendship, love and encouragement throughout good and bad times.

Reproduced with permission of the copyright owner. Further reproduction prohibited without permission.

Table of Contents

Reproduced with permission of the copyright owner. Further reproduction prohibited without permission.

Chapter II. Materials and Methods

Reproduced with permission of the copyright owner. Further reproduction prohibited without permission.

Chapter III. Results

Reproduced with permission of the copyright owner. Further reproduction prohibited without permission.

Reproduced with permission of the copyright owner. Further reproduction prohibited without permission.

Chapter IV. Discussion

Reproduced with permission of the copyright owner. Further reproduction prohibited without permission.

List of Figures

Reproduced with permission of the copyright owner. Further reproduction prohibited without permission.

Reproduced with permission of the copyright owner. Further reproduction prohibited without permission.

Reproduced with permission of the copyright owner. Further reproduction prohibited without permission.

List of Tables

Reproduced with permission of the copyright owner. Further reproduction prohibited without permission.

Reproduced with permission of the copyright owner. Further reproduction prohibited without permission.

Abbreviations

ADP	Adenosine diphosphate
Amp	Ampicillin
AUC	Analytical ultracentrifuge/ultracentrifugation
bp	Base pair
BSA	Bovine serum albumin
CD	Circular dichroism
DNA	Deoxyribonucleic acid
D-2-PGA	Deuterium 2-phosphoglyceric acid at C-2
E. coli	*Escherichia coli*
EDTA	Ethylenediaminetetraacetic acid
ESI-Q-ToF	Electrospray ionization Quadrupole Time-of-Flight
H	Helix
HOAc	Acetic Acid
ITC	Isothermal titration calorimetry
K	Association constant
$\mathbf{k_{cat}}$	Turnover number
$\mathbf{K_d}$	Dissociation constant
$\mathbf{K_i}$	Inhibitory constant
KIE	Kinetic isotope effect
$\mathbf{K_M}$	Michaelis constant
LB	Luria-Bertani medium

Reproduced with permission of the copyright owner. Further reproduction prohibited without permission.

LDH	Lactate dehydrogenase
MD	Molecular dynamics
Me^{2+}	Divalent cation
MeOH	Methanol
MES	2-Morpholinoethanesulfonic acid
$Mg(OAc)_2$	Magnesium acetate
MLE	Muconate lactonizing enzyme
MR	Mandelate racemase
NADH	Nicotinamide dinucleotide
NaOAc	Sodium acetate
PCR	Polymerase chain reaction
PEP	Phosphoenolpyruvate
2-PGA	2-Phosphglyceric acid
PhAH	Phosphonoacetohydroxamate
PK	Pyruvate kinase
S	Strand
SDS-PAGE	Sodium dodecyl sulfate polyacrylamide gel electrophoresis
TAE	Tris/Acetic acid/EDTA
TE	Tris/EDTA
TIM	Triosephosphate isomerase
T_m	Melting Temperature
TMAOH	Tetramethyl ammonium hydroxide
TPCK	L-1-tosylamido-2-phenylethyl chloromethyl ketone
TSP	Tartronate semialdehyde phosphate

Reproduced with permission of the copyright owner. Further reproduction prohibited without permission.

Tris	Tris-(hydroxymethyl)aminomethane
V_{max}	Maximum velocity
UV	Ultraviolet
(*Z*)-3-Cl-P-enolpyruvate	(Z)-3-Chlorophosphoenolpyruvate

Reproduced with permission of the copyright owner. Further reproduction prohibited without permission.

Chapter I: Introduction

I.1 General Introduction

Glycolysis is a universal energy pathway in which a sequence of reactions takes place to convert glucose into pyruvate with the concomitant production of ATP. Glucose, which is stored in the readily mobilized form of glycogen, constitutes the fundamental source of energy for cell metabolism (Stryer, 1995). Inherent defects in the use and storage of glucose and glycogen may lead to metabolic disorders, known as "glycogen storage myopathies" (Tsujuno et al., 2000). Diseases that involve inborn errors of metabolism that are characterized by glycogen accumulation in tissues due to enzyme defects in either the glycolysis or gluconeogenesis pathways are categorized under glycogen storage myopathies. Numerous glycogen storage diseases have been discovered to date, and they have been assigned roman numerals roughly in the order of their discovery.

More recently, Comi et al. (2001) reported a new metabolic myopathy of distal glycolysis in a patient who suffered from a deficiency in an enzyme that catalyzes one of the terminal steps in the glycolytic pathway, enolase. The patient suffers from exercise induced myalgias and muscle weakness and fatigue. The patient was diagnosed with having glycogenosis type XIII disorder, caused by muscle-specific enolase deficiency. What is enolase, and what role does it play in the glycolytic and gluconeogenic pathways?

I.2 Basic Overview of Enolase

Enolase (2-phospho-D-glycerate hydrolyase, E.C. 4.2.1.11) is a ubiquitous enzyme that catalyzes the reversible dehydration of 2-phosphoglyceric acid (2-PGA) to

Reproduced with permission of the copyright owner. Further reproduction prohibited without permission.

phosphoenolpyruvate (PEP). It participates in both glycolysis and gluconeogenesis (Wold, 1971). It catalyzes the only dehydration step in the glycolytic series of reactions. Enolase exhibits an absolute requirement for divalent cations for enzymatic activity, with Mg^{2+} being the natural cofactor and giving the highest activity (Brewer, 1981). It is a metalloenzyme in which metal ions play both structural and catalytic roles. Two equivalents of divalent cation per subunit are required for full enolase activity (Faller et al., 1977). The order of binding to each subunit is the first Me^{2+}, then the substrate, followed by the second equivalent of Me^{2+}.

Enolase has been isolated from a wide variety of organisms. All the eukaryotic enolases characterized to date have been depicted as protein homo- or hetero-dimers with approximate subunit molecular weights of 46 kD. Alternatively, octameric forms of enolase have been depicted for some prokaryotic species (Brown et al., 1998; Pawluk et al., 1986; Schurig et al., 1995; Ehinger et al., 2004).

I.2.1 Mammalian Enolase

In mammals, there are three genes which code for three different enolase isozymes, designated as α, β, and γ enolase. The three different isozymes combine to give either homo- or hetero-dimers of enolases that are tissue specific. The αα-homodimer is implicated mainly in embryonic tissue, where it accounts for the total enolase activity. It is the only form of enolase that is found in liver tissues. The αγ-heterodimer and the γγ-homodimer are specific to neurons, while the αβ-heterodimer and the ββ-homodimer are implicated in striated muscles (Segil et al., 1988). Crystal structures of human neuron-specific enolase (NSE) are now readily available at 1.8 Å and 1.36 Å resolutions (Chai et al., 2004; Quin et al., 2006).

Reproduced with permission of the copyright owner. Further reproduction prohibited without permission.

I.2.2 Yeast Enolase

In spite of the more recent efforts in determining structures of mammalian enolases, the most extensively studied enolase to date is that of Baker's yeast (*Saccharomyces cerevisiae*). In yeast, there are two genes, namely *ENO1* and *ENO2*, which code for the two different enolase isozymes, enolase 1 and 2, respectively (Holland et al., 1981). The nucleotide sequences of the genes coding for the two isozymes are 95% identical. The levels of the two yeast isozymes are under metabolic and developmental control, that is, the intracellular steady-state concentrations of the two polypeptides depends on the carbon source used to cultivate the yeast cultures. Enolase 1 is the predominant and most studied form of the enzyme (McAlister & Holland, 1982). Yeast enolase exists as a dimeric protein with two identical subunits, each containing 436 residues (Chin et al., 1981). Enolase from yeast has been obtainable in reasonably pure form since 1941 (Warburg & Christian, 1942). Several crystal structures of yeast enolase complexed with and without metal cofactors and substrate/inhibitors are available in the protein data bank (Stec & Lebioda, 1990; Lebioda et al., 1989; Lebioda & Stec, 1991; Larsen et al., 1996; Wedekind et al., 1995; Wedekind et al., 1994, Zhang et al., 1997).

I.3 Enolase Orthologues

I.3.1 Primary Amino Acid Comparison of Enolase Orthologues

Enolase has been discovered and studied from numerous sources, including eukaryotes and prokaryotes. An extensive archive of enolase sequences from different species have been determined and deposited into the SWISS PROT sequence database. Enolase is a well conserved enzyme, with the conservation being particularly apparent at the

Reproduced with permission of the copyright owner. Further reproduction prohibited without permission.

catalytic site within isozymes and different species. Figure 1 shows the sequence alignment of yeast with the three different *Homo sapiens* isozymes, rabbit-β, lobster, and *E. coli* enolases.

```
Homosap-beta        -MAMQKIFAREILDSRGNPTVEVDLHTAKGRF-RAAVPSGASTGIYEALELRDGDKGRYL 58
Rabbit-beta         -MAMQKIFAREILDSRGNPTVEVDLHTAKGRF-RAAVPSGASTGIYEALELRDGDKSRYL 58
Homosap-alpha       -MSILKIHAREIFDSRGNPTVEVDLFTSKGLF-RAAVPSGASTGIYEALELRDNDKTRYM 58
Homosap-gamma       --SIQKIWAREILDSRGNPTVEVDLYTAKGLF-RAAVPSGASTGIYEALELRDGDKQRYL 57
Lobster             --SITKVFARTIFDSRGNPTVEVDLYTSKGLF-RAAVPSGASTGVHEALEMRDGDKSKYH 57
yeast               -MAVSKVYARSVYDSRGNPTVEVELTTEKGVF-RSIVPSGASTGVHEALEMRDGDKSKWM 58
E.coli              MSKIVKIIGREIIDSRGNPTVEAEVHLEGGFVGMAAAPSGASTGSREALELRDGDKSRFL 60
                       : *: .* : *********.::    * .  : .*******  ****:**.** ::

Homosap-beta        GKGVLKAVENINNTLGPALLQKKLSVVDQEKVDKFMIELDGTENKSKFGANAILGVSLAV 118
Rabbit-beta         GKGVLKAVEHINKTLGPALLEKKLSVVDQEKVDKFMIELDGTENKSKFGANAILGVSLAV 118
Homosap-alpha       GKGVSKAVEHINKTIAPALVSKKLNVTEQEKIDKLMIEMDGTENKSKFGANAILGVSLAV 118
Homosap-gamma       GKGVLKAVDHINSTIAPALISSGLSVVEQEKLDNLMLELDGTENKSKFGANAILGVSLAV 117
Lobster             GKSVFNAVKNVNDVIVPEIIKSGLKVTQQKECDEFMCKLDGTENKSSLGANAILGVSLAI 117
yeast               GKGVLHAVKNVNDVIAPAFVKANIDVKDQKAVDDFLISLDGTANKSKLGANAILGVSLAA 118
E.coli              GKGVTKAVAAVNGPIAQALIGK--DAKDQAGIDKIMIDLDGTENKSKFGANAILAVSLAN 118
                    **.* :**  :*  :   ::    .. :*   *.:: .:*** ***.:******.****

Homosap-beta        CKAGAAEKGVPLYRHIADLAGN--PDLILPVPAFNVINGGSHAGNKLAMQEFMILPVGAS 176
Rabbit-beta         CKAGAAEKGVPLYRHIADLAGN--HDLVLPVPAFNVINGGSHAGNKLAMQEFMILPVGAS 176
Homosap-alpha       CKAGAVEKGVPLYRHIADLAGN--SEVILPVPAFNVINGGSHAGNKLAMQEFMILPVGAA 176
Homosap-gamma       CKAGAAERELPLYRHIAQLAGN--SDLILPVPAFNVINGGSHAGNKLAMQEFMILPVGAE 175
Lobster             CKAGAAELGIPLYRHIANLANY--DEVILPVPAFNVINGGSHAGNKLAMQEFMILPTGAT 175
yeast               SRAAAAEKNVPLYKHLADLSKSKTSPYVLPVPFLNVLNGGSHAGGALALQEFMIAPTGAK 178
E.coli              AKAAAAAKGMPLYEHIAELNGTP-GKYSMPVPMMNIINGGEHADNNVDIQEFMIQPVGAK 177
                    .:*.*.   :***.*:*:*          :*** :*::***.**.. : :***** *.**

Homosap-beta        SFKEAMRIGAEVYHHLKGVIKAKYGKDATNVGDEGGFAPNILENNEALELLKTAIQAAGY 236
Rabbit-beta         SFREAMRIGAEVYHHLKGVIKAKYGKDATNVGDEGGFAPNILENNEALELLKTAIQAAGY 236
Homosap-alpha       NFREAMRIGAEVYHNLKNVIKEKYGKDATNVGDEGGFAPNILENKEGLELLKTAIGKAGY 236
Homosap-gamma       SFRDAMRLGAEVYHTLKGVIKDKYGKDATNVGDEGGFAPNILENSEALELVKEAIDKAGY 235
Lobster             SFTEAMRMGTEVYHHLKAVIKARFGLDATAVGDEGGFAPNILNNKDALDLIQEAIKKAGY 235
yeast               TFAEALRIGSEVYHNLKSLTKKRYGASAGNVGDEGGVAPNIQTAEEALDLIVDAIKAAGH 238
E.coli              TVKEAIRMGSEVFHHLAKVLKAKG--MNTAVGDEGGYAPNLGSNAEALAVIAEAVKAAGY 235
                    .. :*:*:*:**:* *  : * :        ****** ***:    :.* ::  *:  **:

Homosap-beta        PD--KVVIGMDVAASEFYR-NGKYDLDFKSPD-DPARHITGEKLGELYKSFIKNYPVVSI 292
Rabbit-beta         PD--KVVIGMDVAASEFHR-NGKYDLDFKSPD-DPARHITGQKLGELYKSFIKNYPVVSI 292
Homosap-alpha       TD--KVVIGMDVAASEFFR-SGKYDLDFKSPD-DPSRYISPDQLADLYKSFIKDYPVVSI 292
Homosap-gamma       TE--KMVIGMDVAASEFYR-DGKYDLDFKSPT-DPSRYITGDQLGALYQDFVRDYPVVSI 291
Lobster             TG--KIEIGMDVAASEFYKQNNIYDLDFKTANNDGSQKISGDQLRDMYMEFCKDFPIVSI 293
yeast               DG--KVKIGLDCASSEFFK-DGKYDLDFKNPNSDKSKWLTGPQLADLYHSLMKRYPIVSI 295
E.coli              ELGKDITLAMDCAASEFYK-DGKYVLAG-----EGNKAFTSEEFTHFLEELTKQYPIVSI 289
                        .: :.:* *:***.: .. * *       :  : ::  ::  :  .: : :*:***

Homosap-beta        EDPFDQDDWATWTSFLSGVN--IQIVGDDLTVTNPKRIAQAVEKKACNCLLLKVNQIGSV 350
Rabbit-beta         EDPFDQDDWATWTSFLSGVD--IQIVGDDLTVTNPKRIAQAVEKKACNCLLLKVNQIGSV 350
Homosap-alpha       EDPFDQDDWGAWQKFTASAG--IQVVGDDLTVTNPKRIAKAVNEKSCNCLLLKVNQIGSV 350
Homosap-gamma       EDPFDQDDWAAWSKFTANVG--IQIVGDDLTVTNPKRIERAVEEKACNCLLLKVNQIGSV 349
Lobster             EDPFDQDDWETWSKMTSGTT--IQIVGDDLTVTNPKRITTAVEKKACKCLLLKVNQIGSV 351
yeast               EDPFAEDDWEAWSHFFKTAG--IQIVADDLTVTNPKRIATAIEKKAADALLLKVNQIGTL 353
E.coli              EDGLDESDWDGFAYQTKVLGDKIQLVGDDLFVTNTKILKEGIEKGIANSILIKFNQIGSL 349
                    ** : :.**  :           **:*.*** ***.* :  .:::  ...:*:*.****::

Homosap-beta        TESIQACKLAQSNGWGVMVSHRSGETEDTFIADLVVGLCTGQIKTGAPCRSERLAKYNQL 410
Rabbit-beta         TESIQACKLAQSNGWGVMVSHRSGETEDTFIADLVVGLCTGQIKTGAPCRSERLAKYNQL 410
Homosap-alpha       TESLQACKLAQANGWGVMVSHRSGETEDTFIADLVVGLCTGQIKTGAPCRSERLAKYNQL 410
Homosap-gamma       TEAIQACKLAQENGWGVMVSHRSGETEDTFIADLVVGLCTGQIKTGAPCRSERLAKYNQL 409
Lobster             TESIDAHLLAKKNGWGTMVSHRSGETEDCFIADLVVGLCTGQIKTGAPCRSERLAKYNQI 411
yeast               SESIKAAQDSFAAGWGVMVSHRSGETEDTFIADLVVGLRTGQIKTGAPARSERLAKLNQL 413
E.coli              TETLAAIKMAKDAGYTAVISHRSGETEDATIADLAVGTAAGQIKTGSMSRSDRVAKYNQL 409
                    :*:: *   :   *: .::********* ****.** :******: .**:*:** **:
```


Reproduced with permission of the copyright owner. Further reproduction prohibited without permission.

```
Homosap-beta        MRIEEALGDKAIFAGRKFRNPKAK 434
Rabbit-beta         MRIEEALGDKAVFAGRKFRNPKAK 434
Homosap-alpha       LRIEEELGSKAKFAGRNFRNPLAK 434
Homosap-gamma       MRIEEELGDEARFAGHNFRNPSVL 433
Lobster             LRIEEELGSGAKFAGKNFRAPS-- 433
yeast               LRIEEELGDNAVFAGENFHHGDKL 437
E.coli              IRIEEALGEKAPYNGRKEIKGQA- 432
                    :**** **. * : *.:
```

Figure 1. Primary sequence alignment of yeast, *Homo sapiens* α, β, and γ isoforms, lobster, rabbit muscle β, and *E. coli* enolases. Alignment was obtained from the EBI-ClustalW Sequence Analysis Tool (http://www.ebi.ac.uk/). The amino acids are colour coded, for which red indicates small and hydrophobic amino acids, blue indicates acidic amino acids, magenta indicates basic amino acids, green indicates hydroxyl, amine and basic amino acids, gray indicates other amino acids. The consensus symbols under the alignments with "*" for residues in that column that are identical in all sequences in the alignment, ":" means that conserved substitutions have been observed, according to the colour code above, and "." means that semi-conserved substitutions are observed.

The three *Homo sapiens* isozymes, the α, β, and γ isoforms, exhibit over 80% sequence identity (Chin 1990). Comparison of the eukaryotic mammalian enolases with the prokaryotic *E. coli* enolase also yields sequence identity of over 50% (Table 1). For this, enolase from diverse species seems to share similar kinetic properties (Hannaert et al., 2003).

	Homo sapiens α	*Homo sapiens* β	*Homo sapiens* γ	Lobster	Rabbit β	*E. Coli*
Yeast	63%	63%	62%	64%	64%	51%
Homo sapiens α		83%	83%	72%	83%	52%
Homo sapiens β			84%	71%	97%	55%
Homo sapiens γ				72%	84%	52%
Lobster					71%	50%
Rabbit β						54%

Table 1. Sequence identity between enolases from yeast, *Homo sapiens*, lobster, rabbit, and *E. Coli.*

Reproduced with permission of the copyright owner. Further reproduction prohibited without permission.

I.3.2 Tertiary Structural Comparison of Enolase Orthologues

The three-dimensional structures of the enolase orthologues are similar amongspecies. Kühnel & Luisi (2001) have superimposed the crystal structures of yeast, *E. coli*, and lobster enolases. The main region of structural variability between the prokaryotic and eukaryotic enolases is in the loop comprising residues 248-268 in *E. coli*. *E. coli* enolase has a corresponding five residue deletion between residues 259-260 (Figure 1). In comparison to mammalian enolases, this loop is, on average, four residues shorter in prokaryotic enolases, and two residues longer in plant enolases (Zhang et al., 1997). Figure 2 demonstrates a tertiary structural alignment of enolase from *Saccharomyces cerevisiae*, human neuron, *E. coli*, and lobster enolase. All of the aligned enolase structures are very similar.

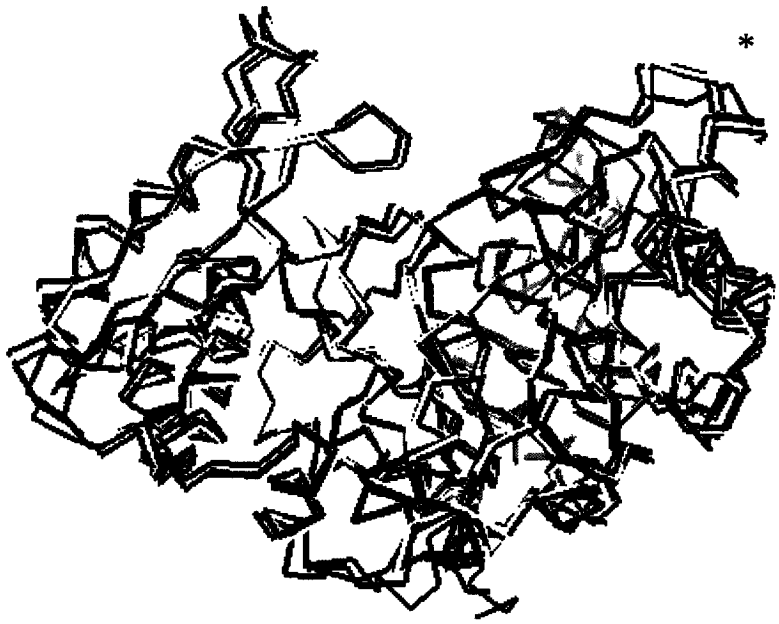

Figure 2. Tertiary structure alignment of yeast (blue; 2ONE), *E. coli* (purple; 1E9I), lobster (yellow; 1PDZ), and human neuron (pink; 1TE6) enolase. An asterisk marks loop 250-267 (*E. coli*), which contains the five residue deletion in *E. coli*. Structure alignment was performed using the CEMC-Multiple Protein Structure Alignment Server provided by the University of Albany, http://bioinformatics.albany.edu/~cemc/. The figure was generated using PyMol.

Reproduced with permission of the copyright owner. Further reproduction prohibited without permission.

I.4 Structure of Yeast Enolase

I.4.1 Overall Structure of Yeast Enolase

Yeast enolase is a dimeric protein with two identical subunits, each composed of 436 amino acid residues. Each subunit comprises a smaller, N-terminal domain, and a larger, C-terminal domain (Lebioda et al., 1989; Stec & Lebioda, 1990). The N-terminal domain consists of three strands followed by four helices linking to the eight-fold α/β-barrel C-terminal domain. The crystal structure of enolase is such that it has been described as a butterfly structure (Figure 3).

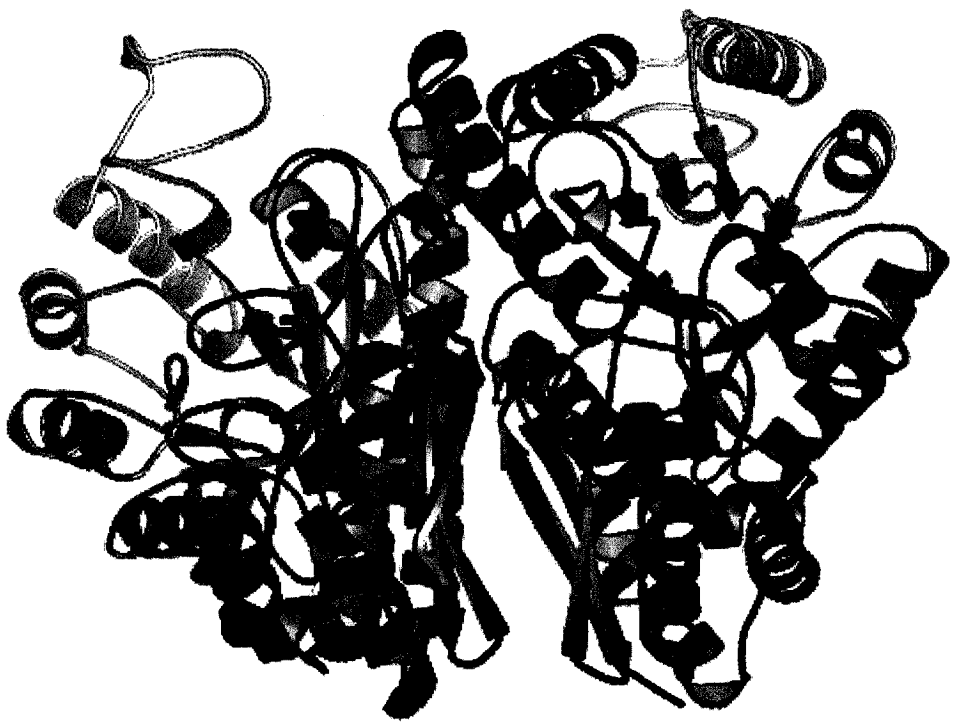

Figure 3. Ribbon structure of yeast enolase (1ONE). Structure was generated using PyMol, and selecting the default publication colouring scheme.

Reproduced with permission of the copyright owner. Further reproduction prohibited without permission.

I.4.2 N-Terminal Domain

The N-terminal domain extends from residues 1-142. It begins with a three-stranded amphiphilic antiparallel β-meander, strands S9-S11. A long loop, consisting of residues 37-60, extends towards the entrance of the active site and forms the extension between the last strand of the meander, S11, and the first of the four α-helices, HI. The helix, HI, is disrupted in the middle by Pro74, which induces a bend that places the two antiparallel helices, HK and HJ, closely packed against the C-terminal domain. HJ is then trailed by HL which terminates the N-terminal domain. The overall secondary structural component of the N-terminal domain is demonstrated in Figure 4.

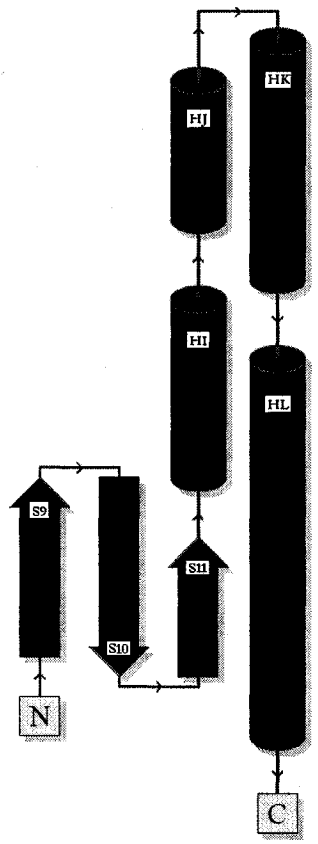

Figure 4. Secondary structural representation of the N-terminal domain of yeast enolase. The N-terminal begins with flat arrows depicting the β sheets, followed by cylinders representing helices.

Reproduced with permission of the copyright owner. Further reproduction prohibited without permission.

I.4.3 C-Terminal Domain

The C-terminal domain extends from residues 143-436. The domain is a construct of α/β supersecondary structures, where eight β-strands, S1-S8, are surrounded by eight α-helices, HA-HH. The first β-strand, S1, of the barrel connects to the second strand, S2, via a long connecting loop which protrudes from the barrel, consisting of residues 155-167. S2 is antiparallel to the other strands of the barrel. It is then followed by two antiparallel helices that is proceeded by a six fold repeat of α/β pattern, forming an $\beta\beta\alpha\alpha(\beta\alpha)_6$ barrel topology (Figure 5). Refer to Table 2 for a full list of secondary structural components of yeast enolase. The $\beta\beta\alpha\alpha(\beta\alpha)_6$ barrel topology is an unusual fold that originates from the $(\beta\alpha)_8$ TIM barrel. TIM, triosephosphate isomerase (E.C. 5.3.1.1), was the first protein that was discovered to have the eight-fold α/β barrel structure (Banner et al., 1975). The TIM barrel is frequently encountered in many proteins. The TIM barrel fold is so common as to be found in about 10% of all known proteins (Gerlt, 2000). TIM barrel enzymes catalyze a vast range of different reactions. The $(\beta\alpha)_8$-barrel is formed from eight twisted parallel β-strands surrounded by eight α-helices. The enolase $\beta\beta\alpha\alpha(\beta\alpha)_6$ barrel topology is a modified form of the common $(\beta\alpha)_8$-barrel. Despite the differences in the barrel topology, all known enzymes with the TIM barrel domain have their active site residues located within the C-terminal face of the barrel, and within the loops that connect the β-strands with the subsequent α-helices (Henn-Sax et al., 2001). The purpose of the evolutionarily diverse $(\beta\alpha)_8$-barrel fold found in different proteins remains a mystery.

Reproduced with permission of the copyright owner. Further reproduction prohibited without permission.

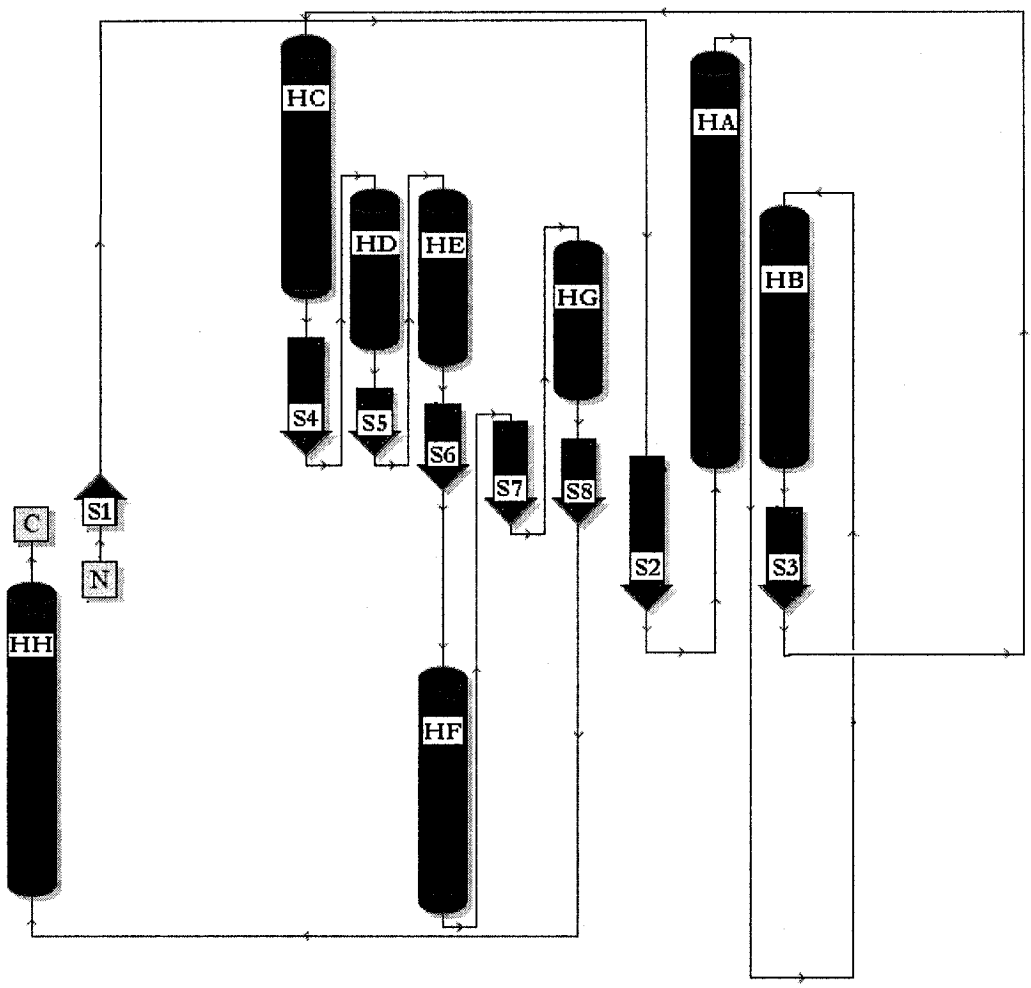

Figure 5. Secondary structural representation of the C-terminal domain of yeast enolase, with flat arrows depicting the β sheets, followed by cylinders representing helices.

Reproduced with permission of the copyright owner. Further reproduction prohibited without permission.

Anti-parallel β meander	Strand 9	5-13
	Strand 10	17-25
	Strand 11	29-35
Helices of N-terminal domain	Helix I	61-80
	Helix J	86-96
	Helix K	107-125
	Helix L	128-136
8-fold β-α barrel	Strand 1	150-153
	Strand 2	168-172
	Helix A	179-200
	Helix B	221-235
	Strand 3	241-247
	Helix C	275-288
	Strand 4	293-296
	Helix D	303-312
	Strand 5	316-320
	Helix E	327-336
	Strand 6	341-345
	Helix F	352-365
	Strand 7	368-373
	Helix G	382-389
	Strand 8	394-397
	Helix H	404-419

Table 2. Secondary structural elements in enolase. Table obtained from Table 7 in Lebioda et al., 1989.

I.4.4 Subunit Interface

The dimer interface is formed by contacts between the main chain of the N-terminal meander, S9 and S10, of one subunit and the side chains of C-terminal HH of the other subunit. The dimer interface is structurally conserved between species (Kühnel & Luisi, 2001). Kühnel and Luisi have demonstrated the dimer interfaces of *E. coli*, lobster, and yeast enolases have similar amounts of buried surface, as well as similar surface contact shapes and charge distributions. The ratio of charged/hydrophobic interface residues for enolase is approximately twice the average for oligomeric proteins since the subunit interface

Reproduced with permission of the copyright owner. Further reproduction prohibited without permission.

of enolase is more polar than that of other oligomeric proteins (Kühnel & Luisi, 2001; Janin et al., 1988). The dimeric interface is held together and strengthened by ionic bonds and H-bonds between the two subunits (Table 3). These interactions account for a relatively small percentage of the solvent accessible surface of the dimer interface (Stec & Lebioda, 1990).

Bond	Residue 1	Residue 2
Ionic Bond	**R8**-NE	OE_2-**E417**
	R8-NH_2	OE_1-**E417**
	R414-NE	OE_1-**E20**
	R414-NH_2	OE_2-**E20**
Hydrogen bond	**E20**-OE_1	NE-**R414**
	E20-OE_2	NH_2-**R414**
	E417-OE_1	NH_2-**R8**
	E417-OE_2	NE-**R8**
	E417-OE_2	NE-**R8**
	N410-ND_2	OE_1-**E379**
	N410-ND_2	O-**Y11**
	N410-OD_1	N-**Y11**
	E404-OE_1	N-**S403**
	E188-OE_1	N-**W56**
	H191-NE_2	O-**R14**
	S13-O	N-**R402**
	V208-O	N-**V208**

Table 3. Ionic and H-bond interactions between enolase subunits (Table 6 and 8 of Stec & Lebioda, 1990). Legend – O: main chain carbonyl oxygen; OD_1: side chain carbonyl group; OE_1 and OE_2: oxygen 1 and 2 of side-chain carboxylic group; N: main chain amino group; ND_2: side chain amino group; NE: side chain guanidinium amino bonded between carbon D and Z; NH_2: side chain guanidiunium amino bonded to carbon Z.

I.5 Subunit Dissociation

Subunit dissociation of enolase depends on several factors. Divalent cations play a significant role in the dimerization of enolase. The dissociation of the dimeric enzyme into

Reproduced with permission of the copyright owner. Further reproduction prohibited without permission.

their respective monomers is increased upon removal of the first Me^{2+}. The binding of the first Me^{2+} aids in the structuring of the enzymatic active site, which increases subunit association (Brewer & Weber, 1968). The first Me^{2+} may be removed with excess EDTA (ethylenediamine tetraacetate) or other chelating agents. Subunit dissociation of enolase may also be affected by salts. Salts containing chaotropic anions such as chloride aid in the dissociation of the subunits (Brewer, 1976; Brewer, 1969; Brewer & Weber, 1969), whereas cosmotropic anions such as acetate, would promote subunit association (Brewer, 1969; Brewer, 1976). High ratio of charged/hydrophobic residues and low solvent accessible surface between the dimer interface accounts for the observed salt dependency for the dimer formation of enolase (Kühnel & Luisi, 2001).

The subunit interface does not seem to have any allosteric function since enolase has no known cooperative effects (Kühnel & Luisi, 2001). The two separate active sites of enolase are well contained within their respective monomeric subunits, independent from each other (Kornblatt et al., 1998). Dissociation of enolase to obtain active monomers is therefore of interest. Many earlier efforts to dissociate enolase into active monomers have failed, though they seem to be properly folded (Kornblatt et al., 1996). Two common methods used for the dissociation studies involve the use of salts or hydrostatic pressure (Brewer & Weber, 1968; Kornblatt et al., 1996; Trepanier et al., 1990; Kornblatt et al., 2004). Dissociation of the dimer with salts produced inactive forms of the monomeric enolase due to many setbacks. The setbacks include loss of the divalent cation, exposure of hydrophobic regions (Brewer, 1969), and destabilization of the protein structure by weakening hydrophobic interactions. Such complications affect the proper formation of the active site (Kornblatt et al., 1996). The other method used to dissociate enolase is exposing enolase to hydrostatic pressure. This is a rather milder method to dissociate enolase. The use of

Reproduced with permission of the copyright owner. Further reproduction prohibited without permission.

hydrostatic pressure yielded either inactive or active monomers, depending on the enolase form subjected to the pressure (Kornblatt et al., 2004). Hydrostatic pressure dissociation of apo-enolase or Mg^{2+}-enolase yielded inactive monomers (Kornblatt et al., 1998). In a later study on the hydrostatic pressure dissociation of Mn^{2+}-enolase, active monomers were obtained (Kornblatt et al., 2004). Structural examination of the monomeric enolases using UV-spectroscopy indicate that Mn^{2+} remains bound to the monomeric enolase whereas the Mg^{2+} is released during dissociation. Kornblatt et al. (2004) therefore suggested that the presence of divalent cation is necessary for production of active enolase monomers.

In addition to the use of hydrostatic pressure, active enolase monomers have also been produced through raising the temperature to above 40°C and lowering the protein concentration to below 7 μg/mL in the presence of Mg^{2+} and substrate (Keresztes-Nagy & Orman, 1971; Holleman, 1973).

I.6 Active Site Geometry

The active site of enolase is located within the deep cavity of the carboxylic end of the barrel (Figure 6). A fragment of the N-terminal domain and two highly mobile loops which protrude from the barrel, form a wide crevice to the active site. The first Me^{2+} binding site is hence accessible to the solvent (Lebioda et al., 1989). Crystal structures of yeast enolase with Mg^{2+} as the metal cofactor illustrate that the first Mg^{2+} binds portions of the active site together by means of six-ligand bonds, arranged into an octahedral geometry. The first Mg^{2+} is coordinated to the highly electronegative donor atoms of the carboxylate side chains of Asp246, Asp320, and Glu295 (Lebioda & Stec, 1989). In addition, its coordination to the bidentate carboxylate group of the substrate/product, and to a single H_2O molecule completes the octahedral coordination shell (Wedekind et al., 1995). One of

Reproduced with permission of the copyright owner. Further reproduction prohibited without permission.

the carboxylate oxygens of the substrate/product bridges the two magnesium ions as it is also liganded to the second Mg^{2+}. An oxygen from the phosphate group of the substrate/product also chelates to the second Mg^{2+}. The octahedral coordination of the second Mg^{2+} is completed with the carbonyl and γ-oxygens of Ser39 and two H_2O molecules (Larsen et al., 1996). Ser39 is part of a flexible active site loop that extends from Gly37 to His43 in the N-terminal domain. The chelation of the second Mg^{2+} to Ser39, in effect, seals off the entrance to the active site. This action has been described by Wedekind et al. (1994), as a "latch to the gate to the active site of enolase".

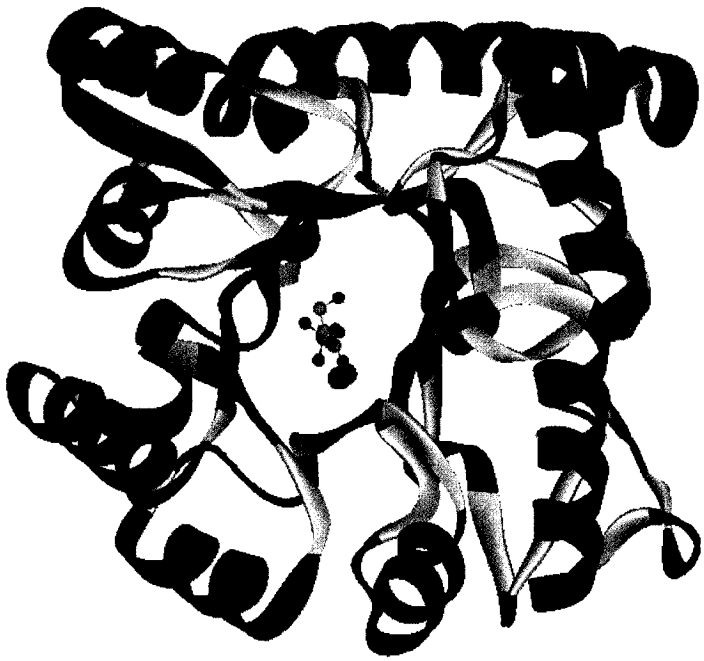

Figure 6. Active site located within the deep cavity of the C-terminal domain. The green spheres in the middle of the barrel represent the two Mg^{2+} cations, and the molecules next to them are 2-PGA and PEP. Helices are red, beta sheets are cyan, turns are green, and coils are white. Figure generated with Weblab ViewerLite using pdb 1ONE.

Reproduced with permission of the copyright owner. Further reproduction prohibited without permission.

Other residues that are found in the active site region are Ala38, His159, Glu168, Glu211, Asp321, Lys345, His373, Arg374, Ser375, and Lys396, some of which are involved in coordinating the substrate molecule as it enters the active site. The phosphoryl oxygens of 2-PGA make H-bond contacts with the amide hydrogens of Ala38, Ser39, and Ser375, along with the side chains of Arg374, Ser375, and His159. The side chain of His373 is in contact with the hydroxyl group of the substrate, and Lys396 interacts with the carboxylic group of 2-PGA. His159 is part of another flexible loop that extends from Val153-Phe169 that fold over the active site alongside with the active site loop to close off the active site. Figure 7 illustrate the residues and bondings involved in the active site geometry of enolase.

I.7 Reaction Mechanism

I.7.1 Overview of the Enolase Reaction Mechanism

The reversible elimination of water from 2-PGA to give PEP proceeds through an *anti* stereochemistry reaction (Cohn et al., 1970). The reaction occurs in a stepwise manner (Dinovo & Boyer, 1971; Stubbe & Abeles, 1980; Anderson et al., 1984; Anderson et al., 1994; Poyner et al., 1996). In the forward direction, an enzymatic base abstracts a proton from C-2 of 2-PGA, forming a carbanion (enolate) intermediate. This step is followed by the loss of an OH^- group from the hydroxymethyl group of the intermediate via a catalytic acid, to give the product of PEP. Hydration of PEP goes through the reverse steps. Figure 8 represents the stepwise reaction of enolase.

Reproduced with permission of the copyright owner. Further reproduction prohibited without permission.

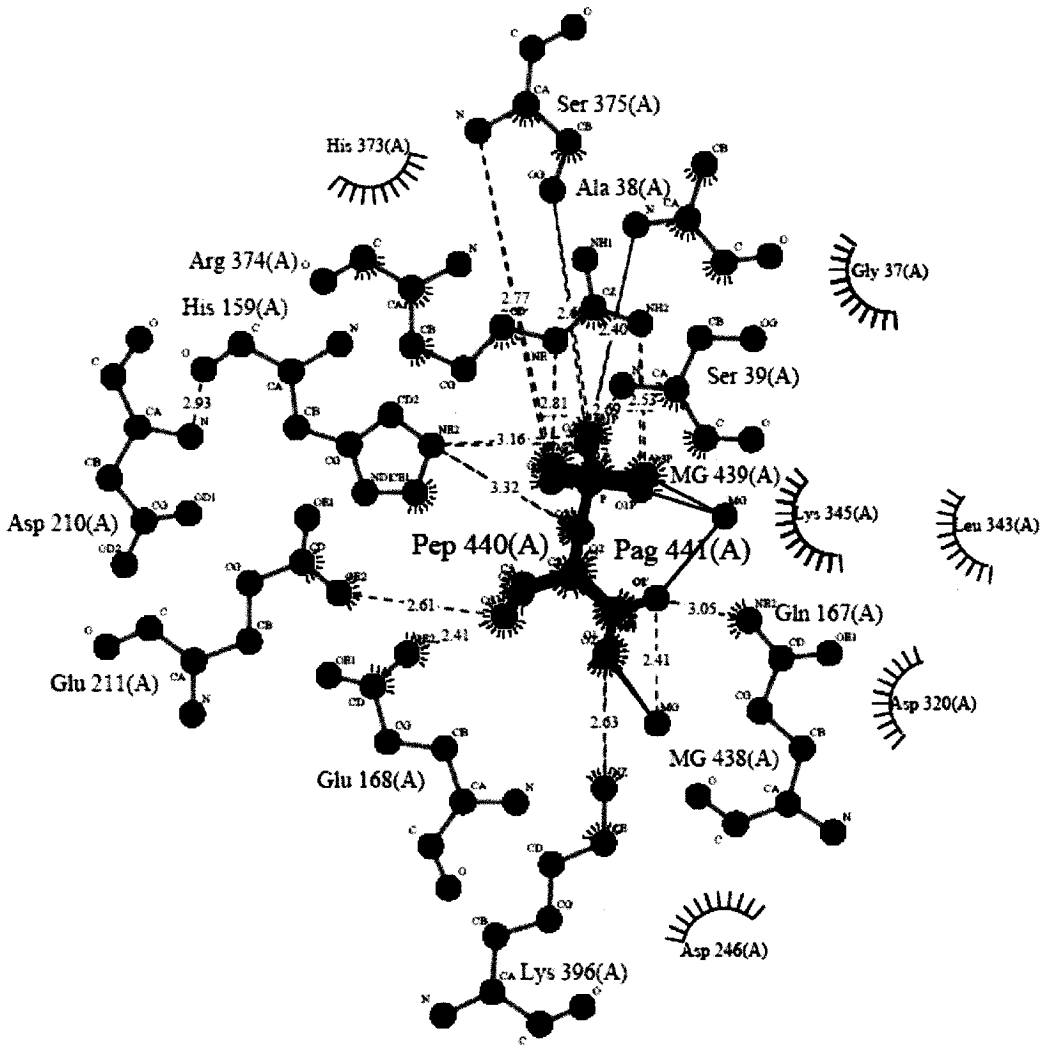

Figure 7. Active site geometry of enolase. H-bonds are represented by dotted green lines, with the distance in Angstroms labeled. The amino acids are coloured according to the CPK scheme. Amino acid residues that are behind the plane of the diagram are represented by quarter circle with dashes. Figure obtained from the Structure Analysis of the pdb 1ONE from the RCSB Protein Data Bank.

Reproduced with permission of the copyright owner. Further reproduction prohibited without permission.

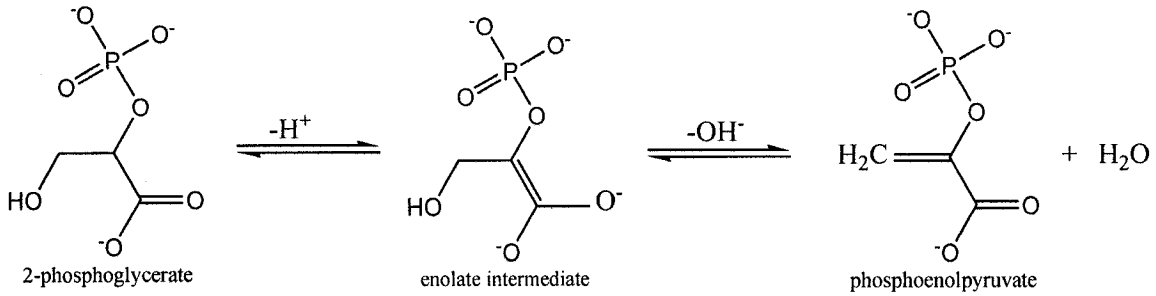

Figure 8. Stepwise reaction of enolase.

For enolase, this form of acid/base mechanism is quite intriguing. This is due to the fact that the abstraction of the C-2 proton involves overcoming a substantial barrier since it is relatively non-acidic with a p*Ka* of ~28 – 32 (Wedekind, 1994), and the removal of a relatively poor leaving OH^- group from C-3 of the intermediate. Therefore, catalysis must provide a means of promoting ionization of the carbon acid, stabilization of the enolate intermediate, and increasing the leaving ability of the OH^-. With this, the questions of which amino acid is the base for the initial proton abstraction, and what roles do the metal ions play, arise.

I.7.2 Mechanistic Schemes

To date, the catalytic mechanism of enolase has not been defined unambiguously. Among the many different proposals of the enolase catalytic machinery, three of them have received the most attention. The contrasting proposals have emerged from separate structural investigations of either yeast enolase (Lebioda & Stec, 1991; Wedekind et al., 1994) or lobster muscle enolase (Duquerroy et al., 1995). One of the earlier schemes was based on the crystal structures of yeast enolase prepared by Lebioda et al. (Lebioda & Stec, 1991; Lebioda et al., 1989). The scheme infers that the catalytic base is a water molecule that is

Reproduced with permission of the copyright owner. Further reproduction prohibited without permission.

activated by two glutamate residues (Lebioda & Stec, 1991). This water molecule is H-bonded to the carboxylic groups of Glu168 and Glu211, and is located in close proximity to the carbon-2 of the substrate in the direction of its proton. The C-2 proton of the substrate is proposed to be primarily transferred to the water molecule, then to Glu168, and further shuttled to the hydroxyl group of the substrate to form the leaving water molecule. H-bonding of the proposed basic water molecule to the carboxylic groups renders it to be strongly nucleophilic, therefore facilitating its role as the catalytic base of enolase, abstracting the proton in the catalytic reaction. In addition to this, Lebioda and Stec have also proposed that the first metal site coordinates to the hydroxyl group of 2-PGA, making it to be a better leaving group. This mechanistic proposal has been supported by experiments done by Brewer et al. (1997), Sangadala et al (1995) and Poyner et al. (1996), who have found that mutation of either Glu168 or Glu211 to glutamate in yeast enolase results in reduced activity of the enzyme by a factor of at least 10^{-4} (Brewer et al., 1993; Sangadala et al., 1995; and Poyner et al., 1996). However, this mechanistic proposal has been challenged since the location and the role of the second metal site were ambiguous in the crystal structures used to support this proposal.

The second mechanistic scheme that has been proposed originates from the analysis of the crystal structure of lobster enolase (Duquerroy et al., 1995). Duquerroy et al. proposed His157 (His159 in yeast enolase) to be the catalytic base which abstracts the carbon-2 proton from 2-PGA. This possible catalytic base has been debated as Vinarov and Nowak (1999) established that the H159A variant yeast enolase has depressed activity by 10^{-4} fold of magnitude, but Brewer et al. (2000) found that H159A has significant activity. Therefore, this reaction scheme became less universally accepted than the other two schemes.

Reproduced with permission of the copyright owner. Further reproduction prohibited without permission.

More recently, the crystal structures of yeast enolase complexed with phosphonoacetohydroxamate (PhAH), a high-affinity inhibitor of enolase, in the presence of either Mg^{2+} or Mn^{2+} (Wedekind et al., 1994 and Zhang et al., 1994 respectively) were obtained. The structure of PhAH is believed to mimic the aci-carboxylate form of the intermediate carbanion in the reaction, and is therefore widely used to study the interactions between enolase and substrate (Anderson et al., 1984). The crystal structures of enolase complexed with PhAH, which have more refined views on the location of the second Me^{2+} site, have lead to a different proposal for the identity of the catalytic base, and have elucidated the role of both metal sites. This reaction scheme proposes Lys345 to be the catalytic base. Lys345 is a more conventional base and is within close proximity to carbon 2 of 2-PGA. It is proposed that Lys345 is in fact the only basic functional group that is accessible to the proton. Moreover, the ε-amino group of Lys396 is within H-bonding distance of a carboxylate oxygen of 2-PGA, which is believed to stabilize, along with the divalent cations, the increased negative charge that builds up on the carboxylate of the enolase intermediate. This mechanistic scheme is supported by the work done by Poyner et al. (1996) where the K345A variant loses the ability to catalyze the exchange of carbon-2 proton of 2-PGA with deuterium in D_2O and has activity severely depressed by a factor of 10^{-5}. According to previous work done by Cohn et al. (1970), the reaction mechanism for the enolase-catalyzed elimination of water from 2-PGA occurs via an *anti*-stereochemistry. It was therefore proposed that the catalytic acid may be the carboxyl side chain of Glu211. Glu211 is on the opposite side to Lys345 and is proximate to the hydroxymethyl group of 2-PGA, facilitating the removal of the C-3-OH. This reaction scheme (Figure 9) is presently the most accepted as the reaction mechanism of enolase.

Reproduced with permission of the copyright owner. Further reproduction prohibited without permission.

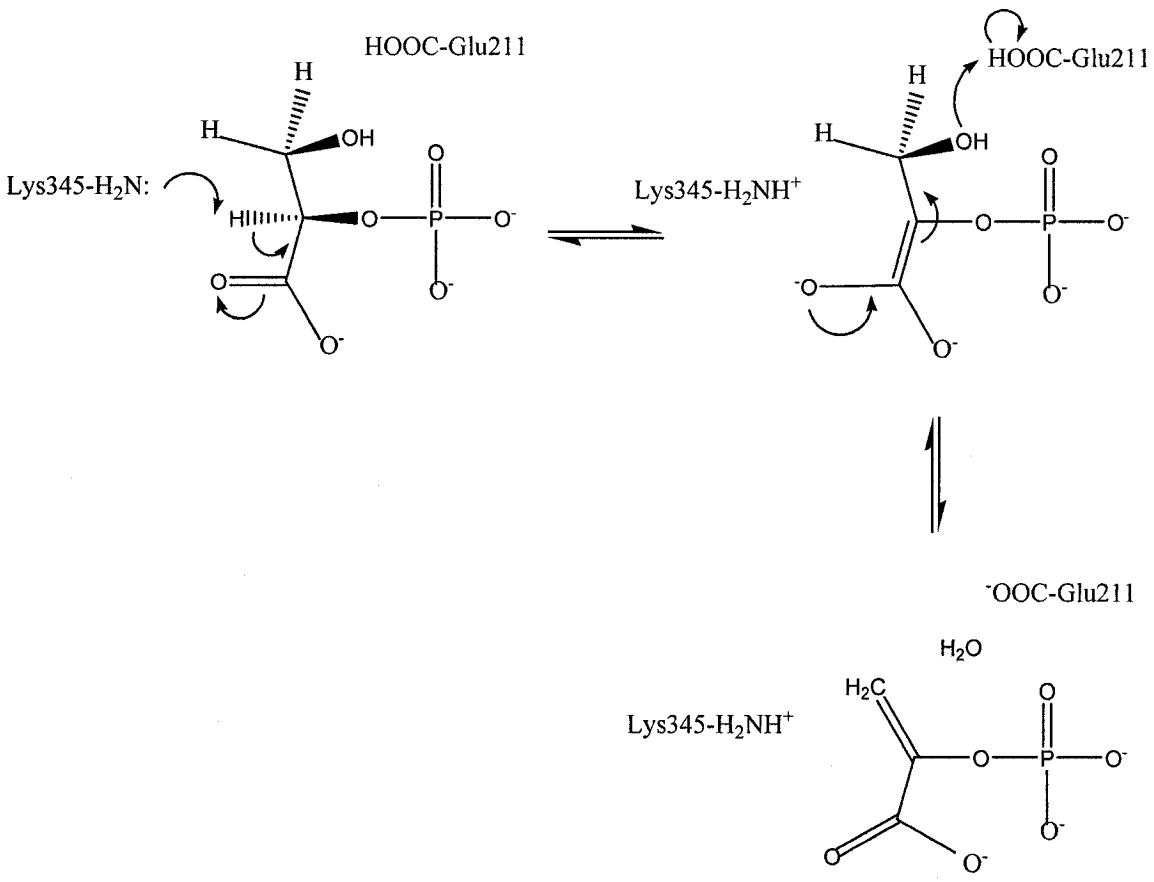

Figure 9. Reaction mechanism of enolase with Lys345 and Glu211 as the catalytic base/acid pair.

I.8 Role of Metal in Enolase

Enolase is a metalloenzyme which requires two equivalents of divalent cations for activity. Binding of the first Me^{2+} to the high affinity cation binding site has a structural function of placing portions of the active site together, facilitating the binding of the substrate/inhibitor. The second equivalent of Me^{2+} binds only upon binding of substrate/inhibitor. The two metal ions not only provide structural purposes, but are

Reproduced with permission of the copyright owner. Further reproduction prohibited without permission.

engaged to stabilize the extra negative charge observed in the enolate intermediate (Larsen et al., 1996). The interactions of the metal with the substrate or enzyme are illustrated in section I.6.

For catalysis to occur, the binding of two metal ions to each monomer is required. The two metal sites are observed in the crystal structures. However, at high concentrations of metal, enzyme inhibition is observed. Faller et al. (1977) first suggested that there is a third inhibitory metal binding site. More recently, in 2003, the crystal structure of *Trypanosoma brucei* enolase was made available (da Silva Giotto et al., 2003). The crystal structure illustrates and confirms the presence of the third inhibitory metal binding site in enolase. The crystal structure revealed four protein ligands interacting with this third metal, namely the Glu208, Glu165, His156, and Gln164 in the *Trypanosoma brucei* numbering system. Experimental results obtained from Vinarov and Nowak (1999) on the study of Mn^{2+} binding to the H159A variant yeast enolase agree with the existence of the third inhibitory binding site. Vinarov and Nowak demonstrated, using EPR spectroscopy, that the metal ion binding affinity for the first two metal sites was similar to that of the wild-type enolase's. However, a weaker third metal ion binding site was observed in comparison to that of the wild-type. These results are consistent with the observation that His159 (*His156 in T. brucei*) is a ligand for this third metal ion, as its mutation led to a decrease in affinity for the metal ion.

I.9 Enolase Superfamily

Enolase belongs to the enolase superfamily. The enolase superfamily is divided into three subgroups: the mandelate racemase (MR), muconate lactonizing enzyme (MLE I), and the enolase subgroups. Mandelate racemase catalyzes the interconversion of the (R)- and

Reproduced with permission of the copyright owner. Further reproduction prohibited without permission.

(S)-enantiomers of mandelate, muconate lactonizing enzyme I catalyzes the reversible cycloisomerization of *cis,cis*-muconate to muconolactone, and enolase catalyzes in the interconversion of 2-phosphoglycerate to phosphoenolpyruvate. Although members of this superfamily catalyze different overall reactions, they are catergorized into the same superfamily as they catalyze the same initial step. The members of the enolase superfamily share the initial divalent metal ion-assisted removal of the α-proton from a carboxylate anion substrate, forming an enolic intermediate (Babbitt et al., 1996).

All members of the superfamily contain a small N-terminal and a large C-terminal mixture of the α/β-barrel domain as described previously. They share similar active site architectures, where their active site functional groups are located within the loops connecting the β-sheets with the α-helices (Gerlt, 2000). The difference in substrate specificities depends on the N-terminal domain that closes over the active site in the barrel domain. Members of the enolase superfamily are assigned to their respective subgroups according to their active site general base(s). The mandelate racemase subgroup abstracts the α-proton via one lysine and/or histidine residue, whereas the muconate lactonizing enzyme I subgroup catalyzes this initial step via two lysine residues, and the enolase subgroup probably uses one lysine residue (please refer to the section I.6 Reaction Mechanism). Structural alignment of MR, MLE I, and enolase demonstrate global homology between the three subgroups The functional group of Lys345 from enolase is spatially homologous to those of Lys273 in the active site of MLE I, and His297 in the active site of MR (Babbitt et al., 1996). On the other hand, Glu211, the proposed catalytic acid of enolase do not have homologous active sites of MR or MLE I. This is anticipated as the subgroups catalyze different overall chemical mechanisms.

Reproduced with permission of the copyright owner. Further reproduction prohibited without permission.

I.10 Mobile Loop Movement

Loop movements in enzymes are associated with the proper positioning of catalytically important residues (Joseph et al., 1990). Enolase has a wealth of loop structures that are involved in forming the connections between the α-helices and β-barrels. Among them, three large loops that extend over the active site are of significance. They are highly mobile loops that differ significantly in position between the holoenzyme and holoenzyme with substrate bound structures. The first loop, Loop1 (L1) is located within the N-terminal domain. It is composed of residues Ser36-Ala45. The other two loops are within the C-terminal domain, termed Loop2 (L2) composed of residues Val153-Phe169, and Loop 3 (L3) composed of residues Ser250-Ser267. These loop structures experience positional shifts as the substrate and metals bind to the enzyme. On the binding of Me^{2+} and substrate, Loop 1 from the N-terminal domain and Loops 2 and 3 from the C-terminal domain fold over the active site to form the closed conformation (Larsen et al., 1996; Zhang et al., 1997). Little change in these mobile loops is observed as the first Me^{2+} binds to the apoenzyme (Wedekind et al., 1995). The three mobile loops in the apo-enzyme are in the opened-loop structure. These mobile loops undergo a large shift upon substrate and second metal binding. This is termed the closed-loop structure (Larsen et al., 1996). In the crystal structure of the asymmetric dimer of yeast enolase with an equilibrium mixture of PGA and PEP, the three loop conformations differ between the PGA-bound subunit and the PEP-bound subunit. In the PEP-bound subunit, Loop 1 resembles the closed-loop conformation, whereas Loops 2 and 3 resemble the open-loop conformation (Zhang et al., 1997). Figure 10 illustrates the superimposition of the two forms of the loop structures, noting the huge different in positions of the three mobile loops.

Reproduced with permission of the copyright owner. Further reproduction prohibited without permission.

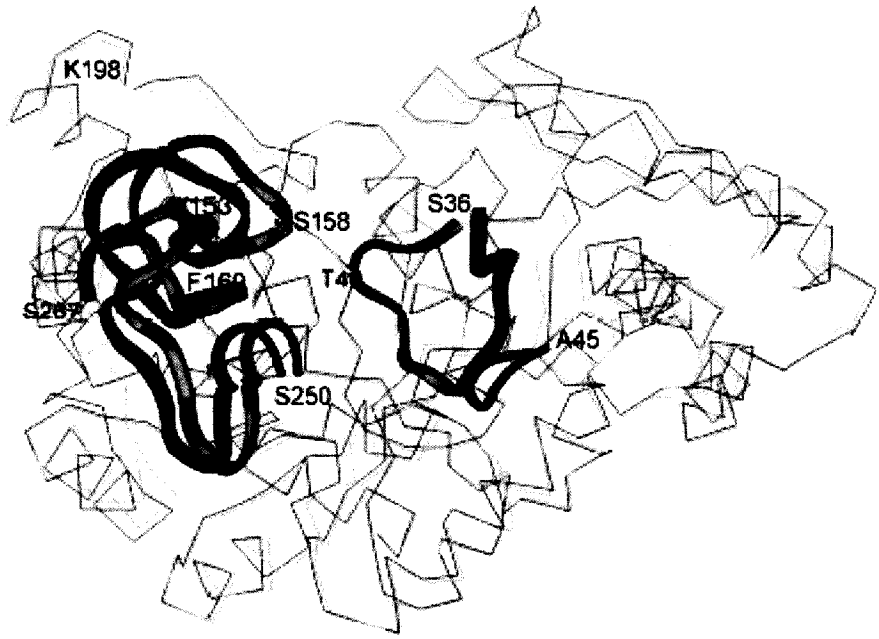

Figure 10: Tertiary structural alignment of the opened (apo: purple) and closed (holo: cyan) loop conformations of enolase. Three loops show structural vatiation, with Loop 1 (Ser36-Ala45) showing large positional displacement. The positions of glycine residues in these loops are shown in blue. The figure was obtained from Figure 6 of Gunasekaran et al., 2003.

As mentioned previously, Ser39 and His159 interact with the metal and substrate as they bind. Such interactions form anchors for L1 and L2 to effectively seal off the active site. The mobility of these loops is facilitated by the presence of glycine residues that form hinge sites. For example, in Loop 1, Gly37 and Gly41 form the hinge sites that permit Ser39 to rotate into position to interact with the substrate and the second metal. Also, in Loop 2, Gly156, Gly157, Gly161, and Gly162 are responsible for providing Loop 2 with enough space and mobility to properly position His159 to coordinate with the substrate (Gunasekaran et al., 2003).

Reproduced with permission of the copyright owner. Further reproduction prohibited without permission.

I.11 Research Objective

The muscle specific β-enolase accounts for over 90% of muscle enolase activity. Deficiency in β-enolase leads to the metabolic myopathy, glycogenosis type XIII. Comi et al. (2001) are the first to report on a patient suffering from this muscle-specific enolase deficiency, with only 5% normal activity. The patient experiences exercise-induced myalgias and generalized muscle weakness. Certain clinical, biochemical and genetic features of the patient were observed. Primarily, no rise in venous lactate level was observed upon exercise. This was the first indication of a glycolytic pathway defect. Glycolytic enzyme activities were then measured in muscle homogenate supernatant. Results indicate ~20-fold decrease in the patient's muscle enolase activity compared to the control. In addition, negative immunostaining with specific antibodies for β-enolase and Western blot analysis of the muscle tissue points to reduced β-enolase protein level. Figure 11 represents the Western blot analysis of α- and β-enolase.

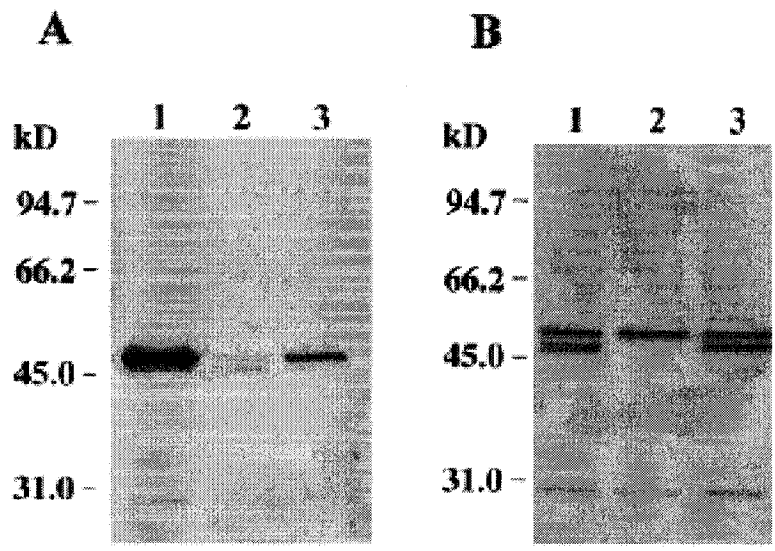

Figure 11. Western blot analysis of α- and β-enolase. **(A)** β-enolase; Lane 1: Control muscle; Lane 2: patient muscle; Lane 3: purified muscle enolase. **(B)** Immunoblot with rabbit α-enolase antibodies; Lane 1 and 3: control muscles; Lane 2: patient muscle. Figure was obtained from Comi et al., 2001.

Reproduced with permission of the copyright owner. Further reproduction prohibited without permission.

In Figure 11 (A), control muscle β-enolase and purified muscle enolase show strong bands at ~46 kDa. Only a faint doublet of immunoreactivity is observed in the patient. In Figure 11 (B), both control muscles show two bands when immunoblotted with rabbit α-enolase antibodies, with only one band showing in the patient. The second band is believed to be a cross-reacting β-enolase immunoreactivity. The results indicate that the patient carries normal levels of α-enolase, with an isolated deficiency of β-enolase.

Further analysis reveals that the patient carries two heterozygous missense mutations changing G156 to an aspartate or G374 to a glutamate. The current research objective is to study the role of one of the missense mutations, G156 (G157 in yeast enolase) that the patient carries. Yeast enolase is used as a model to study the effects of the G156D mutation in human ββ-enolase. The G157D mutation will be introduced into yeast enolase. Yeast enolase may be obtained in high quantities, and has high sequence and structural similarities with mammalian enolase, hence the yeast enzyme is a good model to study the ββ-enolase variant.

G157 is part of the highly mobile Loop 2. Glycine residues are of great popularity in mobile loop structures as it is a small amino acid which may form good hinges that facilitate movement. Changing a glycine residue to another larger and charged one such as aspartate may hinder the appropriate movement of the loop itself. In addition, L2 in enolase plays a crucial role in closing off the active site as the metal and substrate are bound. Within this loop, His159 is of mechanistic significance. His159 interacts with the substrate as it binds, generating an anchorage point for L2 to close over the active site. Hence, mutation of the small, non-polar Gly157 residue, located two amino acid residues from His159, to a large, polar aspartate residue, may hinder the interaction of His159 with the substrate. The hindering of this interaction may then impair the proper positioning of L2 as catalysis

Reproduced with permission of the copyright owner. Further reproduction prohibited without permission.

occurs. His159 is also believed to be a ligand to the third inhibitory metal binding site. If the mutation of G157D affects the local environment of L2, then there should be a significant difference in the binding of this third inhibitory metal.

With this, the current research study involves introducing the G157D point mutation into the wild-type enolase. To see the effects of the increase in size and charge of the mutation, the G157A, G157N, and G157L variants would also be constructed. Basic characterization of the G157 variants, looking at differences in the structure, stability, and kinetic properties from the wild-type protein, is performed in order to elucidate the role of the G157 in yeast enolase, and thus infer the role of G156 in human ββ-enolase.

Reproduced with permission of the copyright owner. Further reproduction prohibited without permission.

Chapter II: Materials and Methods

II.1 Bacterial Growth Media

Luria Broth (LB) was prepared with 1% bacteriological grade tryptone, 0.5% yeast extract, and 1% A.C.S. grade NaCl, all purchased from Fisher Scientific. LB plates are made with 1% agar purchased from Becton Dickinson.

Bacterial growth for protein expression was carried out in expression medium prepared with 1% tryptone, 0.5% yeast extract and 1.6% of A.C.S. grade α-Lactose, obtained from Fisher Scientific. The medium is supplemented with M9 salt, (Sambrook et al.,1989), using Na_2HPO_4, KH_2PO_4, NH_4Cl, NaCl, all certified A.C.S. grade purchased from Fisher Scientific. All growth media were pH adjusted to 7.0.

BioTech grade ampicillin (sodium salt), purchased from Fisher Scientific, was prepared as 100 mg/mL solution sterilized using 0.45 μm Nalgene syringe filters and stored at -20°C. Ampicillin was added into medium to a concentration of 100 μg/mL.

II.2 Agarose Gel

Agarose gels are used to analyze DNA samples. Agarose, genetic technology grade, purchased from ICN Biomedical, is dissolved to 1% concentration in TAE buffer (40 mM Tris, 20 mM acetic acid, and 1 mM EDTA, pH 8.0) by heating 1-1.5 min in the microwave. The 1% agarose solution is supplemented with 0.5 μg/mL of ethidium bromide (prepared as a 10 mg/mL stock in dH_2O and kept from light) before the gel solidifies. Loading dye (purchased as 6X from Promega) is diluted to 1X and added to the all samples and to 0.5 μg of the molecular weight standard, Lambda (λ) DNA (*Eco*RI/*Hin*dIII), purchased from

Reproduced with permission of the copyright owner. Further reproduction prohibited without permission.

Promega, before loading onto the gel. Electrophoresis was carried out at 80 V-100 V in TAE buffer for 1-2 hrs. Gels are visualized under UV-transillumination and photographed.

II.3 SDS-PAGE

Separating proteins under denaturing conditions was performed using SDS-PAGE. The gels were prepared with 12% resolving gel and 4% stacking gel. Stock solutions of buffer and bis/acrylamide were prepared and stored at 4°C. Bis/acrylamide, 30%) was prepared with 29.2% acrylamide (99.9% pure) and 0.8% N'N'-bis-methylene-acrylamide (97.0% pure), both purchased from Bio-Rad. SDS (Fluka) was prepared as 10% w/v in dH_2O and stored at room temperature. APS, 10%, was prepared and stored at -20°C. The APS, TEMED, 2-mercaptoethanol, and Coomassie brilliant blue R were of electrophoresis purity grades and purchased from Bio-Rad. Table 4 illustrates the contents of the stacking and resolving gels.

Solutions	Stacking Gel	Resolving Gel
30% bis/acrylamide	2.0 mL	325 µL
dH_2O	1.7 mL	3.0 µL
1.5M Tris-HCl, pH 8.8	1.25 mL	------
0.5M Tris-HCl, pH 6.8	------	620 µL
10% SDS	50 µL	25 µL
10% APS	25 µL	12.5 µL
TEMED	2.5 µL	2.5 µL

Table 4. SDS-PAGE preparation contents.

Reproduced with permission of the copyright owner. Further reproduction prohibited without permission.

Samples containing 10 μg of protein, were diluted with sample buffer (2.5% 0.5M Tris-HCl pH 6.8, 4% SDS, 2% glycerol, 1% 2-β-metcaptoethanol: electrophoresis grade, purchased from Bio-Rad, and a pinch of Brilliant Blue R from Sigma) and boiled for 1.5 min before loading onto the gel. SDS-PAGE low protein molecular weight standards, purchased from Bio-Rad, and standard yeast enolase, purchased from Sigma, were electrophoresed routinely with the samples. Electrophoresis was carried out at 200 V, and the gels were framed after Coomassie staining for 30 min in staining solution (0.1% Coomassie blue, 40% MeOH, 10% HOAc) and destaining for 2 hrs in destaining solution (40% MeOH, 10% HOAc).

II.4 Removal of Metals

Solutions or protein samples that needed to be metal free were passed through chelex columns. Chelex 100 resin (sodium form, analytical grade) was purchased from Bio Rad. Bottles and vials that were used to contain samples that were metal free were soaked in 20% Nitric acid (A.C.S. grade, purchased from Fisher Scientific) for ≥1 hr, and rinsed thoroughly with dH_2O prior to use.

II.5 Standard Enolase Assay

Enolase activity assays were preformed by monitoring the production of PEP at 240 nm for 1 min using the Varian Cary 1 UV-visible spectrophotometer. Assays were carried out in 1 cm quartz cuvettes. Enolase assay buffer was prepared as 50 mM imidazole (pH 7.1), 1 mM $Mg(OAc)_2$, 250 mM KCl (all A.C.S. certified grade from Fisher Scientific), and 0.1 mM EDTA (≥99% from Fluka). The assays were initiated by addition of enzyme to 1 mM 2-PGA in 1 mL of enolase assay buffer at 25°C. The concentration of enzyme used for

Reproduced with permission of the copyright owner. Further reproduction prohibited without permission.

the assays varied between the wild-type and variant enolase in order to yield a maximum optimal slope of ΔOD_{240} of 0.1/min.

II.6 LDH/PK Linked Assay for 2-PGA Determination

The concentration of PGA was determined using a lactate dehydrogenase/pyruvake kinase (LDH/PK from rabbit muscle, purchased from Roche) linked assay. The assay was performed in a freshly prepared assay mix that contained 0.25 mL of 5.4 mM NADH (≥97.0% HPLC grade from BioChemika), 0.25 mL of 40.5 mM ADP (sodium salt, from Bacterial source, purchased from Sigma), and 9.5 mL of enolase assay buffer. The concentration of 2-PGA was determined from the drop in absorbance at 340 nm due to the consumption of NADH. $OD_{340(1)}$ was measured with 2.5 mL of the assay mix with 15 μL of LDH/PK and 2 μL of the 2-PGA sample. The assay was begun with the addition of 5 μL of concentrated enolase and the $OD_{340(2)}$ was measured once no further change occurred. The concentration of 2-PGA was calculated with $\varepsilon_{340\ 2\text{-PGA}} = 6.22\ mM^{-1}$, as equation 1:

$$[2\text{-PGA}] = \frac{(OD_{340(2)} - OD_{340(1)}) \times \text{dilution factor}}{6.22\ mM^{-1}} \qquad (1)$$

II.7 2-PGA Synthesis

Since the enolase substrate, 2-PGA, is no longer commercially available, 2-PGA was synthesized enzymatically. The synthesis of 2-PGA was prepared following a modified method from Sims & Reed (2004). D-glycerate-2-kinase was used to convert D-glycerate to 2-PGA with ATP. The conversion began with mixing 1.9 g of ATP with 0.48 g of DL-glyceric acid (hemi calcium salt hydrate, minimum 98% purchased from Sigma), 14 mL dH_2O, and 40 μL of 1 M $Mg(OAc)_2$. The pH of the mixture was adjusted to 7.0-8.0 with 2

Reproduced with permission of the copyright owner. Further reproduction prohibited without permission.

N KOH. The OD_{260} was measured with 1 μL of the mixture in 2.5 mL of dH_2O. Approximately 4 mg of D-glycerate-2-kinase (prepared and purified in the Kornblatt lab as described in Sims & Reed, 2004) was mixed into the solution and incubated at 4°C overnight. The overnight incubation mixture was then passed through the charcoal column. The charcoal column was prepared with two layers of Whitman filter paper, followed by coating it with a thick bottom layer of celite and topping the celite layer with ~7 g of activated carbon powder (USP). After applying the sample, the column was then washed three times of 1 column volume of dH_2O. Assays for 2-PGA were carried out for the overnight incubation mixture, the charcoal eluted mixture, and the three dH_2O washes by measuring the change in OD_{340} using the LDH/PK linked assay. OD_{260} was monitored for the samples as well. Samples containing 2-PGA were pooled together and stored at -20°C overnight. The pooled sample was thawed the next day and diluted with 100 mL dH_2O to bring down the ionic strength. 1 N HCl, 1.0 mL, (A.C.S. grade purchased from Fisher Scientific) was added to the diluted sample and loaded onto a 20 mL Dowex (1×2-400 ion-exchange resin purchased from Sigma) column that has been thoroughly washed and equilibrated with dH_2O. The samples were loaded at a flow rate of approximately 1 mL/min. The 2-PGA was then eluted with 0.04 M HCl at the same flow rate and 5 mL fractions were collected. OD_{260} and ΔOD_{340} were monitored for every fourth fraction. The fractions containing high amounts of 2-PGA and low OD_{260} (≤ 0.6) were pooled together and pH adjusted to 7.5-8.0 using TMAOH (tetramethyl ammonium hydroxide, purum purchased from Fluka). The pooled 2-PGA sample was quickly frozen with liquid nitrogen and stored at -20°C. The 2-PGA was then lyophilized and diluted in dH_2O to the desired concentration of 2-PGA and stored at -20°C.

Reproduced with permission of the copyright owner. Further reproduction prohibited without permission.

II.8 D-PGA Synthesis

Deuterated 2-PGA was prepared by dissolving 300 mg of PEP (Roche) and 12 mg of $MgSO_4 \cdot 7H_2O$ (A.C.S. grade from Fisher Scientific) in 10.0 mL of D_2O (100.0 atom %D, purchased from Aldrich). The pH of the mixture was adjusted to just below 6 with solid MES (≥99.0%, Fluka Biochemika). The concentration of PEP was determined by measuring its OD_{240}, using a molar extinction coefficient of 1.25 mM^{-1}. Approximately 2 mg of yeast enolase was added to the mixture, which was then incubated over night at 4°C. The conversion of PGA was determined the following day by the decrease in concentration of PEP (approximately 25% conversion is expected). 1 N HCl, 0.5 mL, and 100 mL of dH_2O were added to the overnight mixture. The mixture was then loaded onto a Dowex column with a flow rate of approximately 1 mL/min. The D-PGA was separated from PEP by eluting with 0.02 M HCl, and 3 mL fractions were collected. D-PGA was measured enzymatically by monitoring the increase in PEP production upon addition of 5 μL of concentrated yeast enolase. The fractions with D-PGA were pooled together and pH adjusted to 7.0 with TMAOH. The pool was then frozen with liquid nitrogen and stored at -20°C until it was lyophilized. The D-PGA was then dissolved in dH_2O to the desired concentration and stored at -20°C.

II.9 Plasmid DNA Extraction

Small-scale plasmid DNA extraction was performed using the Wizard Plus Miniprep DNA Purification System purchased from Promega. Large-scale plasmid DNA extractions were performed according to the large scale isolation of plasmid DNA from *E. coli* (Kreig & Melton, 1991). Lysis buffer was prepared with 25 mM Tris-HCl pH 7.5 (molecular biology grade), 10 mM EDTA (Ultra ≥99%), 1.5% sucrose (A.C.S. grade), and 2 mg/mL of chicken

Reproduced with permission of the copyright owner. Further reproduction prohibited without permission.

egg white Lysozyme from Sigma. Phenol, ultra pure for molecular biology, was purchased from Fluka BioChemika. PEG 13% was prepared using PEG 8000 from Boehringer Mannheim. RNAse A from bovine pancreas (Boehringer Mannheim) was prepared as 10 mg/mL solution, and heat inactivated according to Sambrook et al. (1989). The final DNA products were resuspended in TE buffer (10 mM Tris-HCl, 1 mM EDTA, pH 8.0). The concentration and purity of the DNA were determined according to the OD_{260} and OD_{280} ratio. The purified DNA are then used to transform into competent cells or alternatively kept at -20°C for long term storage.

II.10 Determination of Protein Concentration

The concentration of enolase was calculated by dividing the OD_{280} of the enolase samples by the ε_{280} of 0.895 $mLmg^{-1}cm^{-1}$ (Warburg, 1942). Alternatively, the Bio Rad BSA, based on the Bradford method (Engel, 1996), was used to determine protein concentration. BSA was purchased from Sigma, and the Bio Rad Protein Assay Dye Reagent was purchased from Bio Rad. A standard curve was prepared with 2-8 μg of BSA measured at OD_{595}.

II.11 Site-directed Mutagenesis

The open reading frame of the gene coding for yeast enolase was ligated into the pET-3a vector polycloning site, between the *Nde*I and *Bam*HI restriction site by Isabelle Rajotte. Site-directed mutagenesis was carried out on the plasmid DNA carrying the wild-type yeast enolase gene as directed in the Quick Change (Stratagene) method. The following HPLC grade oligonucleotide primers (Table 5) were designed using the PC Gene software (PC/Gene: the nucleic acid and protein sequence analysis software system © A. Bairoch/University of Geneva/Switzerland; ™ IntelliGenetics Inc. Released 6.60/July 1,

Reproduced with permission of the copyright owner. Further reproduction prohibited without permission.

1991), and purchased from BioCorp Inc. (Montreal, Que.) for introducing site-specific mutations.

Yeast Enolase Variant	Oligonucleotide
G157D	3' GGTAAGAACTTGCAAAA**T**TTGCCAC**T**AAGGGTGCGACCACC 5' 5' CCATTCTTGAACGTTTT**A**AACGGTG**A**TTCCCACGCTGGTGG 3'
G157A	3' GGTAAGAACTTGCAAAA**T**TTGCCAC**G**AAGGGTGCGACCACC 5' 5' CCATTCTTGAACGTTTT**A**AACGGTG**C**TTCCCACGCTGGTGG 3'
G157N	3' GGTAAGAACTTGCAAAA**T**TTGCCA**TT**AAGGGTGCGACCACC 5' 5' CCATTCTTGAACGTTTT**A**AACGGT**AA**TTCCCACGCTGGTGG 3'
G157L	3' GGTAAGAACTTGCAAAA**T**TTGCCA**GA**AAGGGTGCGACCACC 5' 5' CCATTCTTGAACGTTTT**A**AACGGT**CT**TTCCCACGCTGGTGG 3'

Table 5. Oligonucleotide primer sequences for mutagenesis of yeast enolase.

The bold and underlined nucleotides indicate those used to alter codons, while the underlined regions nucleotide indicates the silently introduced restriction site, *Dra*I, for selection of variants. The oligonucleotides were dissolved and diluted in sterile dH_2O, and quantitated by measuring their OD_{260}, where each OD_{260} unit is equivalent to 33 μg of oligonucleotide (Brown, 1991).

PCR samples were prepared by addition of 200 ng of the double-stranded parental DNA, 250 ng of each of the forward and reverse oligonucleotide primers, and 40 μM dNTP into 10 μL of *Pfu* buffer containing $MgSO_4$. Sterile dH_2O was used to dilute the sample to a total volume of 100 μL volume. Mutagenesis was then carried out using 0.5 units of the highly thermostable *Pfu* DNA polymerase, purchased from Fermentas Life Science. PCR amplification was performed according to the temperature cycles elucidated in Table 6. The

Reproduced with permission of the copyright owner. Further reproduction prohibited without permission.

methylated and hemi-methylated parental DNA was then digested with 10 units of *Dpn*I (Fermentas Life Science) for 1 hr at 37°C. The digests were analyzed by 1% agarose (ICN Biomedics, Genetic Technology grade) gel electrophoresis.

Segment	Number of Cycles	Temperature	Duration
1	1	95°C	2 min
		54°C	1 min
		72°C	14 min
2	16	95°C	30 sec
		54°C	1 min
		72°C	14 min

Table 6. Temperature cycles for PCR

II.12 Screening of Variant Yeast Enolase

Wild-type and mutant forms of yeast enolase DNA are transformed into the XL1-Blue *E. coli* competent cells using heat shock. DNA of interest is incubated with 100 μL the competent cells on ice for approximately 40 min. Sterile dH_2O is used as a negative control. The incubation is followed by 1.5 min of heat shock at 42°C (Capage & Hill, 1979; Lederberg & Cohen, 1974). The cells are grown in LB for 1.5 hr at 37°C, 225 rpm, and then plated onto LB plates containing ampicillin and incubated at 37°C for 16 hrs. Colonies were picked and inoculated into 10 mL LB+Amp and grown for 16 hrs at 37°C, 225 rpm. DNA was purified according to the small-scale plasmid preparation. DNA (1 μg) was double-digested with 10 units each of *Bam*HI and *Nde*I restriction enzymes, purchased from

Reproduced with permission of the copyright owner. Further reproduction prohibited without permission.

Fermentas, or alternatively digested with the newly inserted silent mutation restriction enzyme, *Dra*I, purchased from Promega. Samples were complemented with 1X of the appropriate buffer and 0.1 mg/mL of acetylated BSA. Digests were then analyzed on agarose gels to screen for samples that generated the appropriate fragments.

Mutant DNA samples were re-transformed into XL1-Blue *E. coli* competent cells, and 100-200 mL cultures are grown for 16 hrs in LB+Amp. This is followed by large-scale plasmid preparation, and the purified DNA was sent for DNA sequencing at Bio S&T Inc. (Lachine, Que.). Results of the variant sequences were aligned with parental DNA (Accession number: J01322) using protein-protein Blast tool in NCBI (http://www.ncbi.nlm.nih.gov/) to ensure the desired product was obtained.

II.13 Glycerol Stocks

Wild-type and mutant DNAs were transformed into XL1-Blue. 100-fold dilution of overnight 10 mL cultures were inoculated into fresh 10 mL LB+Amp and grown for 2-3 hrs, until it reached an OD_{600} of approximately 0.5. Cultures were then prepared by mixing with sterile glycerol (A.C.S. certified, purchased from Fisher Scientific) to give a final glycerol concentration of 15% in sterile cryogenic vials, and stored at -86°C.

II.14 Dialysis

The dialysis tubing was purchased from BioDesign, with a molecular weight cut off of 30 kD. The tubing was treated two times in boiling water for 30 min and then stored in 10 mM EDTA at 4°C. Before using, the tubing is washed thoroughly with dH_2O and soaked in the dialysis buffer. Samples containing salt are then placed into the dialysis tubing

Reproduced with permission of the copyright owner. Further reproduction prohibited without permission.

and stirred in 100-fold volume of buffer. After 2 hrs, dialysis continued overnight in another 100-fold volume of fresh buffer.

II.15 Recombinant Protein Expression

Wild-type and variant proteins were over-expressed as the method described in Poyner et al. (1996). DNA was transformed into BL21(DE3) *E. coli* competent cells, and plated onto LB+Amp plates. Overnight colonies were suspended with 5 mL of LB and diluted 200-fold into 50 mL of media containing 1% tryptone and 0.5% yeast extract supplemented with 1X M9 salt and ampicillin. Cells were grown for 2-3 hrs at 37°C, 225 rpm, until they reached an OD_{600} of approximately 0.5. Induction was carried out by diluting the cells 100-fold into fresh 4 L of expression medium with 1X M9 medium and ampicillin and grown for 14 hrs under the same conditions. The cells were then harvested by centrifugation for 10 min at 5 krpm, JA-10 rotor, at 4°C in a Beckman J2-HS centrifuge. The wet cell paste was weighed and used for protein isolation, or alternatively, stored at -20°C.

II.16 Recombinant Protein Purification

Recombinant protein purification was performed on ice or at 4°C. The cell pastes were resuspended in Tris buffer (50 mM Tris, 1 mM $Mg(OAc)_2$, and 1 mM EDTA, pH 7.4) at 2 mL/g of cell paste. The suspensions were treated with a bit of both DNAse I (Roche) and RNAse (Boehringer Mannheim), both from bovine pancreas. The substrate analogue, phosphonoacetic acid (Aldrich Chem. Co.), was added to obtain a final concentration of approximately 1 mM. Cells were then subjected to sonication to lyse cell walls, using a Branson 250 Sonifier. Six 30 sec bursts with 1 min cooling periods between bursts, were

Reproduced with permission of the copyright owner. Further reproduction prohibited without permission.

used per 10 g of cell paste. The pH of the extracts was adjusted to 7.0-7.5 using 1 M Tris, and tested with pH paper. The extracts were then centrifuged at 4°C for 30 min at 14 krpm, JA-20 rotor. The supernatant was centrifuged a second time under the same conditions. The supernatant was collected and kept on ice while salting out with ammonium sulfate (Anhydrous A.C.S. grade purchased from Fisher Scientific). For the wild-type, G157A, G157N, and G157L variants, the supernatants were brought to 40% $(NH_4)_2SO_4$ saturation, whereas for the G157D, the supernatant was brought to 60% $(NH_4)_2SO_4$ saturation. The $(NH_4)_2SO_4$ was allowed to dissolve and equilibrate in the supernatant by stirring at low speed for 30 min. The supernatant was then centrifuged for 30 min at 4°C, at 14 krpm, JA-20 rotor, and the pellet was discarded. A second $(NH_4)_2SO_4$ fractionation was carried out at 85% $(NH_4)_2SO_4$ saturation for the wild-type, G157A, G157N, and G157L variants, and at 95% $(NH_4)_2SO_4$ saturation for the G157D variant enolase. The $(NH_4)_2SO_4$ was allowed to dissolve and the extract was centrifuged under the same conditions as the first fractionation. The final pellet was resuspended in 6.0 mL of the Tris buffer, and allowed to desalt by dialysis in Tris buffer. The extract was centrifuged at 12 krpm, JA-20 rotor, 4°C for 30 min before loading onto the 200 mL Q-Sepharose Fast Flow resin (purchased from Amersham) anion exchange column that has been washed and equilibrated in the Tris buffer. The extract was loaded and eluted with the same buffer at a flow rate of approximately 0.5 mL/min. Fractions were collected every 10 min and every third fraction was tested for OD_{280} and OD_{260}, and assayed for activity under the standard enolase assay conditions. Fractions with protein $OD_{280/260}$ ratios above 1.7 were separated on SDS-PAGE. Fractions with high content and purity determined by its activity, SDS-PAGE and ratio of $OD_{280/260}$ were pooled together. The enolase pool was precipitated to 85% $(NH_4)_2SO_4$ saturation for

Reproduced with permission of the copyright owner. Further reproduction prohibited without permission.

the wild-type, G157A, G157N, and G157L variants and to 95% $(NH_4)_2SO_4$ saturation for the G157D enolase variant for storage at 4°C.

II.17 Mass Spectrometry

The molecular masses of the wild-type and G157 variant yeast enolases were obtained by using an ESI-Q-ToF 2 mass spectrometer (Micromass). Approximately 0.3 mg/mL samples in Tris buffer were prepared and passed through a C-18 trap before being directly injected into the mass spectrometer. The raw data were deconvoluted using the MassLynx software (V4.0 SP1, Copyright © 2003 Micromass Ltd.) Mass Spectrometry was carried out by Alain Tessier from the Center for Biological Applications of Mass Spectrometry of Concordia University.

II.18 Dissociation of Enolase with Sodium Perchlorate

A stock solution of 4 M $NaClO_4$ (monohydrate, A.C.S. ≥98.0% purchased from Fluka Chemika) was prepared and stored at 4°C. Samples contained 1 mg/mL enolase in Tris buffer and varying concentrations of $NaClO_4$ and NaOAc in a total volume of 2.5 mL. The concentrations of $NaClO_4$ varied from 0-0.3 M, where enolase is completely dissociated (Kornblatt et al., 1998), and the samples were incubated typically for 24 hrs at 15°C before measurements were made. To maintain constant ionic strength of 0.3 M Na^+, the concentration of Na^+ was balanced by addition of NaOAc. The dissociation of enolase was monitored by aromatic UV CD (Jasco 710 spectropolarimeter), under a continuous N_2 gas flow of 3 L/hr. All aromatic UV CD scans were recorded between 250-340 nm, with a scan speed of 20 nm/min at 0.2 nm step resolution, and 1 nm bandwidths, and 5 accumulations of each sample were taken. Appropriate blanks were subtracted from the spectra of the

Reproduced with permission of the copyright owner. Further reproduction prohibited without permission.

protein. The dissociation constant, K_d, was calculated using equation 2 (Kornblatt et al., 1996; Kornblatt et al., 1998):

$$K_d = 4(f_M)^2[\text{enolase}]/(f_D) \qquad (2)$$

where f_M stands for the fraction of monomeric enolase and f_D stands for the fraction of dimeric enolase. The fractions of monomeric and dimeric enolase were monitored by the change in signal intensity at 284 nm, taking the spectrum of the enolase at 0.3 M $NaClO_4$ to be that of the completely monomeric enolase. The dissociation constant of the wild-type and G157D variant enolase were calculated by extrapolation of the linear plots of ln K_d vs the concentration of $NaClO_4$ to zero concentration of $NaClO_4$.

II.19 Denaturation of Enolase with Urea

Urea (A.C.S. ≥ 99.5%, Fluka Chemika) was prepared as a 10 M stock solution in Tris buffer, stored at room temperature (expires in 1 month). Samples containing 0.5 mg/mL of the wild-type and G157D variant enolases and 0-8 M of urea were incubated for ≥20 hrs at 15°C. The extent of denaturation was monitored by loss of secondary structure using peptide-bond CD. A 1 mm quartz cuvette was used and the scans were made between 210-260 nm, with a scan speed of 50 nm/min at 0.25 sec response time, and 1 nm bandwidths, and 5 accumulations of each sample were taken (all far-UV CD spectra were taken with the above parameters unless otherwise specified). The loss of signal at 222 nm at increasing concentrations of urea was taken to monitor the denaturation process of enolase with urea.

Reproduced with permission of the copyright owner. Further reproduction prohibited without permission.

II.20 Temperature Denaturation of Enolase

Temperature denaturation of wild-type and G157 variant enolases was monitored by the loss of secondary structure in the far-UV peptide bond CD region. A 1 mm quartz circular jacketed CD cuvette was used. The temperature was raised from 30-80°C at a temperature slope of 15°C/hr with a wait time of 2 min. The scans were made between 210-260 nm with a step resolution of 0.2 nm, response time of 0.25 s, and bandwidth of 1 nm. Protein samples were diluted to 0.5 mg/mL in Tris buffer before reading. The T_m is taken to be the temperature at which the CD signal at 222 nm is at the midpoint of the fully native and denatured.

II.21 Fluorescence Spectroscopy

Enolase at a concentration of 0.1 mg/mL (1.06 μM) in Tris buffer was excited at λ_{ex} = 280 with a 2 nm slit. The fluorescence spectra were monitored from 300-400 nm with a 2nm slit, and a scan rate of 1.0nm/sec. Samples were placed in 1.0 cm quartz cuvettes with a 3.0 mL volume capacity. The spectrum of the buffer was subtracted from all the protein spectra

II.22 Titration of the First Metal Site

The K_d for the first metal binding site in wild-type and G157D enolase was determined by titrating in $Mg(OAc)_2$ in metal free enolase. Apo-enolases were prepared by passing the protein sample twice through a chelex column that has been washed and equilibrated with metal free Mes/Tris (25 mM Mes monohydrate ≥99.0% from Fluka BioChemika, 25 mM Tris A.C.S. grade from Fisher Scientific). The change in fluorescence signal at 335 nm was monitored as subsequent aliquots of $Mg(OAc)_2$ were added to the 1 cm

Reproduced with permission of the copyright owner. Further reproduction prohibited without permission.

fluorescent cuvette containing 0.1 mg/mL of protein sample. The apo-enzyme was stirred in the fluorescent compartment for 15 min to equilibrate the oxygen levels and the sample temperature to 25°C prior to the first reading. The sample was stirred for 15 s after each addition of $Mg(OAc)_2$, and 15 s time traces were taken at 335 nm at λ_{ex} of 280 nm, with a 2 nm slit, for each addition of $Mg(OAc)_2$ and the fluorescent intensity (after 5 point smoothing) at 10 s was recorded. As a control, the same experiment was performed by titrating the enzyme with chelexed dH_2O. The percentage of fluorescence change was corrected for the volume change. The results were fitted to ligand binding – low K_d equation (Clarke, 1996). The equation was inserted into the EnzFitter program, single user version 2.0.18.0 (published and distributed by BioSoft, Copyright © Biosoft, 2004).

II.23 Analytical Ultracentrifugation

Sedimentation velocity experiments were performed using an analytical ultracentrifuge (Beckman Optima XL-I). The sedimentation of wild-type and G157 variant enolases was determined by centrifuging 400 μL samples at 42 krpm in a 60-Ti rotor at 15°C. Sedimentation was scanned at either 230 or 280 nm, depending on the concentration of the sample. The sedimentation coefficients, $S_{20,w}$, were obtained by analyzing the data using the DCDT+ software (version 1.14). Reference samples (samples without protein) were centrifuged side-by-side to the protein samples. Sedimentation coefficients were corrected for buffer density and viscosity at different temperatures, which were calculated using the Sednterp (Sedimentation Interpretation) program version 1.08. Centrifugation was performed by either Dr. P. Ulycznj or Dr. M. J. Kornblatt.

Reproduced with permission of the copyright owner. Further reproduction prohibited without permission.

II.24 Enzyme Kinetic Studies

The enzymatic activities of wild-type and G157 yeast enolase variants were examined by monitoring the production of PEP at OD_{240} upon addition of appropriate metal and/or substrate ligands. All assays were performed in duplicate in 1 cm quartz cuvettes. The change in absorbance was monitored for 1 min after adding enzyme. The ε_{240nm} for PEP in the presence of Mg^{2+} and Mn^{2+} are 1.376 $mM^{-1}cm^{-1}$ and 1.308 $mM^{-1}cm^{-1}$ respectively (Kornblatt, 2005). Kinetic studies that examined the enolase activity at varying concentrations of metal were performed in chelexed Mes/Tris, pH 7.1 buffer with the addition of 1 mM 2-PGA to each assay. Stock solutions of 2 M $Mg(OAc)_2$ and 1 M $MnCl_2$ were prepared, serial diluted to appropriate concentrations and stored at 4°C. Kinetic studies that examined the activity of enolase at varying concentrations of 2-PGA were performed in Mes/Tris, pH 7.1 with addition of concentrations of $Mg(OAc)_2$ or $MnCl_2$ giving maximum activity. Kinetic analyses were performed using the EnzFitter software. The kinetic parameters of V_{max}, K_m, and/or K_i were obtained by fitting the data either to the Michaelis-Menton (equation 3), Modified Substrate Inhibition (equation 4), or Substrate Inhibition equations (equation 5), depending on whether inhibition at high ligand concentrations was observed.

$$V_o = (V_{max}[S])/ K_M + [S] \quad (3)$$

$$V_o = (V_{max} * [S] + V_2 [S]^2/ K_i)/(K_m + [S] + ([S]^2/K_i)) \quad (4)$$

$$V_o = (V_{max} * [S])/(K_m + [S] + ([S]^2/K_i)) \quad (5)$$

Kinetics that followed the substrate saturation model were analyzed using equation 3. If partial enzyme inhibition was observed at high concentrations of ligand, equation 4 was used

Reproduced with permission of the copyright owner. Further reproduction prohibited without permission.

for the analyses. In the case where complete enzyme inactivation was observed at high concentrations of ligand, equation 5 was used.

The turnover rate, k_{cat}, for the enzymes were obtained by equation 6:

$$k_{cat} = V_{max} / ([protein]_{total} * 2) \quad (6)$$

where the protein concentration was multiplied by a factor of 2 to account for the total number of active sites. The catalytic efficiency of the enzymes was determined as the ratio of k_{cat}/K_m.

II.25 Kinetic Isotope Effect

The primary isotope effect was determined for the wild-type and G157D enolases by examining the rate change by substituting the C-2 proton of 2-PGA to a deuteron (refer to D-PGA synthesis). The enzymatic kinetics with D-PGA were performed as the enzyme kinetic studies mentioned above.

II.26 Isothermal Titration Calorimetry

ITC measurements were carried out at 25°C using a VP-ITC microcalorimeter. Samples were prepared in Mes/Tris buffer, pH 7.1. Enzyme samples for measurements testing the binding of metal were chelexed briefly to remove excess metal not bound to the first metal binding site. 100 mM stock $MnCl_2$ solutions were prepared in chelexed Mes/Tris buffer and stored at 4°C. Before loading the sample cell and the injection syringe with the sample solution and titrant respectively, the solutions were degassed. Titrant solutions were added as 1 μL for the first injection and the rest as 4 μL injections delivered over an 8 s

Reproduced with permission of the copyright owner. Further reproduction prohibited without permission.

period with an interval of 240 s between injections to reach equilibrium. A total of 60 injections were made. For metal and PGA/PEP (equilibrium mixture) titrations, 100 μM active site enzyme was titrated with 2.5 mM titrant. For the potent inhibitor substrate analogue, PhAH titration, 10 μM active site enzyme was titrated with 0.2 mM PhAH. The titrations were performed with a reference power of 10 μCal/sec and a 60 s initial delay. The data were analyzed using the ORIGIN software (Microcal Origin, version 5.0).

II.27 Limited Proteolysis

Wild-type and G157D enolase were subjected to TPCK treated trypsin (bovine pancreas, purchased from Sigma) treatment to test their relative susceptibility to proteolytic cleavage. The 1 mg/mL enolase proteins in Tris buffer were subjected to trypsin digestion using 1:100 and 1:1000 (w/w) trypsin:enolase. As a control, monomeric wild-type enolase was subjected to the same treatment. Monomeric enolase was prepared by incubating the wild-type enolase in 0.3 M $NaClO_4$ for ≥2 hrs prior to experimenting with protease. Once the trypsin was added to the protein samples, the samples were incubated in a 15°C water bath, and 10 μL aliquots were removed at 15, 30, 45, 60, and 120 min. To each aliquot, 2 μL of 10 mM TPCK trypsin inhibitor (Fluka) was immediately added, followed by addition of 10 μL of 2X loading buffer. Samples were quickly boiled for 2 min to denature the protein and protease before loading onto SDS-PAGE.

Reproduced with permission of the copyright owner. Further reproduction prohibited without permission.

Chapter III: Results

III.1 Site-directed Mutagenesis and Screening of Variants

The yeast enolase gene had previously been ligated to the cloning/expression region, between the *Bam*HI and *Nde*I restriction site, of the pET-3a vector by Isabelle Rajotte. Site-directed mutagenesis to generate the G157D, G157A, G157N, and G157L variant enolases was achieved by subjecting the wild-type recombinant yeast enolase to QuikChange Mutagenesis. Individual oligonucleotides were designed to insert the desired mutation at G157 and to create a new restriction site, *Dra*I, by introducing a silent mutation in close proximity. The starting material composed of the 1316 bp yeast enolase insert and the 4602 bp pET-3a vector, is 5918 bp in total. The pET-3a vector with the wild-type enolase itself contains three *Dra*I restriction sites, generating fragments of 19 bp, 692 bp and 5207 bp, but only the fragments of **692 bp** and **5207 bp** are visible on a 1% agarose gel upon digestion with *Dra*I restriction enzyme. With the introduction of an extra *Dra*I restriction site during mutagenesis, four fragments of 19 bp, **692 bp**, **3424 bp**, and **1783 bp** are generated upon *Dra*I restriction enzyme digest, with the latter three being visible on an agarose gel. Figure 12 exhibits the agarose gels used to confirm achievement of G157L and G157D products. Similar results were obtained for the production of the G157 variant enolases (results not shown). DNA sequencing by Bio S&T (Montreal, Que.) confirms the introduction of G157D, G157A, G157N, and G157L mutations into yeast enolase.

Reproduced with permission of the copyright owner. Further reproduction prohibited without permission.

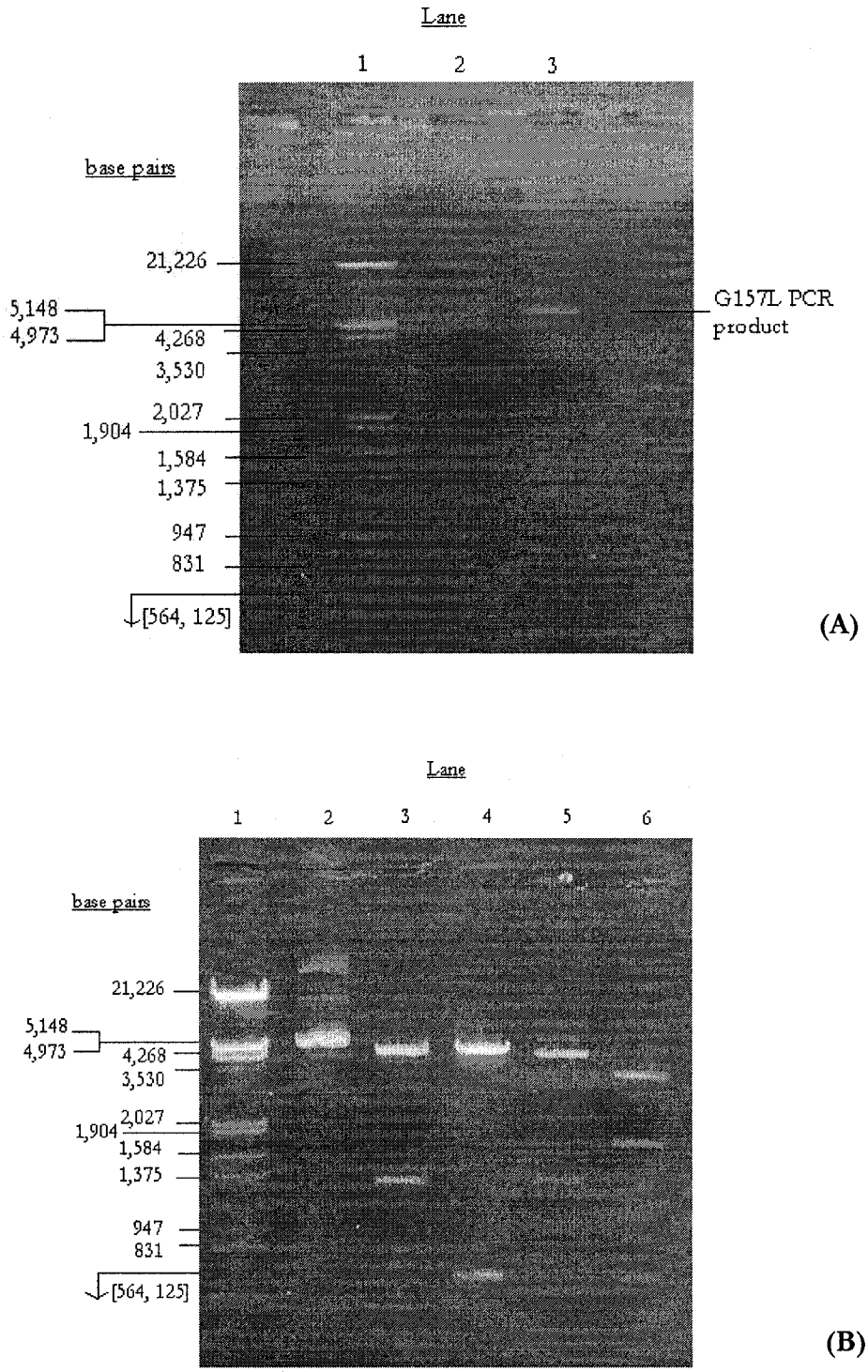

Figure 12. 1% agarose gel of **(A)** G157L QuikChange product upon digestion with *Dpn*I. Lane 1: λ DNA marker; Lane 2: Control (wt DNA without primers); Lane 3: G157L product. **(B)** Wild-type and G157D DNA digested with restriction enzymes to screen for insertion of mutation. Lane 1: λ DNA marker; Lane 2: undigested wt; Lane 3: wt digested with *Bam*HI and *Nde*I; Lane 4: WT digested with *Dra*I; Lane 5: G157D digested with *Bam*HI and *Nde*I; Lane 6: G157D digested with *Dra*I.

Reproduced with permission of the copyright owner. Further reproduction prohibited without permission.

III.2 Purification of Yeast Enolase

III.2.1 Purification of Recombinant Wild-type Yeast Enolase

A plasmid expressing wild-type yeast enolase plasmid was transformed into BL21(DE3) competent cells. Figure 13 illustrates that the increase in activity coincides with the increase of protein concentration. Protein content and purity at each stage of the purification process and Q-Sepharose fractions were monitored via SDS-PAGE. Under SDS and heat denaturating conditions, the wild-type enolase is expected to appear at approximately 46 kD on the SDS-PAGE. Figure 14 shows representative gels of a wild-type enolase purification. Fractions with high activity, an A_{280}/A_{260} ratio ≥ 1.7, and high purity based on SDS-PAGE were pooled together. The final pure wild-type protein showed a single highly pure protein around 46 kD on the SDS-PAGE. Table 7 summarizes the purification of the wild-type enolase. Typically, 250-300 mg of wild-type protein is obtained per 4 L cell culture.

Reproduced with permission of the copyright owner. Further reproduction prohibited without permission.

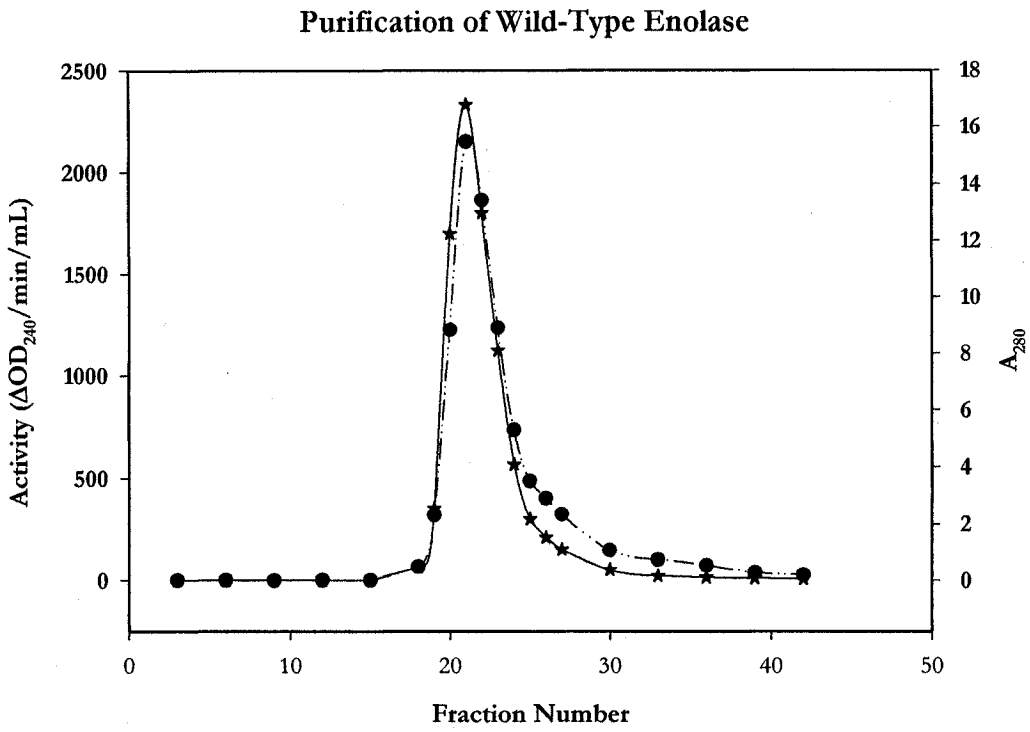

Figure 13. Elution profile of wild-type yeast enolase using Q-Sepharose anion exchange column. Stars with solid line: Activity of fractions (ΔOD_{240}/min/mL); Circles with dot-dashed line: A_{280} of fractions. Fractions 18-23 were pooled.

Purification Step	Volume (mL)	Total Protein (mg)	Total Activity (ΔOD_{240}/min)	Specific Activity (ΔOD_{240}/min/mg)	Purification Fold
Crude extract	51	1530	70380	46	------
0-40% $NH_4(SO_4)_2$	10	260	4410	17	0.37
40-85% $NH_4(SO_4)_2$	21	1260	55493	44	0.95
Q-Sepharose pool	35	278	31500	113	2.47

Table 7. Purification summary of wild-type yeast enolase. Activity assays were conducted in enolase assay buffer plus 1 mM of 2-PGA by monitoring the formation of PEP at 240 nm. Specific activity is the total activity per mg of protein, and was calculated by dividing the total activity by the total protein. Purification fold is obtained by dividing the specific activity of a given sample by that of the crude extract.

Reproduced with permission of the copyright owner. Further reproduction prohibited without permission.

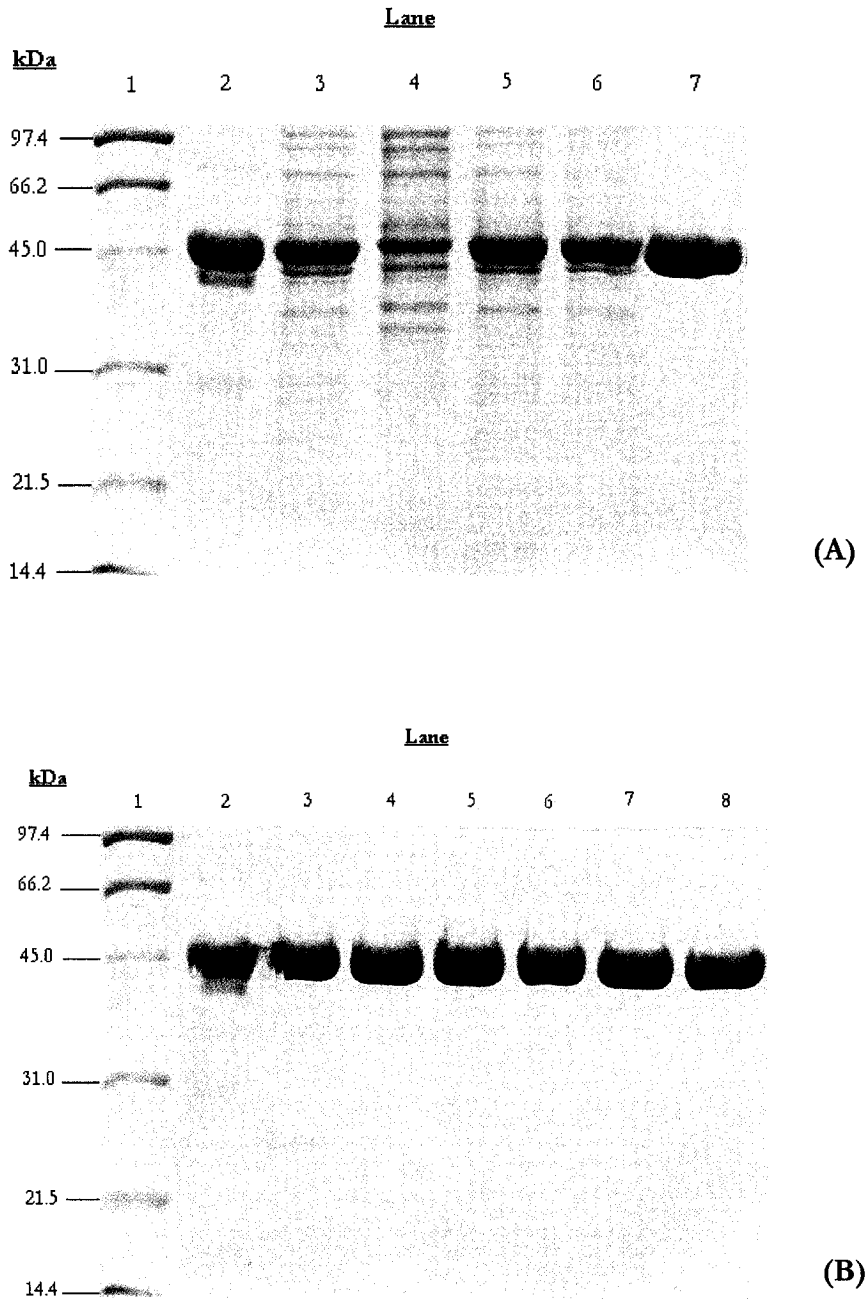

Figure 14. SDS-PAGE of wild-type purification process **(A)** protein from different purification steps, Lane 1: Low molecular weight ladder; Lane 2: Yeast enolase standard (Sigma); Lane 3: Crude extract; Lane 4: 0-40% $NH_4(SO_4)_2$ cut; Lane 5: 0-40% $NH_4(SO_4)_2$ supernatant; Lane 6: 40-85% $NH_4(SO_4)_2$ cut; Lane 7: wild-type Q-Sepharose pool. **(B)** protein from Q-Sepharose purified fractions that were pooled together, Lane 1: Low molecular weight ladder; Lane 2: Yeast enolase standard (Sigma); Lane 3-8: fractions 18-23 respectively.

Reproduced with permission of the copyright owner. Further reproduction prohibited without permission.

III.2.2 Purification of G157D Variant Yeast Enolase

Plasmid expressing G157D variant yeast enolase was transformed into competent BL21(DE3) expression cells. The elution profile of the 60-95% $NH_4(SO_4)_2$ G157D is shown on Figure 15. A clear peak demonstrating the elution of protein is apparent around fractions 20-30. The purity of the protein was monitored by the relative ratio of $A_{280/260}$. The protein content and purity at each stage of the purification process were monitored via SDS-PAGE, with the expected mass of 46 kD (as the wild-type). Fractions with high $A_{280/260}$ ratio and high protein content were also electrophoresed on SDS-PAGE. Activity assays were also performed at each stage of the purification. Since the variant was relatively inactive, the G157D variant was collected according to the purity of the fractions based on SDS-PAGE and $A_{280/260}$ (Figure 16). The final pure G157D pool demonstrates a single highly pure band on SDS-PAGE. Typically, approximately 80-100 mg of protein is obtained per 4 L culture.

Reproduced with permission of the copyright owner. Further reproduction prohibited without permission.

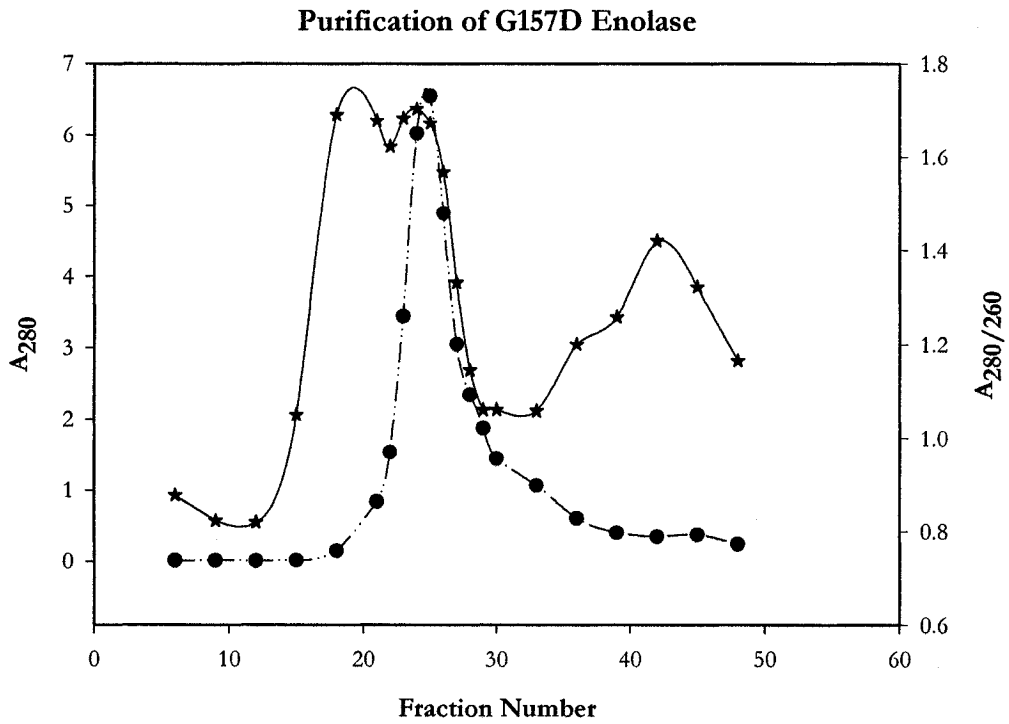

Figure 15. Elution profile of G157D enolase upon anion-exchange in Q-Sepharose resin. Circle dot-dashed line: A_{280}; Star solid line: ratio of $A_{280/260}$. Fractions 22-28 were pooled.

Reproduced with permission of the copyright owner. Further reproduction prohibited without permission.

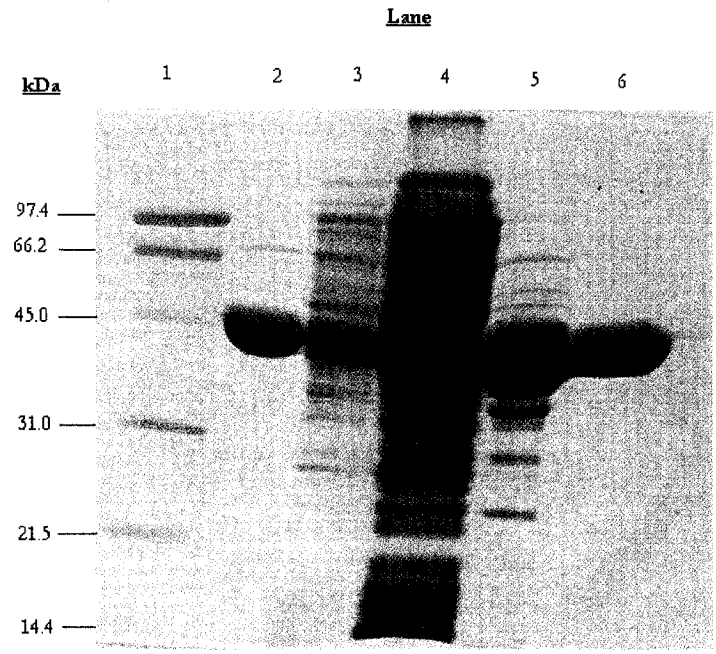

(A)

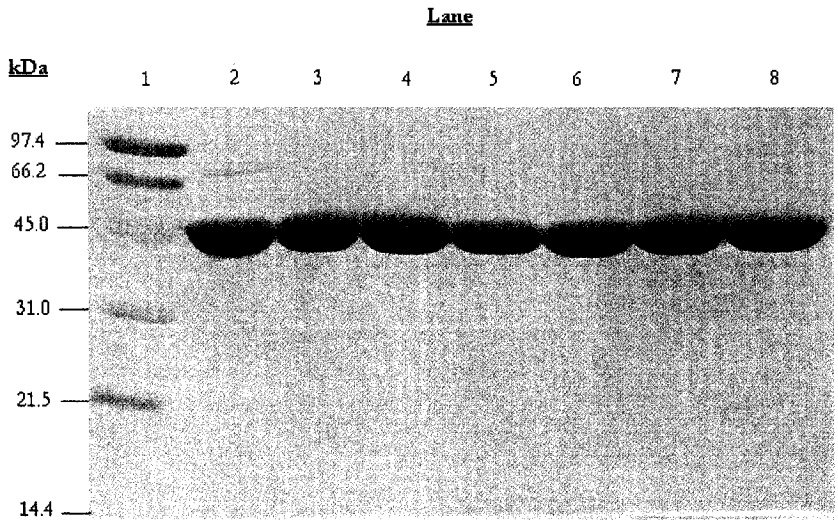

(B)

Figure 16. SDS-PAGE of G157D purification process **(A)** protein from different purification steps, Lane 1: Low molecular weight ladder; Lane 2: Yeast enolase standard (Sigma); Lane 3: Crude extract; Lane 4: 0-60% $NH_4(SO_4)_2$ cut; Lane 5: 60-95% $NH_4(SO_4)_2$ cut; Lane 6: G157D Q-Sepharose pool. **(B)** protein from Q-sepharose purified fractions that were pooled together, Lane 1: Low molecular weight ladder; Lane 2: Yeast enolase standard (Sigma); Lane 3-8: fractions 22-26 respectively.

Reproduced with permission of the copyright owner. Further reproduction prohibited without permission.

III.2.3 Purification of the G157A, G157N, and G157L Variant Enolases

The G157A, G157N, and G157L proteins were obtained using the wild-type procedure for growth and purification of the wild-type protein. The purification processes were monitored by activity, $A_{280/260}$ ratio, and SDS-PAGE. When assayed for activity, only the G157A variant demonstrated sufficient activity to locate the bulk of the protein. The G157N and G157L variants seemed to possess relatively little or no activity. With the low activity of the G157N and G157L enolases, the purification processes were monitored solely by SDS-PAGE and $OD_{280/260}$ ratio. Figures 17-19 illustrate the elution profiles of the G157A, G157N, and G157L proteins, respectively. The purification summary of the G157A enolase is given in Table 8. In essence, for all three protein purifications, fractions with high activity (if applicable), high $A_{280/260\ ratio}$, and high purity demonstrated on SDS-PAGE were pooled together. The final pure G157A, G157N, and G157L pools demonstrate a single highly pure band on the SDS-PAGE (data not shown, refer to figures 14 and 16 for similar SDS-PAGE results). For the three variant purifications, approximately 250-300 mg of each protein was obtained.

Reproduced with permission of the copyright owner. Further reproduction prohibited without permission.

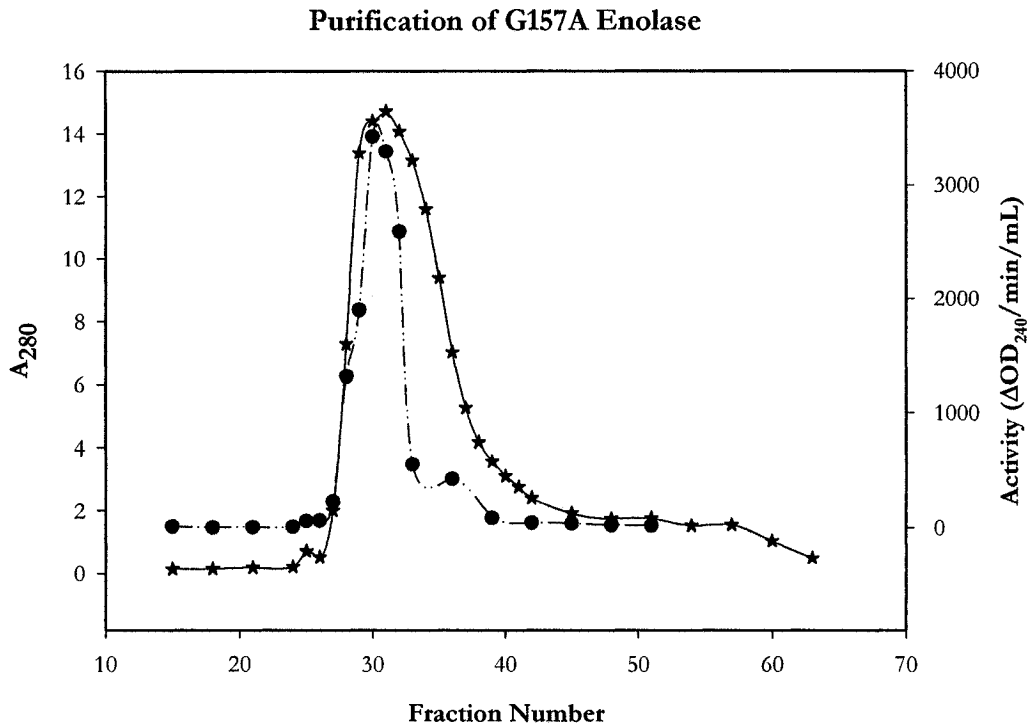

Figure 17. Elution profile of G157A enolase upon anion-exchange in Q-Sepharose resin. Circle dot-dahsed line: A_{280}; Star solid line: Activity of fractions (ΔOD_{240}/min/mL). Fractions 26-33 were pooled.

Purification Step	Volume (mL)	Total Protein (mg)	Total Activity (Units)	Specific Activity (Units/mg)	Purification Fold
Crude extract	50	1275	40650	32	------
0-40% $NH_4(SO_4)_2$	15	190	2721	14	0.45
40-85% $NH_4(SO_4)_2$	17	1224	32509	27	0.83
Q-Sepharose pool	29.5	275	20584	75	2.35

Table 8. Purification summary of G157A yeast enolase. Activity assays were conducted in enolase assay buffer plus 1 mM of 2-PGA by monitoring the formation of PEP at 240 nm. Specific activity is the total activity per mg of protein, and was calculated by dividing the total activity by the total protein. Purification fold is obtained by dividing the specific activity of a given sample by that of the crude extract's.

Reproduced with permission of the copyright owner. Further reproduction prohibited without permission.

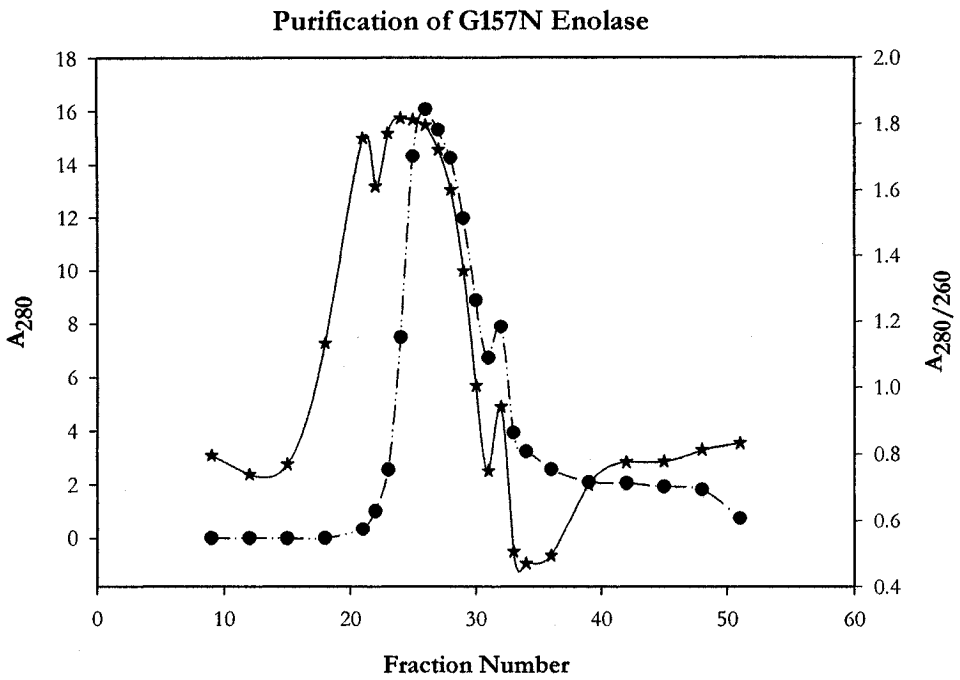

Figure 18. Elution profile of G157N enolase upon anion-exchange in Q-Sepharose resin. Circle dot-dashed line: A_{280}; Star solid line: ratio of $A_{280/260}$. Fractions 22-29 were pooled.

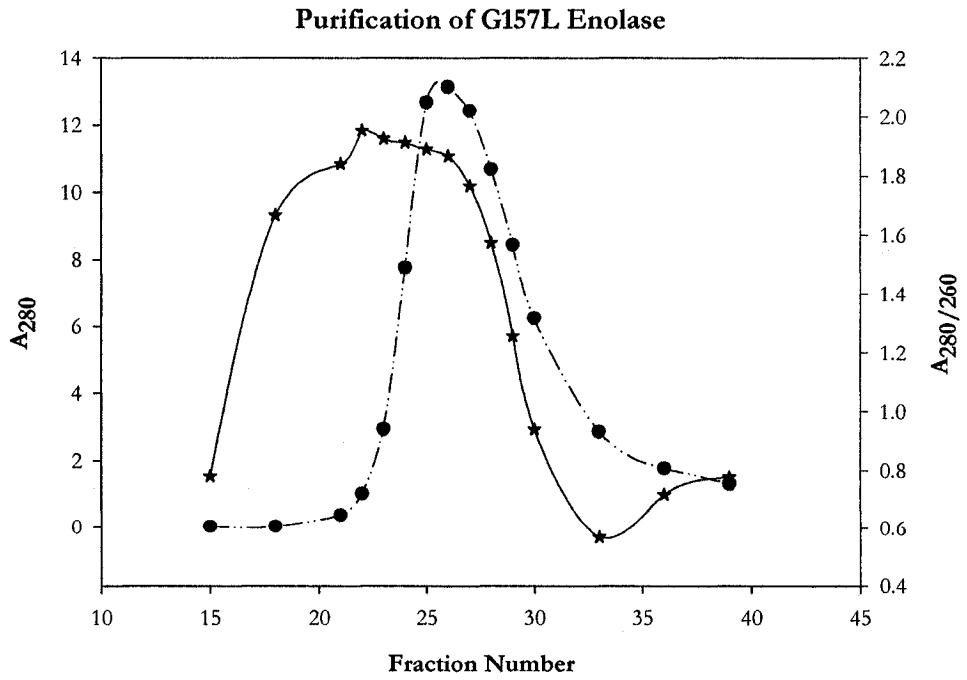

Figure 19. Elution profile of G157L enolase upon anion-exchange in Q-Sepharose resin. Circle dot-dashed line: A_{280}; Star solid line: ratio of $A_{280/260}$. Fractions 22-28 were pooled.

Reproduced with permission of the copyright owner. Further reproduction prohibited without permission.

III.3 Mass Spectrometry

The purified wild-type, G157D, G157A, G157N, and G157L enolases were analyzed by ESI-Q-ToF mass spectrometry. Their molecular masses were obtained and confirmed the identity of the variant enolases. The molecular weights of the wild-type and G157 variant enolases as calculated from the amino acid compositions are listed in Table 9.

Enolase	Theoretical Molecular Mass (Da)	Molecular Mass (Da)
Wild-Type	46670.0	46670.0
G157D	46728.0	46728.0
G157A	46684.0	46684.0
G157N	46727.0	46727.0
G157L	46726.0	46726.0

Table 9. Molecular weights of enolase as calculated from the amino acid contents and confirmed by mass spectrometry.

The mass spectra of wild-type, G157D, G157A, G157N, and G157L enolases are shown in Figure 20 (A-E). The mass spectra were generated using the program MassLynx. The mass of the individual enolase sample corresponds to the respective molecular mass determined from the amino acid composition (Table 9).

Reproduced with permission of the copyright owner. Further reproduction prohibited without permission.

(A)

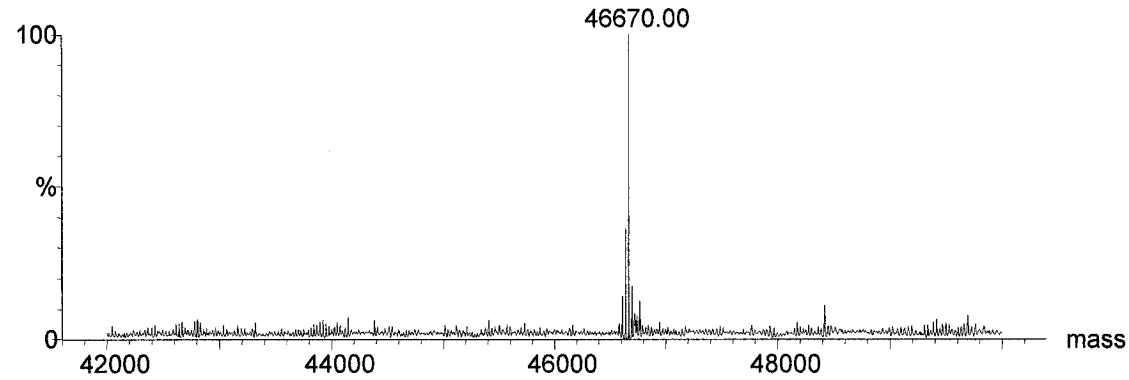

(B)

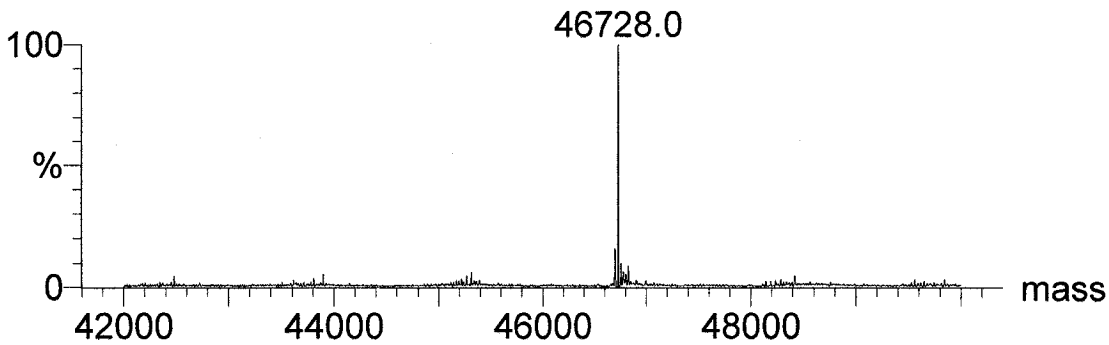

(C)

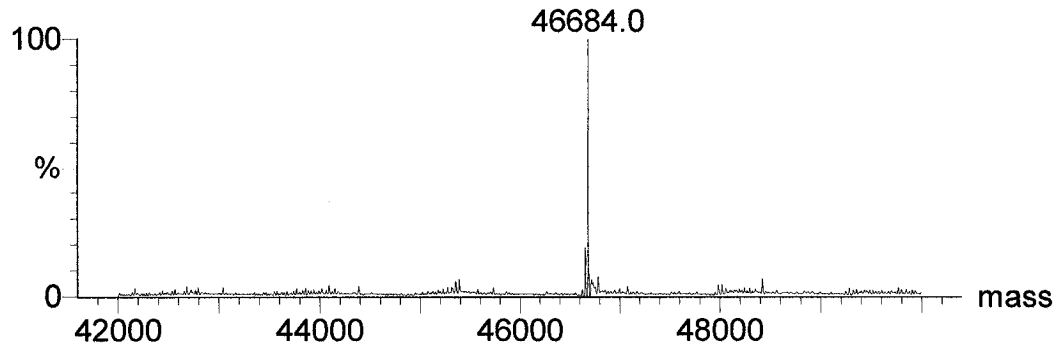

Reproduced with permission of the copyright owner. Further reproduction prohibited without permission.

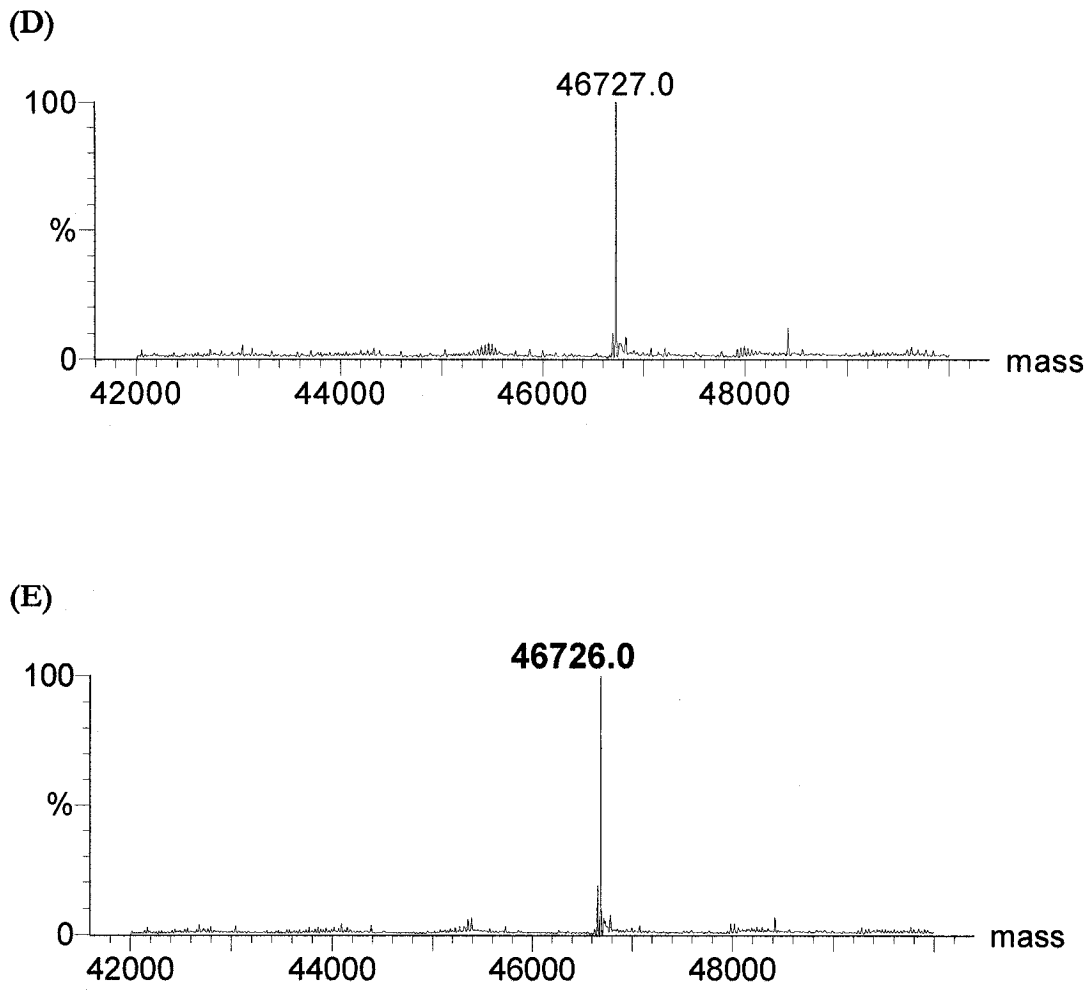

Figure 20. Mass spectrum of **(A)** wild-type, **(B)** G157D, **(C)** G157A, **(D)** G157N, or **(E)** G157L enolase.

Reproduced with permission of the copyright owner. Further reproduction prohibited without permission.

III.4 Optical Spectroscopy

III.4.1 Secondary Structure Examination through Peptide-Bond Circular Dichroism

Wild-type enolase was compared to the G157 variants in order to verify the structural consequences of the mutation at position G157. Far UV (peptide-bond) CD was used to reveal the secondary structural conformations of the enolases. Figure 21 portrays the peptide-bond spectra of the wild-type and G157 variant enolases. Protein, 0.5 mg/mL (5.3 μM), in Tris buffer was used for the scans. The spectra are nearly superimposable, all showing the double minima at 208 and 222 nm, which is characteristic of proteins with high α-helical contents. The main secondary structural elements of enolase are α-helices and β-sheets (Section I.4.1 and I.4.2). This indicates that the G157 variants are properly folded and that the mutations have not disrupted the overall secondary structural folding.

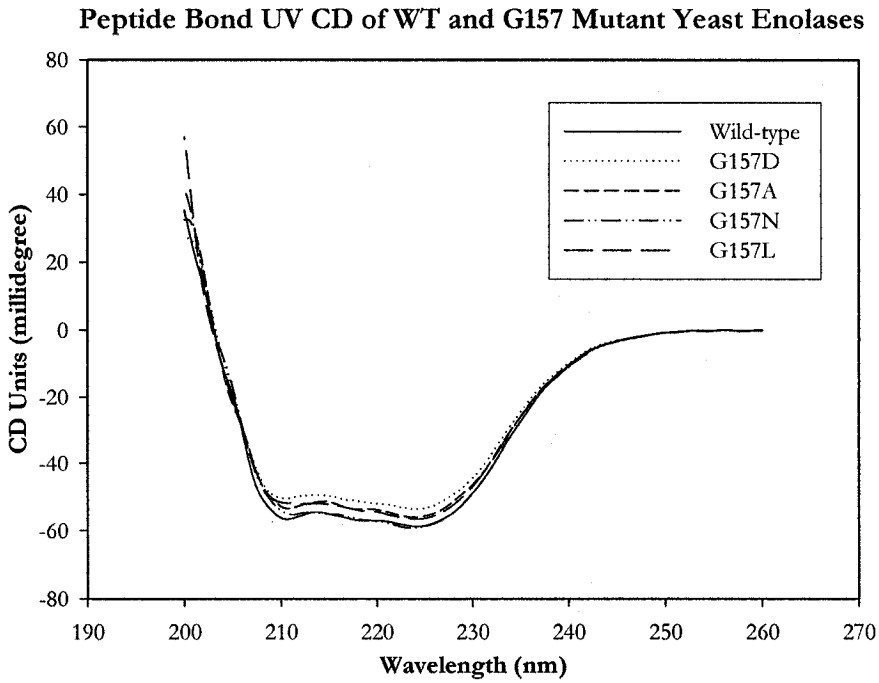

Figure 21. Peptide-bond UV circular dichroic spectra of wild-type, G157D, G157A, G157N, and G157L proteins. A 1 mm quartz cuvette was used and the scans were made between 200-260 nm, with a scan speed of 50 nm/min at 0.25 sec response time, and 1 nm bandwidths, and 5 accumulations of each sample were taken. The spectrum of the buffer was subtracted from all the protein spectra.

Reproduced with permission of the copyright owner. Further reproduction prohibited without permission.

III.4.2 Tertiary Structure Examination through Aromatic UV Circular Dichroism

Upon determining that the G157 variants are properly folded, near UV CD (aromatic UV) was used to compare the tertiary structure of the proteins. The environmental polarity of the immobilized aromatic amino acids of the protein accounts for the spectral features of the protein, in terms of the intensity of the absorption bands and λ_{max}. Yeast enolase contains 5 tryptophan, 9 tyrosine, and 16 phenlyalanines that give rise to characteristic signals. The near-UV CD spectrum is highly indicative of the native state of a protein (Schmid, 1997). The near-UV circular dichroic spectra of the G157 variants are comparable to that of the wild-type (Figure 22). The spectra of the variants show slight intensity differences in the peaks, relating to either concentration differences or slight environmental changes in the chromophoric amino acids.

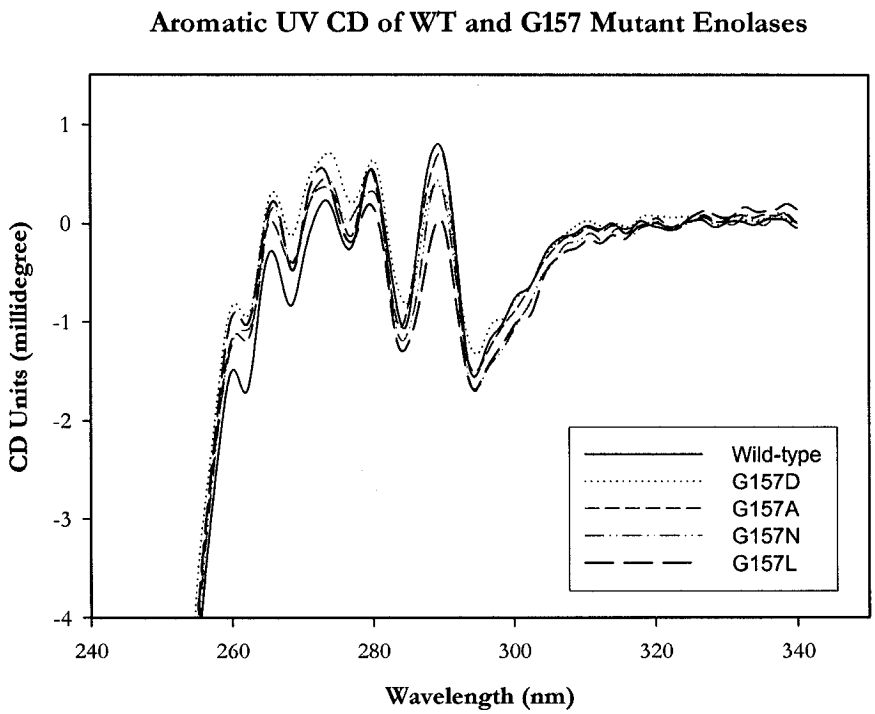

Figure 22. Aromatic UV circular dichroic spectra of wild-type, G157D, G157A, G157N, and G157L protein. Protein, 1 mg/mL (10.6 μM), in Tris buffer was used for the measurements. Scans were made between 250-340 nm, with a scan speed of 20 nm/min at 0.2 nm step resolution, and 1 nm bandwidths, and 5 accumulations of each sample were taken. The spectrum of the buffer was subtracted from all the protein spectra.

Reproduced with permission of the copyright owner. Further reproduction prohibited without permission.

III.4.3 Tertiary Structure Examination through Fluorescence Spectroscopy

The tertiary structure of the proteins was also examined using fluorescence spectroscopy. Fluorescence of proteins is based on the environment of the aromatic amino acids, with the emission usually dominated by the contribution of the tryptophan residue (Schmid, 1997). Shifts in the environment of aromatic amino acid side chains affect the emission spectra due to fluorescence quenching or to their exposure to different solvent polarities. Figure 23 illustrates the fluorescence spectra of the different enolases. They all exhibit a λ_{max} at 335 nm, with differences in the intensity of the peaks. At such low concentrations of protein, the magnitude of error introduced is greater, which may in part explain the difference in fluorescence intensity between the variants and wild-type enolase.

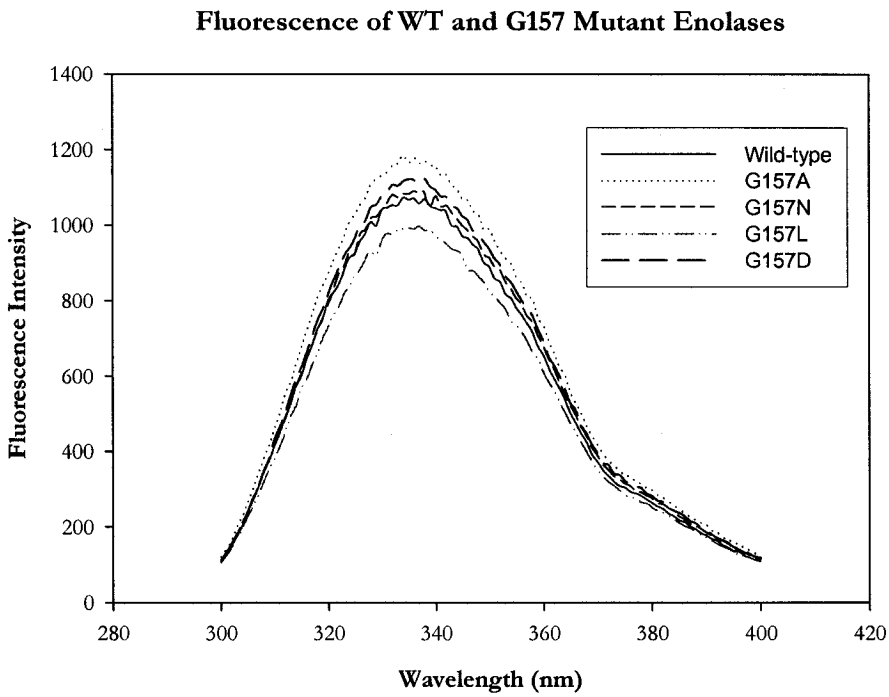

Figure 23. Fluorescence spectra of wild-type, G157D, G157A, G157N, and G157L enolases. Samples were prepared to a concentration of 0.1 mg/mL protein in Tris buffer and equilibrated to 15°C. Fluorescence parameters: 300-400 nm range, λ_{ex} = 280, 2 nm slit, and a scan rate of 1.0 nm/sec.

Reproduced with permission of the copyright owner. Further reproduction prohibited without permission.

III.4.4 Quaternary Structure Examination through Analytical Ultracentrifugation

The quaternary structures of the variants compared to the wild-type were examined via AUC (analytical ultracentrifugation). The sedimentation velocities of the G157 variant enolases were compared to that of the wild-type at two different concentrations, 1 mg/mL (10.6 μM) and 0.1 mg/mL (1.06 μM). The sedimentation coefficient, $S_{20,w}$, is related to the average molecular weight of the species that are present in the sample and thus provides information about the quaternary state of the protein and can help determine whether dissociation or aggregation has occurred. Two different concentrations of protein were examined for the wild-type and variant enolases to determine the extent, if any, of dissociation. The degree of association of the two monomers of enolase increases with increasing concentration (Ralston, 1993). At low concentrations of protein, dissociation is promoted. Significant association or dissociation of enolase would therefore be reflected in the $S_{20,w}$ at different concentrations.

The addition of the salt was necessary to prevent primary charge effects that may impede or reduce the speed of sedimentation of the protein (Ralston, 1993). All samples were centrifuged under the same conditions, described in section II.23.

The sedimentation coefficients of the wild-type and G157 variant enolases are listed in Table 10. The results confirm the retention of the dimeric form of enolase in the G157 variants, with no appreciable dissociation observed as the $S_{20,w}$ values of the variants at both concentrations do not differ significantly from that of the wild-type.

Reproduced with permission of the copyright owner. Further reproduction prohibited without permission.

Enolase	$S_{w,20}$	
	10.6μM	1.06μM
Wild-type	5.599 ± 0.004	5.590 ± 0.002
G157D	5.650 ± 0.002	5.518 ± 0.003
G157A	5.661 ± 0.003	5.573 ± 0.002
G157N	5.622 ± 0.003	5.544 ± 0.002
G157L	5.555 ± 0.003	5.540 ± 0.004

Table 10. Sedimentation coefficients of the wild-type and G157 enolases at 10.6 μM and 1.06 μM concentrations.

III.5 Conformation Stability Examination

III.5.1 Thermal Denaturation of Wild-type and G157 Variant Enolases

The thermal stabilities of the G157 variants compared to the wild-type enolase were examined by measuring the far-UV CD as a function of temperature. As denaturation of protein progresses, there is loss in the secondary structure. This feature was used to assess the melting temperature of the proteins. The loss in the α-helical signal at 222 nm as the protein denatures at increasing temperature was therefore used as to probe the extent of denaturation. Enolase (0.5 mg/mL or 5.3 μM) in Tris buffer was subjected to heat denaturation as described in section II.20. Figure 24 displays the melting curves of the G157 variant and wild-type enolases. The initial CD signal of the protein was taken to be that of the fully native form of the protein, and the final signal upon subjecting the protein to increasing temperatures was taken to be that of the fully denatured protein. The melting temperature, T_m, of the proteins indicates the temperature at which protein is 50% denatured. The T_m of each enolase is listed in Table 11. It is evident that the melting temperatures of the G157 variant proteins are lower than that of the wild-type protein, with

Reproduced with permission of the copyright owner. Further reproduction prohibited without permission.

the G157A more thermally stable as compared to the other three variants (G157D, G157N, and G157L).

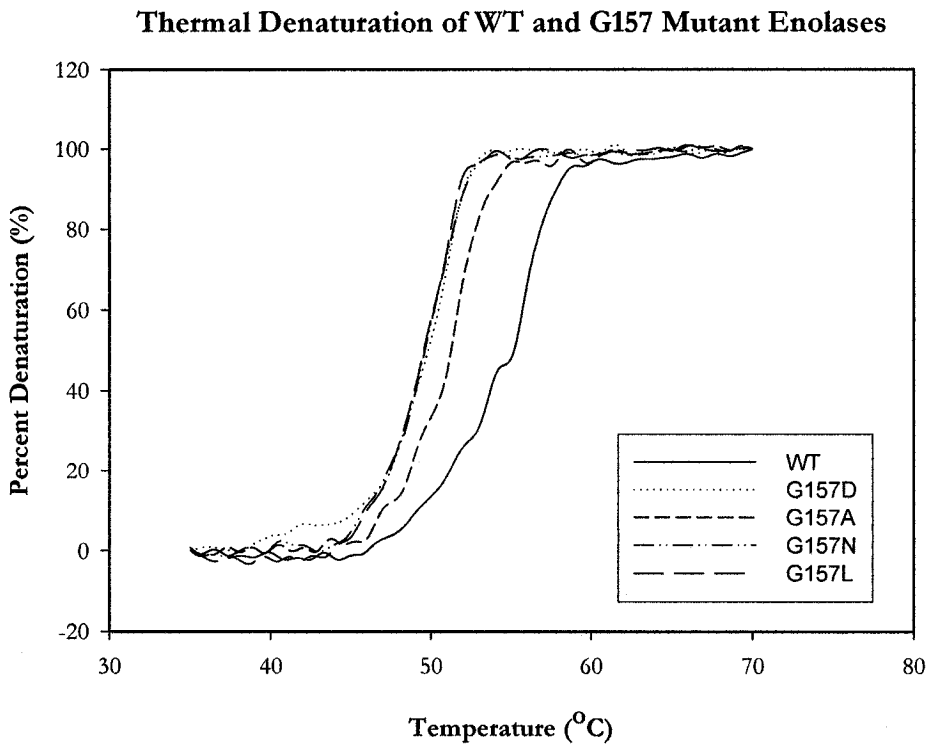

Figure 24. Thermal denaturation of wild-type and G157 variant enolases monitored by the loss in α-helical contents by far-UV CD.

Enolase	T_m (°C)
Wild-type	55.1
G157D	49.9
G157A	51.1
G157N	49.7
G157L	49.5

Table 11. Melting temperatures of wild-type and G157 variant enolases.

Reproduced with permission of the copyright owner. Further reproduction prohibited without permission.

III.5.2 Chemical Denaturation of Wild-type and G157D Variant Enolases

The stability of the G157D variant compared to the wild-type enolase was examined by subjecting the proteins to chemical denaturation using urea. Urea is a mild denaturant which functions by decreasing water-water interactions and H-bond strength, thereby increasing exposure of nonpolar groups to solvent (Bennion & Daggett, 2003). The subsequent loss in CD signal at 222 nm was monitored at increasing concentrations of urea. It was essential that the unfolding reaction has reached equilibrium before making any measurements. The samples were therefore incubated for 24 hrs in different concentrations of the denaturant (Section II.19). The course of denaturation of the wild-type and G157D variant enolase is shown in Figure 25. As the denaturation process does not seem to follow a simple two-state model, the ΔG was not determined. It is apparent however, that the denaturation of G157D occurs more readily than the wild-type as 50% loss in CD signal of the protein is at ~1.3 M urea for G157D enolase compared to ~1.7 M urea for the wild-type enolase.

Reproduced with permission of the copyright owner. Further reproduction prohibited without permission.

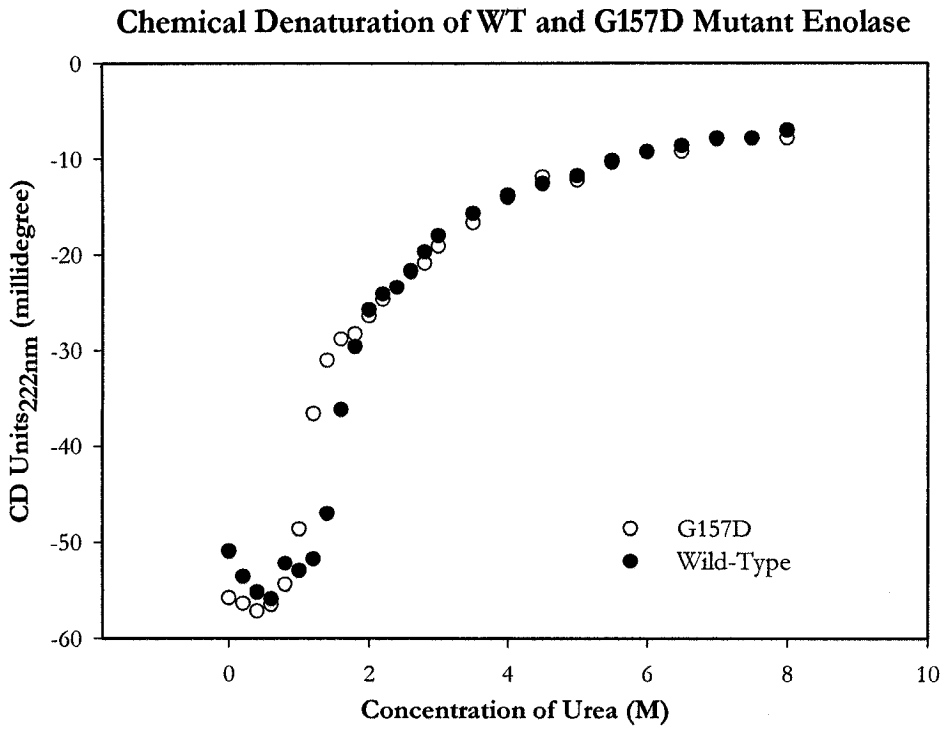

Figure 25. Denaturation of wild-type and G157D variant enolase by urea. Solid circle: wild-type; Open circle: G157D.

III.5.3 Sodium Perchlorate Dissociation of Wild-type and G157D Variant Enolase

The dissociation of wild-type and G157D enolases was examined using $NaClO_4$. $NaClO_4$ is a chaotropic salt that destabilizes protein structures by weakening hydrophobic interactions, leading to exposure of buried protein surfaces (Arakawa & Timasheff, 1982). Protein samples were incubated at varying concentrations of $NaClO_4$, up to 0.3 M where complete dissociation was assumed (Kornblatt et al., 1996). Ionic strength was maintained by balancing the concentration of Na^+ with NaOAc as ionic compositions of the buffer affect dimer association/dissociation (Kühnel & Luisi, 2001). Tyr6, Tyr11, and Try130, and Trp56 are located near the subunit interface and give rise to CD signal differences when the subunits dissociate. The dissociation of wild-type and G157D enolases were monitored by

Reproduced with permission of the copyright owner. Further reproduction prohibited without permission.

changes in spectral characteristics in the aromatic-UV CD. Figure 26 illustrates the change in spectral properties of the enolases at varying concentrations of $NaClO_4$ and is consistent with published results from Kornblatt et al. (1998) in that the dissociation of enolase is accompanied by an increase in signal intensities in the near-UV region. The signal intensities between the dimeric and monomeric enolases differ mainly at 277 nm, 284 nm, and 293 nm, with the change in signal at 284 nm being the most prominent. Hence, the change in signal intensity at 284 nm was used to monitor the dissociation progress, with the signal of the protein in the absence of $NaClO_4$ being that of the fully dimeric protein, and the signal obtained in 0.3 M $NaClO_4$ being that of the fully monomeric protein. The fraction of dimer to monomer was calculated for the proteins at each concentration of $NaClO_4$. The dissociation constant, K_d, was obtained according to the method described in II.18. A linear plot of ln K_d versus [$NaClO_4$] of the wild-type and G157D enolase is shown in Figure 27. Extrapolation to 0 M $NaClO_4$ determines the dissociation constant of the enolases in the absence of $NaClO_4$. G157D variant enolase dissociates more readily than the wild-type enolase as determined from their respective K_d values ($4.65 \times 10^{-8} \pm 6.05 \times 10^{-10}$ M for the wild-type and $1.78 \times 10^{-7} \pm 3.56 \times 10^{-9}$ M for the G157D variant).

Reproduced with permission of the copyright owner. Further reproduction prohibited without permission.

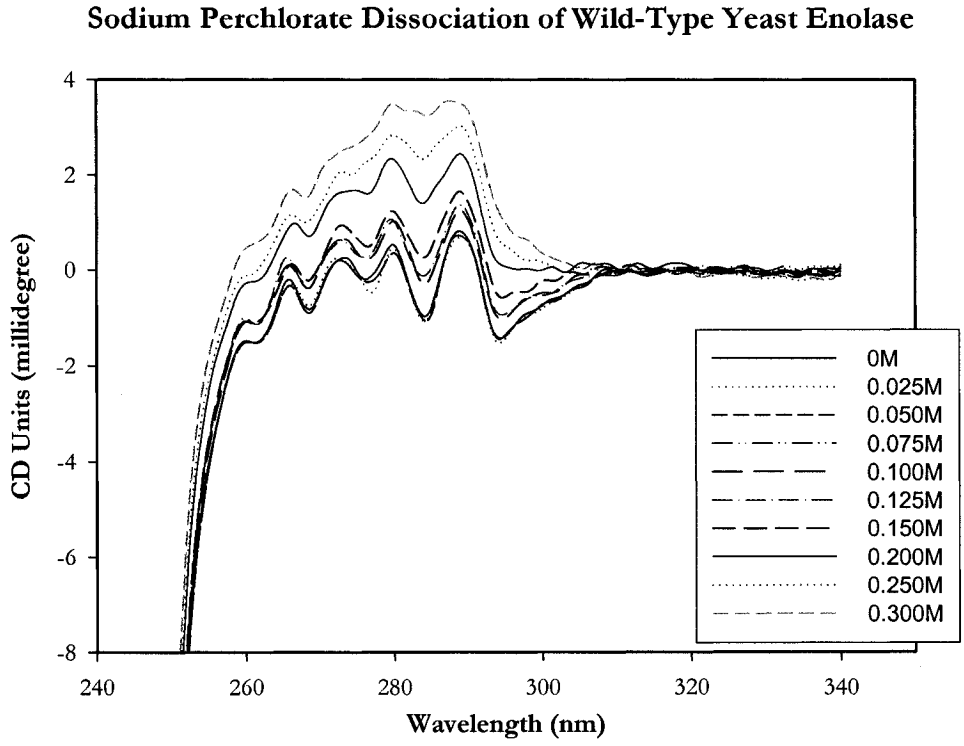

(A)

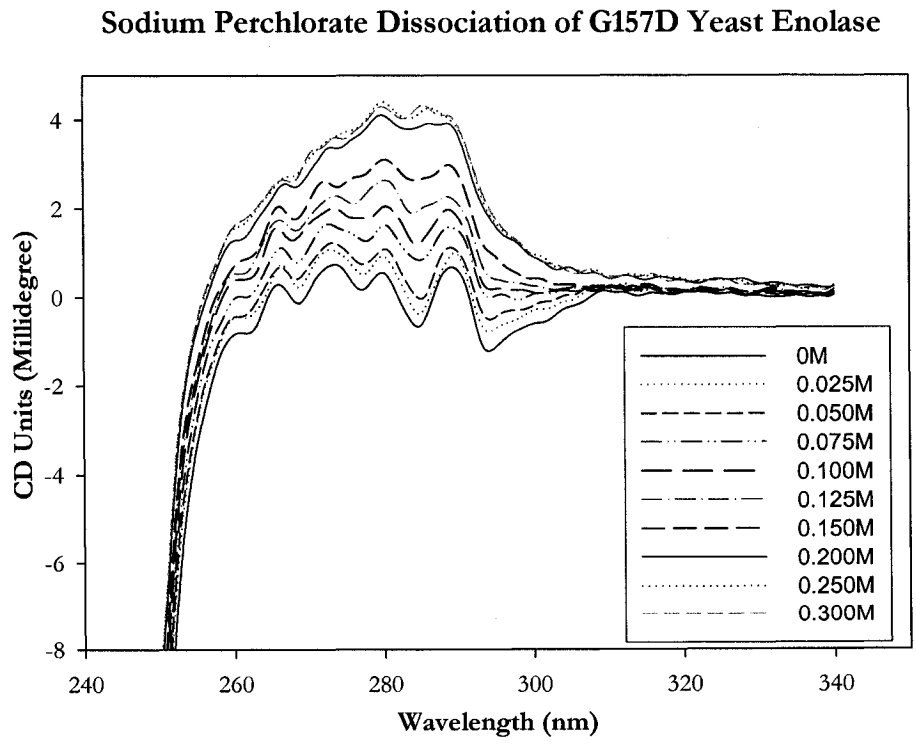

(B)

Figure 26. Dissociation of **(A)** Wild-type enolase and **(B)** G157D enolase monitored by spectral changes in the aromatic-UV region.

Reproduced with permission of the copyright owner. Further reproduction prohibited without permission.

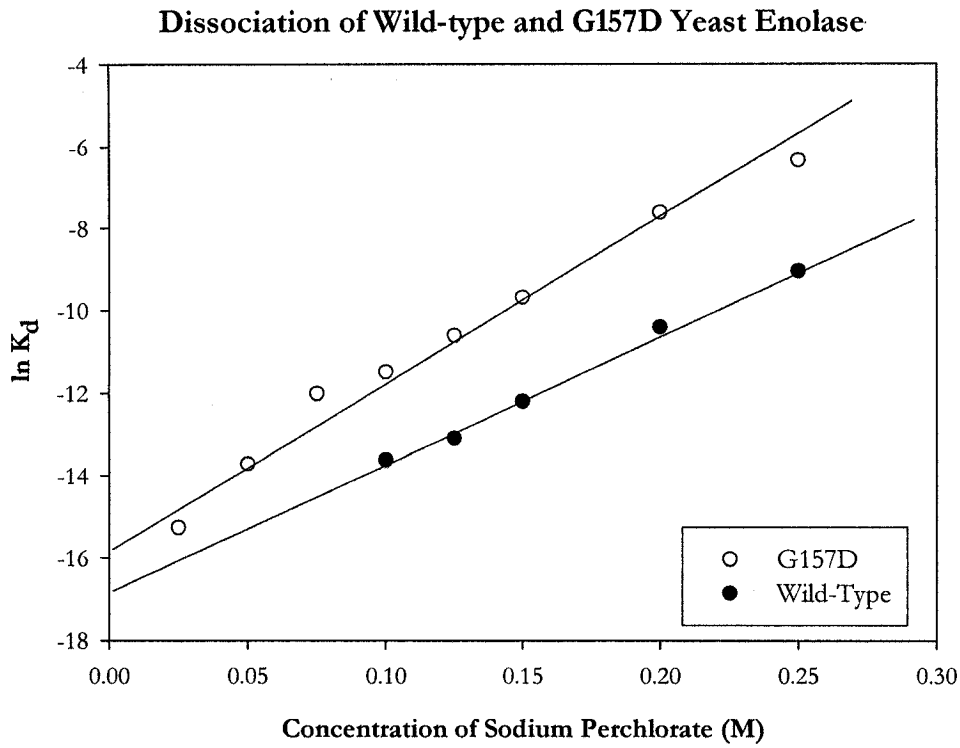

Figure 27. Determination of the dissociation constants, K_d, for the wild-type and G157D enolase. The wild-type K_d is $4.65 \times 10^{-8} \pm 6.05 \times 10^{-10}$ M and the G157D K_d is $1.78 \times 10^{-7} \pm 3.56 \times 10^{-9}$ M.

II.5.4 Limited Proteolysis

The susceptibility to proteolytic cleavage of the G157 variant enolases was examined using trypsin. Trypsin is a protease that degrades enzymes by cleaving proteins at the carboxyl side of the amino acids lysine and arginine. Most native proteins are quite resistant to the action of proteolytic enzymes, and increases in susceptibility to proteolysis are generally results of changes in the protein structure. The wild-type and G157 variant proteins were subjected to trypsin digestion with a weight ratio of trypsin to protein of 1:100. The wild-type enolase was resistant to trypsin digestion whereas the G157 variants showed degradation by 60 min. Figure 28 shows the wild-type and G157 variant enolases before and after 60 min incubation with trypsin.

Reproduced with permission of the copyright owner. Further reproduction prohibited without permission.

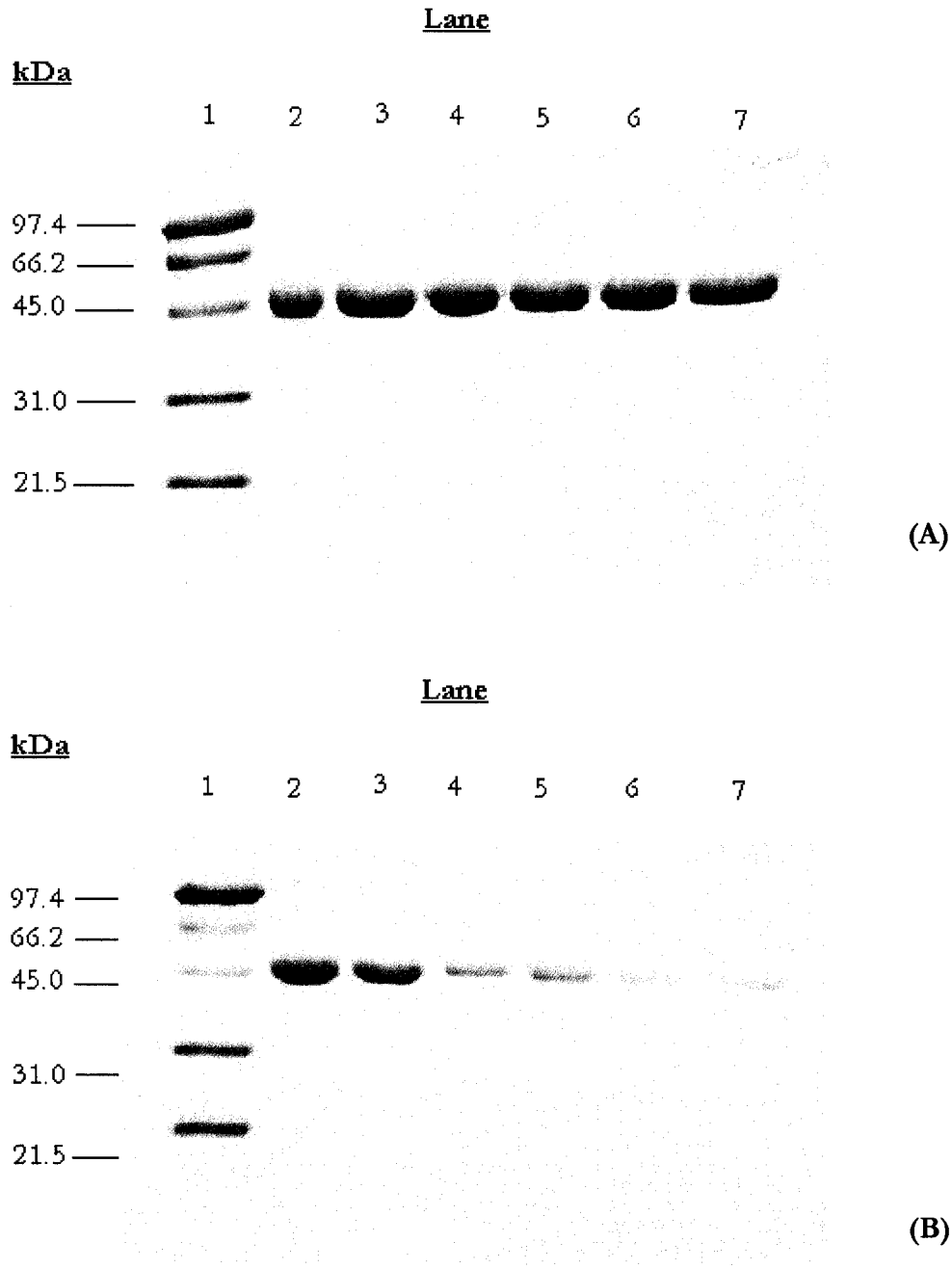

Figure 28. Limited proteolysis with a 1:100 ratio of trypsin to protein. SDS-PAGE of **(A)** wild-type and G157 variant enolases before trypsin digestion, Lane 1: Low molecular weight ladder; Lane 2: Yeast enolase standard; Lane 3: Wild-type; Lane 4: G157D; Lane 5: G157A; Lane 6: G157N; Lane 7: G157L enolase. **(B)** wild-type and G157 variant enolases after incubation with a 1:100 ratio of trypsin to protein for 60 min, Lane 1: Low molecular weight ladder; Lane 2: Yeast enolase standard; Lane 3: Wild-type; Lane 4: G157D; Lane 5: G157A; Lane 6: G157N; Lane 7: G157L enolase.

Reproduced with permission of the copyright owner. Further reproduction prohibited without permission.

At low concentrations of trypsin, 1:1000 ratio of trypsin to protein, there is no cleavage of the wild-type and G157D proteins within 2 hrs of incubation as demonstrated by the SDS-PAGE analysis (Figure 29, A & B). In addition, the wild-type monomeric protein (obtained from dissociation of the dimer with $NaClO_4$) was also subjected to 1:1000 ratio of trypsin to protein. Interestingly, the monomeric protein shows a time dependent digestion pattern (Figure 29, C). As the incubation time increases, the monomeric band of ~46 kD disappears and three bands of ~30 kD-45 kD become more and more apparent. The G157D variant protein does not show appreciable digestion at the 1:1000 ratio of trypsin to protein compared to the monomeric wild-type enolase, consistent with the fully dimeric structure of the G157D variant.

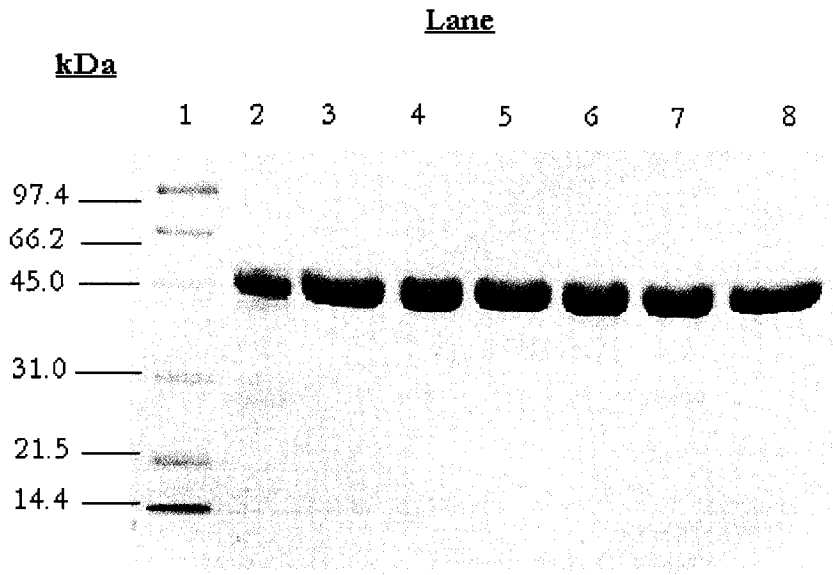

(A)

Reproduced with permission of the copyright owner. Further reproduction prohibited without permission.

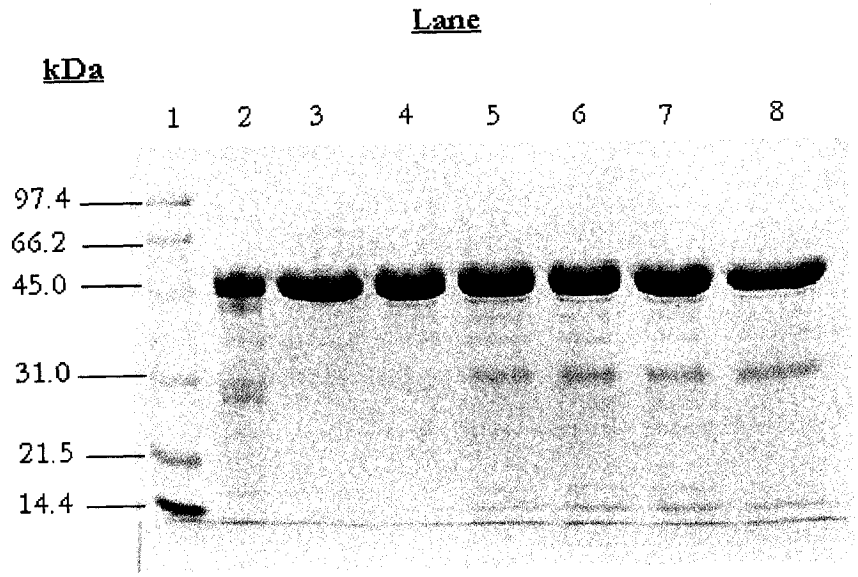

(B)

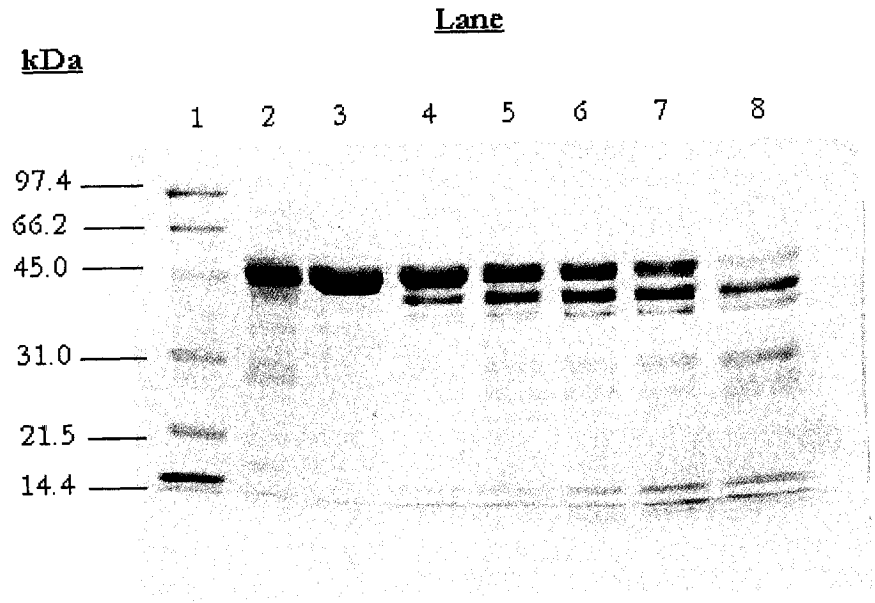

(C)

Figure 29. Limited proteolysis with a 1:1000 ratio of trypsin to protein. SDS-PAGE of **(A)** wild-type enolase incubated with trypsin at, Lane 1: Low molecular weight ladder; Lane 2: Yeast enolase standard; Lane 3: no trypsin; Lane 4: 15 min; Lane 5: 30 min; Lane 6: 45 min; Lane 7: 60 min; Lane 8: 120 min. **(B)** G157D variant enolase incubated with trypsin at, Lane 1: Low molecular weight ladder; Lane 2: Yeast enolase standard; Lane 3: no trypsin; Lane 4: 15 min; Lane 5: 30 min; Lane 6: 45 min; Lane 7: 60 min; Lane 8: 120 min. **(C)** monomeric wild-type enolase incubated with trypsin at, Lane 1: Low molecular weight ladder; Lane 2: Yeast enolase standard; Lane 3: no trypsin; Lane 4: 15 min; Lane 5: 30 min; Lane 6: 45 min; Lane 7: 60 min; Lane 8: 120 min.

Reproduced with permission of the copyright owner. Further reproduction prohibited without permission.

III.6 Steady State Kinetics

III.6.1 Activity of WT and G157 Variant Enolases under Standard Assay Conditions

The activities of the wild-type and G157 variant enolases were examined under standard assay conditions (Section II.5). The reactions were initiated by addition of 1 mM 2-PGA. These conditions provide saturating concentrations of both divalent cation and substrate required for wild-type enolase activity. The activity of the G157 variant enolases is depressed significantly under these standard conditions. Figure 30 demonstrates the percentage of wild-type activity of the variant proteins.

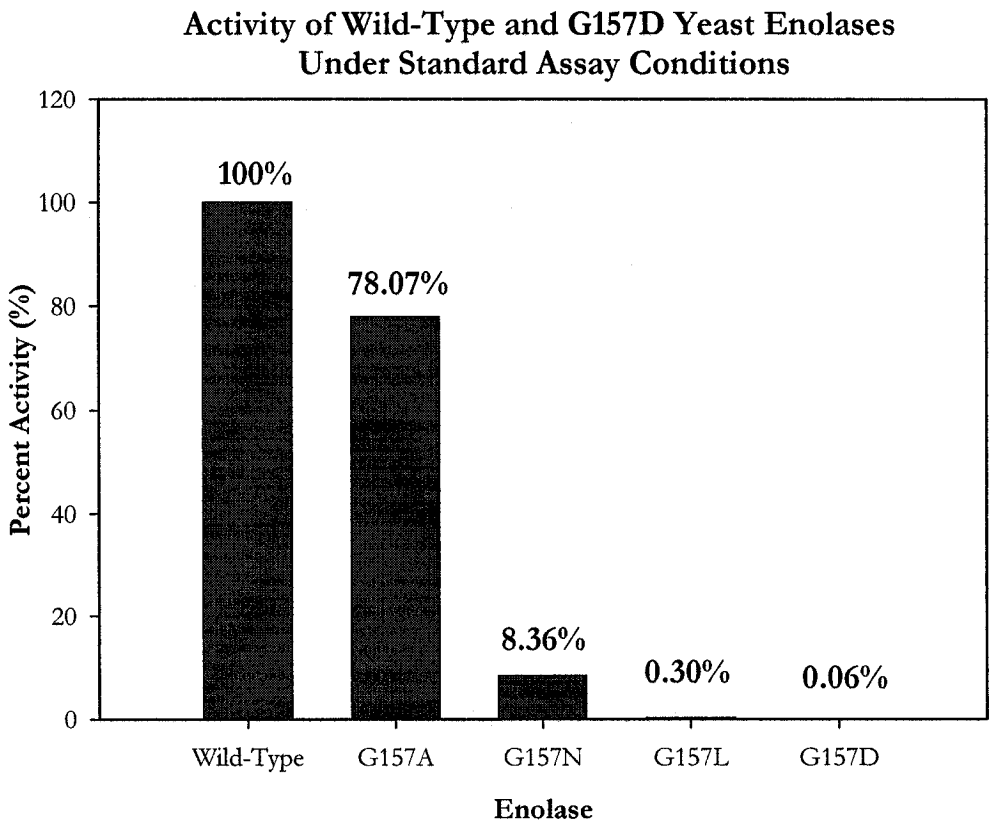

Figure 30. Activity of wild-type and G157 variant enolases under standard enolase assay conditions.

Reproduced with permission of the copyright owner. Further reproduction prohibited without permission.

III.6.2 Determination of Kinetic Constants of Wild-type and G157 Variant Enolases

III.6.2.1 Variation of Activity of Wild-type and G157 Variant Enolases with Mg^{2+}

The effects of magnesium concentration on enzyme activity were investigated for the wild-type and G157 variant enolases. Activity assays at increasing concentrations of Mg^{2+} were performed in metal free Mes/Tris buffer plus 1 mM 2-PGA. The activity was monitored by the rate of appearance of product, PEP, at 240 nm for 1 min. The kinetic parameters were obtained by fitting the data to the equations listed in section II.24 (Table 12). Results indicate a severely depressed k_{cat} and catalytic efficiency for the G157N, G157L or G157D enolase. The K_M for Mg^{2+} has increased significantly for the G157 variants, with the G157L variant having the highest K_M, which may indicate altered affinity for the Mg^{2+} cofactor. Higher concentrations of Mg^{2+} are required for inhibition of enzyme activity with the G157A and inhibition by Mg^{2+} is virtually lost from the G157D, G157N, and G157L enolases. Figure 31 A and B demonstrates the fit of the wild-type and G157D data to the modified substrate inhibition and Michaelis-Menten models respectively. In both cases, the fitted data are in good agreement with the raw data. The extent of depressed k_{cat} in the G157 variants is illustrated more clearly in Figure 32.

Enolase	K_M (Mg^{2+}) (μM)	k_{cat} (s^{-1})	k_{cat}/K_M ($s^{-1}\mu M^{-1}$)	K_i (mM)
Wild-type	35 ± 3	60 ± 1	1.6	8 ± 2
G157D	962 ± 2	0.64 ± 0.01	$6.7x10^{-4}$	No Inhibition
G157A	129 ± 10	41 ± 1	0.3	31 ± 5
G157N	3760 ± 74	15 ± 0.07	$4.0x10^{-3}$	No Inhibition
G157L	23800 ± 450	0.98 ± 0.01	$4.1x10^{-5}$	No Inhibition

Table 12. Kinetic parameters for Mg^{2+} of the wild-type and G157 variant enolases.

Reproduced with permission of the copyright owner. Further reproduction prohibited without permission.

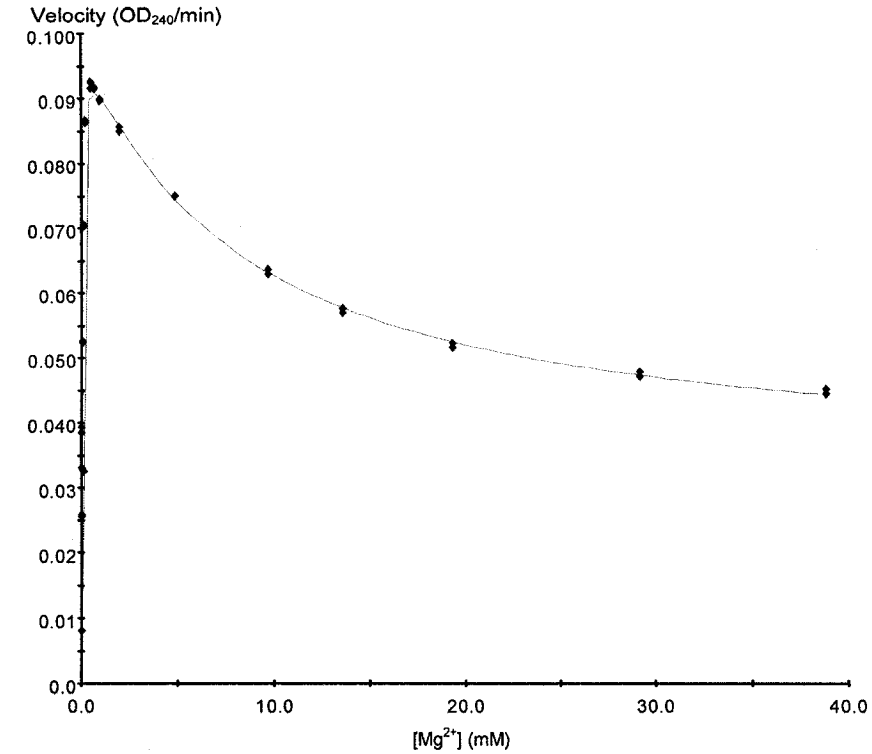

(A)

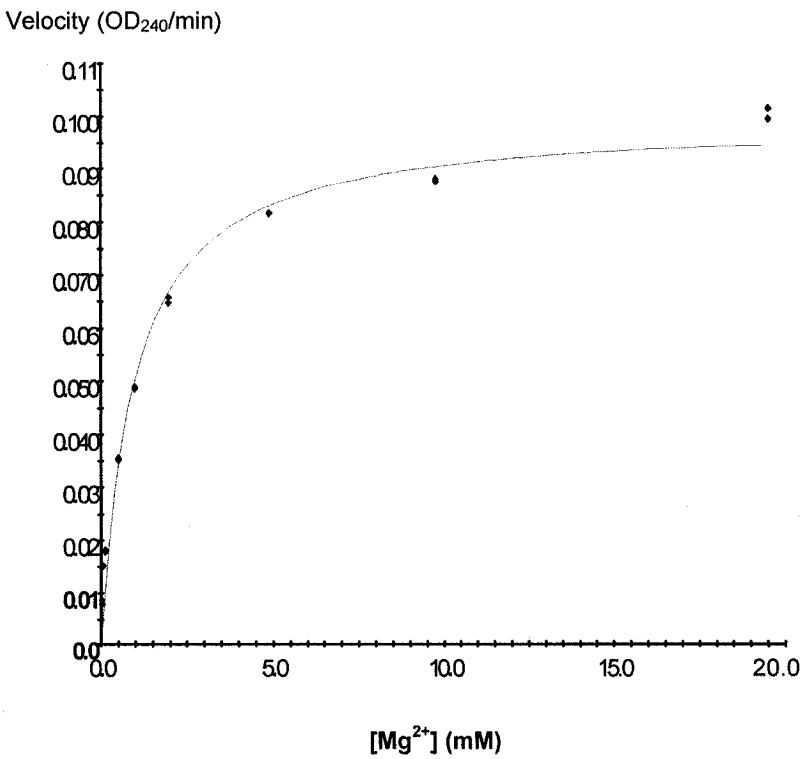

(B)

Figure 31. (A) Wild-type and **(B)** G157D enolase kinetics at increasing [Mg^{2+}] and saturating [2-PGA].

Reproduced with permission of the copyright owner. Further reproduction prohibited without permission.

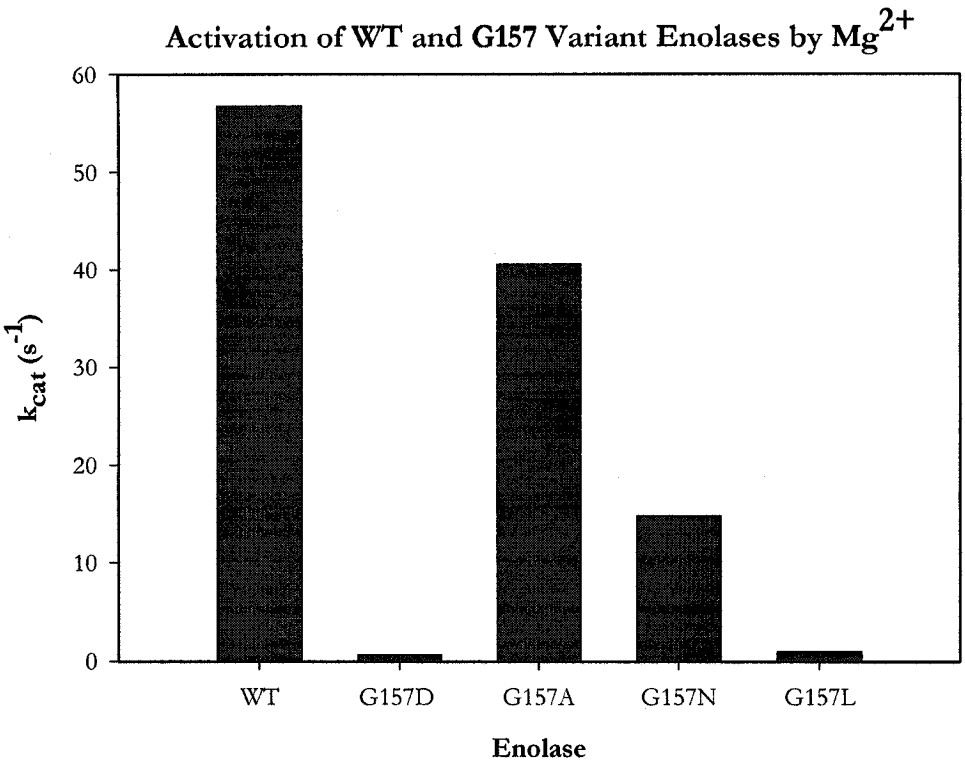

Figure 32. Comparison of k_{cat} of the wild-type and G157 variant enolases at increasing concentrations of Mg^{2+}.

III.6.2.2 Variation of Activity of Wild-type and G157 Variant Enolases with Mn^{2+}

Manganese is the second most active cation for enolase (Poyner et al., 2002). The dependence of enolase activity on Mn^{2+} concentration was therefore also investigated. Kinetic assays in the same buffer and concentration of 2-PGA as in III.6.2.1 were performed by varying the concentrations of Mn^{2+}. Table 13 lists the kinetic parameters obtained by fitting the data to the appropriate models in section II.24. The K_M for Mn^{2+} for the G157 variant enolases do not show such drastic differences from the wild-type as does the K_M for the Mg^{2+}, leading to less severely reduced catalytic efficiencies. Nonetheless, the loss of inhibition by high concentrations of metal is once again observed for the G157D, G157N,

Reproduced with permission of the copyright owner. Further reproduction prohibited without permission.

and G157L enolases. Similar trends in depressed k_{cat} for the G157 variant enolases are observed for the catalytic dependency of Mn^{2+} as for the dependency of Mg^{2+}.

Enolase	K_M (Mn^{2+}) (μM)	k_{cat} (s^{-1})	k_{cat}/K_M ($s^{-1}\mu M^{-1}$)	K_i (μM)
Wild-type	7.7 ± 0.8	29 ± 2	3.7	150 ± 37
G157D	3.4 ± 0.1	0.76 ± 0.01	0.22	No Inhibition
G157A	9.3 ± 0.3	33 ± 1	3.5	132 ± 7
G157N	2.0 ± 0.1	9.3 ± 0.1	4.7	No Inhibition
G157L	6.8 ± 0.1	0.97 ± 0.01	0.14	No Inhibition

Table 13. Kinetic parameters for Mn^{2+} of the wild-type and G157 variant enolases.

Figure 33 A and B demonstrates the fit of the wild-type and G157D data to the modified substrate inhibition and Michaelis-Menten models, respectively. The fitted data is in well agreement with the raw data. The extent of depressed k_{cat} in the G157 variants is illustrated more clearly in Figure 34.

Reproduced with permission of the copyright owner. Further reproduction prohibited without permission.

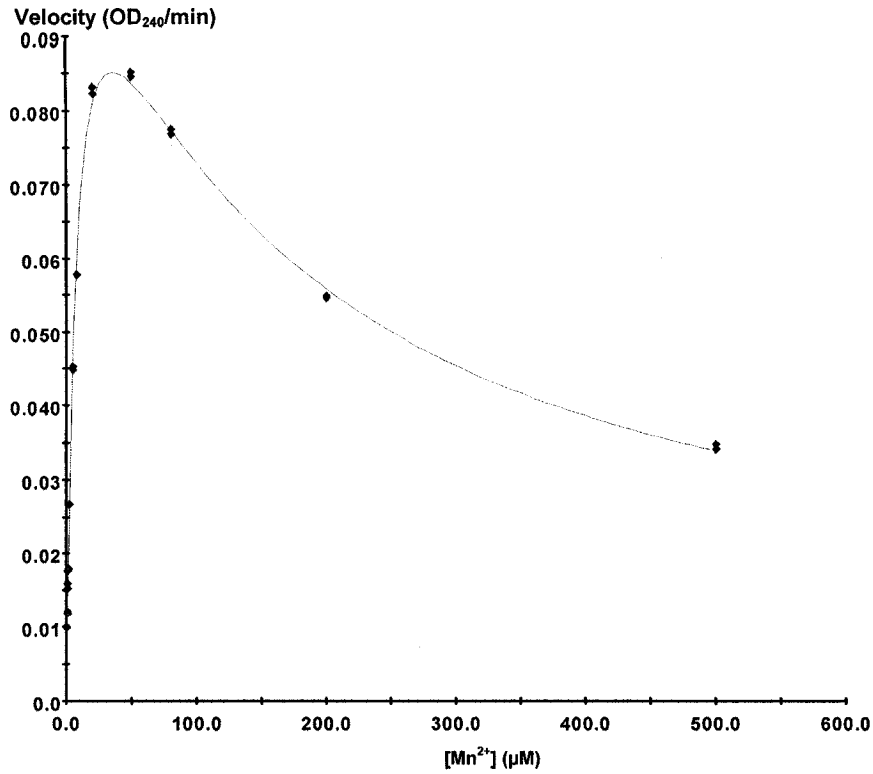

(A)

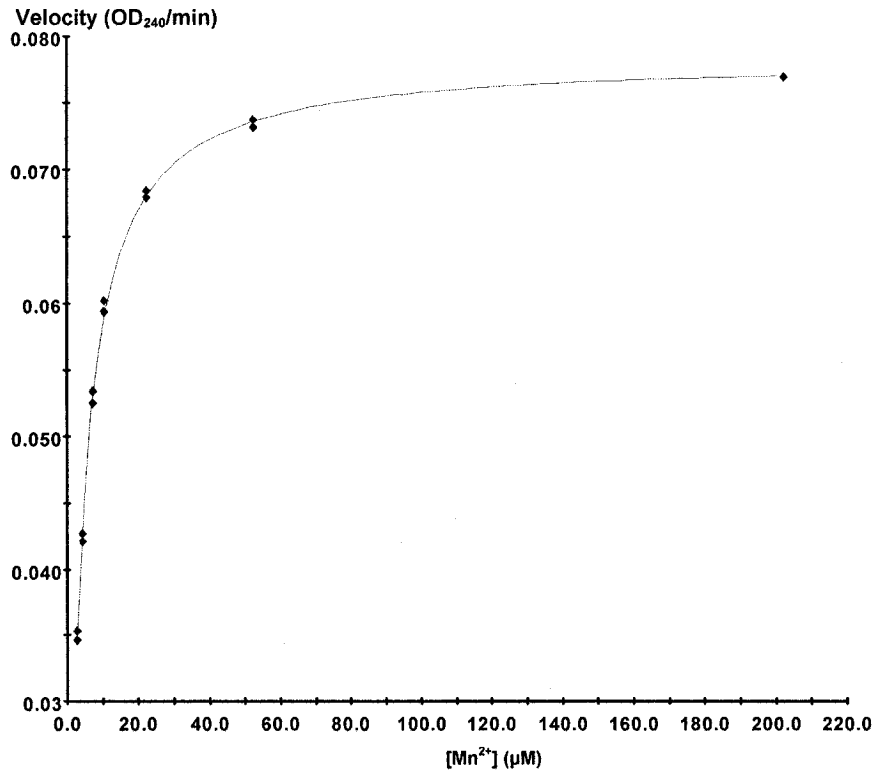

(B)

Figure 33. (A) Wild-type and **(B)** G157D enolase kinetics at increasing [Mn^{2+}] and saturating [2-PGA].

Reproduced with permission of the copyright owner. Further reproduction prohibited without permission.

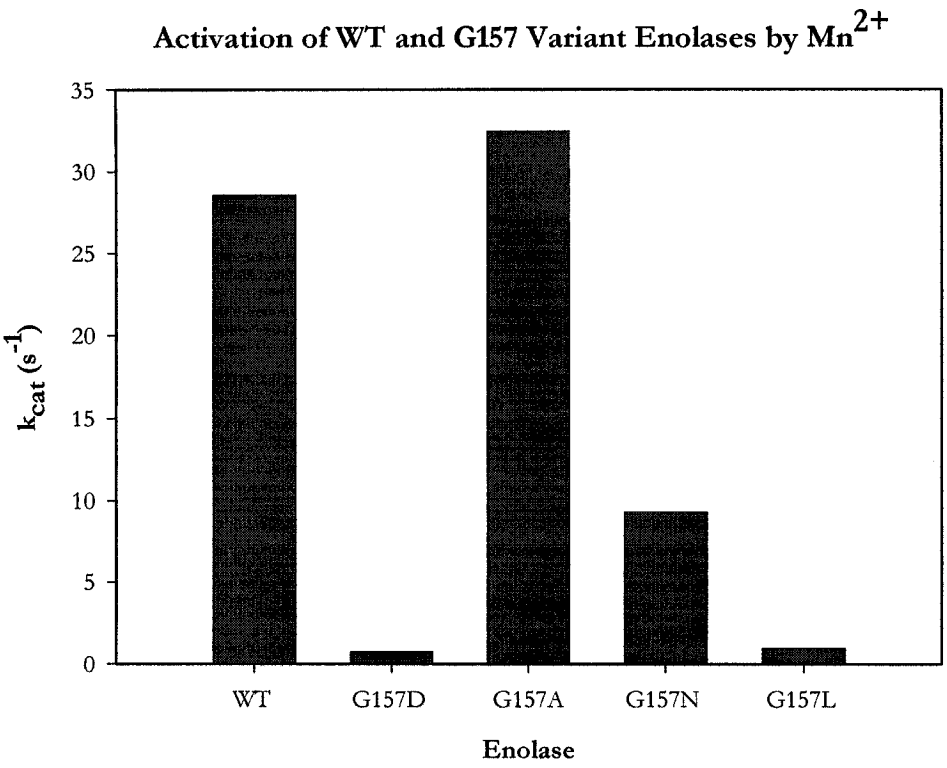

Figure 34. Comparison of k_{cat} of the wild-type and G157 variant enolases at increasing concentrations of Mn^{2+}.

III.6.2.3 Activity of Wild-type and G157 Variant Enolases with 2-PGA at [Mg^{2+}] giving Maximal Activity

The substrate dependency of the wild-type and G157 variant enolases has been examined by supplementing chelexed Mes/Tris buffer with saturating concentrations of Mg^{2+} (determined from III.6.2.1). Assays were performed and monitored in the same fashion as III.6.2.1 and III.6.2.2. Table 14 displays the kinetic parameters obtained for the different enolase by fitting the data to the Michaelis-Menten model. The K_M for 2-PGA for the G157D and G157L variant proteins has increased several fold, and that for the G157A and G157N enolases remain similar to the wild-type's. The k_{cat}s were depressed to similar extents as determined for the dependency of the enzymes for the metal cofactors (Figure 36)

Reproduced with permission of the copyright owner. Further reproduction prohibited without permission.

(III.6.2.1 and III.6.2.2). Figure 35 displays the fit of the kinetic data of the wild-type and G157D enolases.

Enolase	$[Mg^{2+}]$ (mM)	K_M (2-PGA) (μM)	k_{cat} (s^{-1})	k_{cat}/K_M ($s^{-1}\mu M^{-1}$)
Wild-type	1	40 ± 1	44 ± 1	1.1
G157D	20	211 ± 2	0.87 ± 0.01	$4.1x10^{-3}$
G157A	2	42 ± 1	37 ± 1	0.87
G157N	10	33 ± 1	8.3 ± 0.1	0.25
G157L	200	159 ± 7	1.2 ± 0.1	$7.4x10^{-3}$

Table 14. Kinetic parameters of the wild-type and G157 variant enolases by varying [2-PGA] at $[Mg^{2+}]$ giving maximal activity.

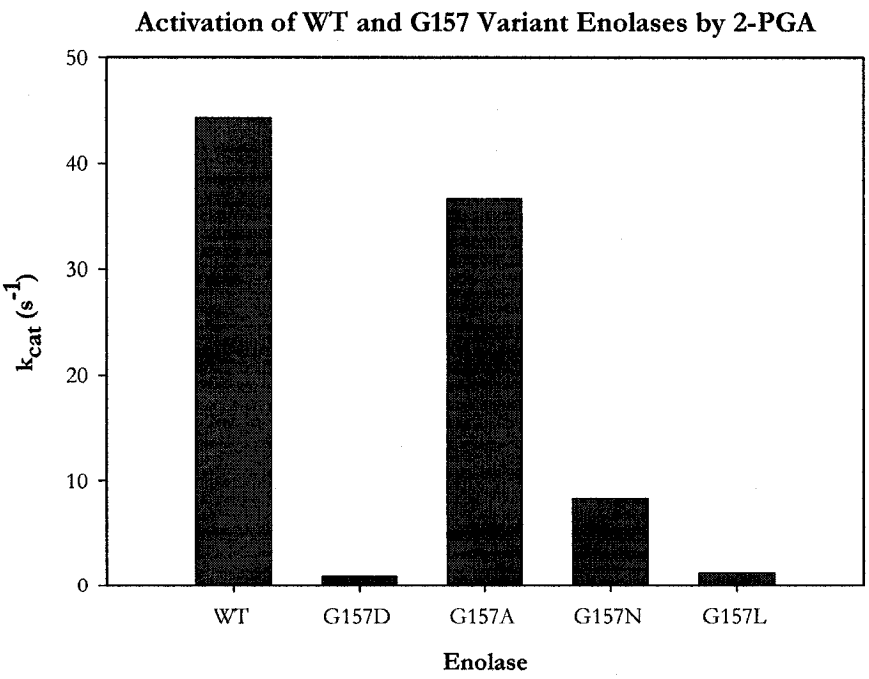

Figure 35. Comparison of k_{cat} of the wild-type and G157 variant enolases on the dependency of 2-PGA at saturating $[Mg^{2+}]$.

Reproduced with permission of the copyright owner. Further reproduction prohibited without permission.

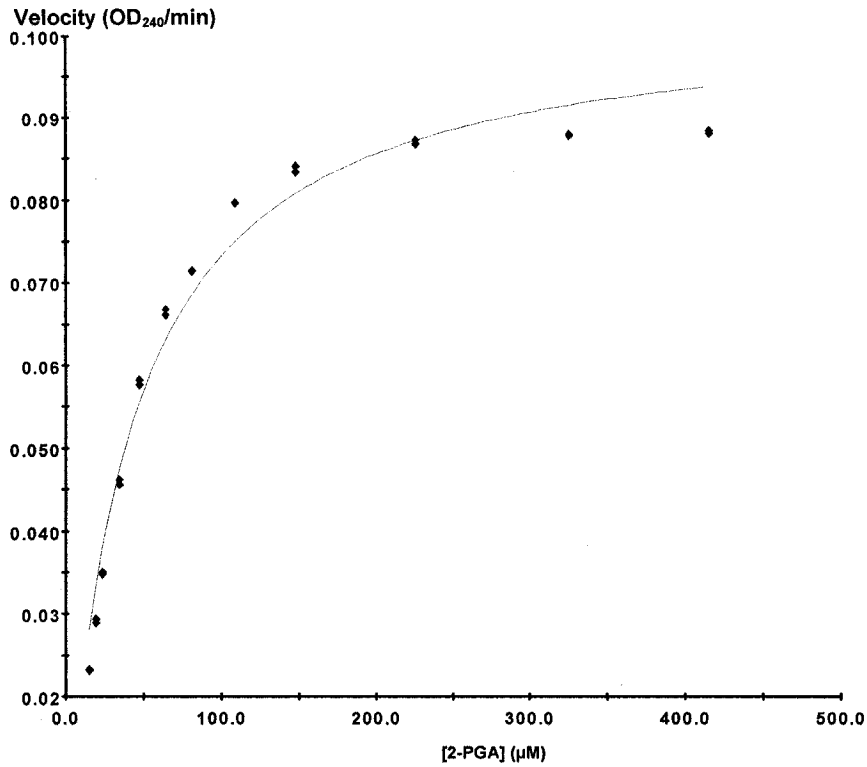

(A)

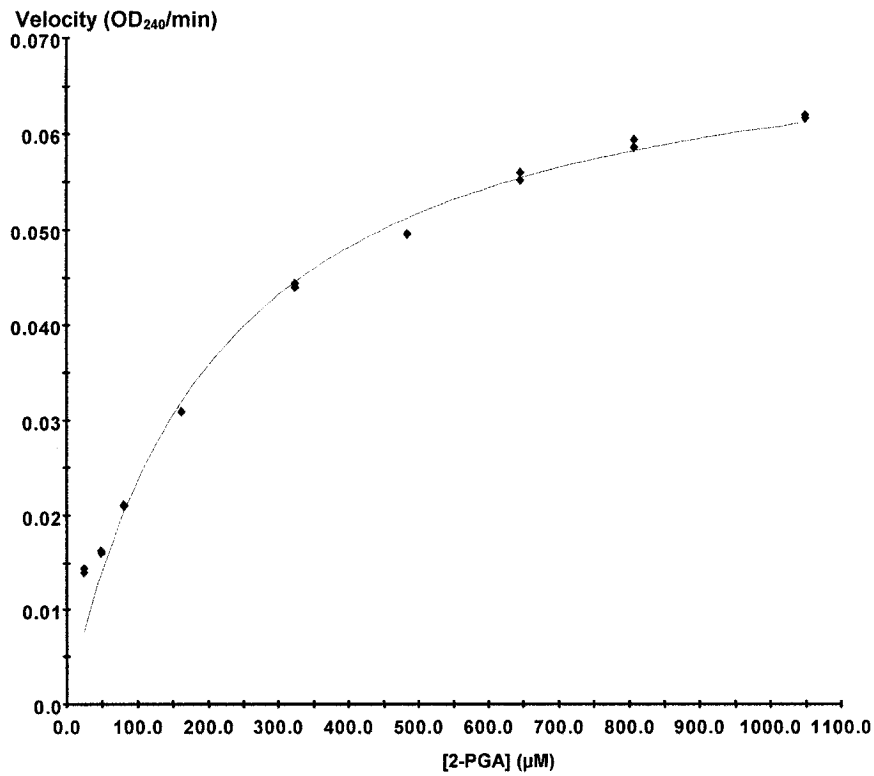

(B)

Figure 36. (A) Wild-type and **(B)** G157D enolase kinetics at increasing [2-PGA] and saturating [Mg^{2+}].

Reproduced with permission of the copyright owner. Further reproduction prohibited without permission.

III.6.2.4 Activity of Wild-type and G157 Variant Enolases with 2-PGA at [Mn^{2+}] giving Maximal Activity

The substrate dependency of the wild-type and G157 variant enolases is investigated by supplementing the assay system with saturating levels of Mn^{2+} (determined from III.6.2.2). Assays were performed and monitored in the same fashion as III.6.2.1 and III.6.2.2. Table 15 displays the kinetic parameters obtained for the different enolase by fitting the data to the Michaelis Menton model. No inhibition at high concentrations of 2-PGA were observed. The K_M for 2-PGA for the G157D variant proteins has increased several fold and that for the G157A, G157N, and G157L enolases remained similar to the wild-type enzyme. The k_{cat}s were depressed with similar trends to those determined for the dependency of the enzymes for the metal cofactors, with that for the G157D being the lowest (Figure 38). The catalytic efficiency of the G157D and G157L enolases are greatly reduced. Figure 37 A and B demonstrates the fit of the kinetic data for wild-type and G157D respectively.

Enolase	[Mn^{2+}] (μM)	K_M (2-PGA) (μM)	k_{cat} (s^{-1})	k_{cat}/K_M ($s^{-1}\mu M^{-1}$)
Wild-type	50	53 ± 3	19 ± 1	0.36
G157D	200	190 ± 1	0.86 ± 0.01	$4.5x10^{-3}$
G157A	50	44 ± 1	22 ± 1	0.49
G157N	20	58 ± 2	8.4 ± 0.1	0.15
G157L	200	42 ± 3	0.95 ± 0.02	0.02

Table 15. Kinetic parameters of the wild-type and G157 variant enolases by varying [2-PGA] at [Mn^{2+}] giving maximal activity.

Reproduced with permission of the copyright owner. Further reproduction prohibited without permission.

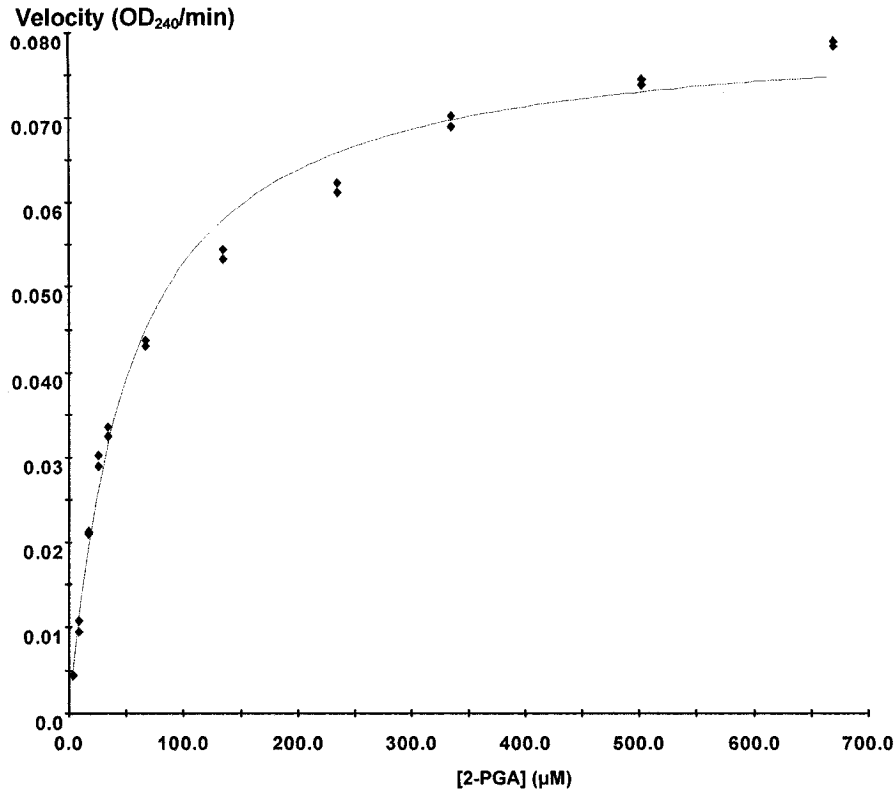

(A)

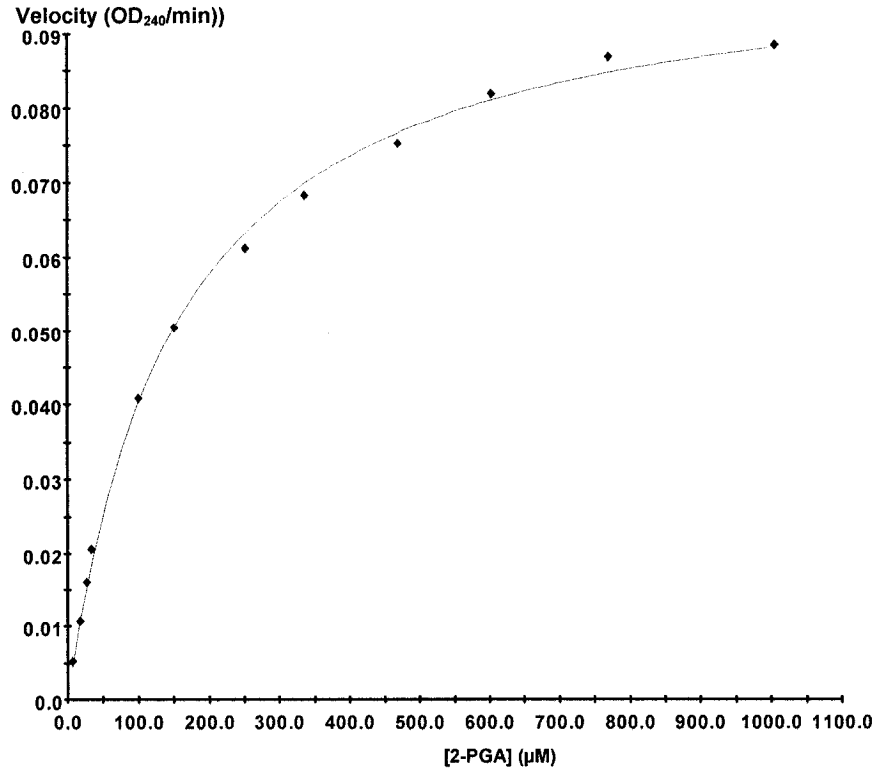

(B)

Figure 37. (A) Wild-type and **(B)** G157D enolase kinetics at increasing [2-PGA] and saturating [Mn^{2+}].

Reproduced with permission of the copyright owner. Further reproduction prohibited without permission.

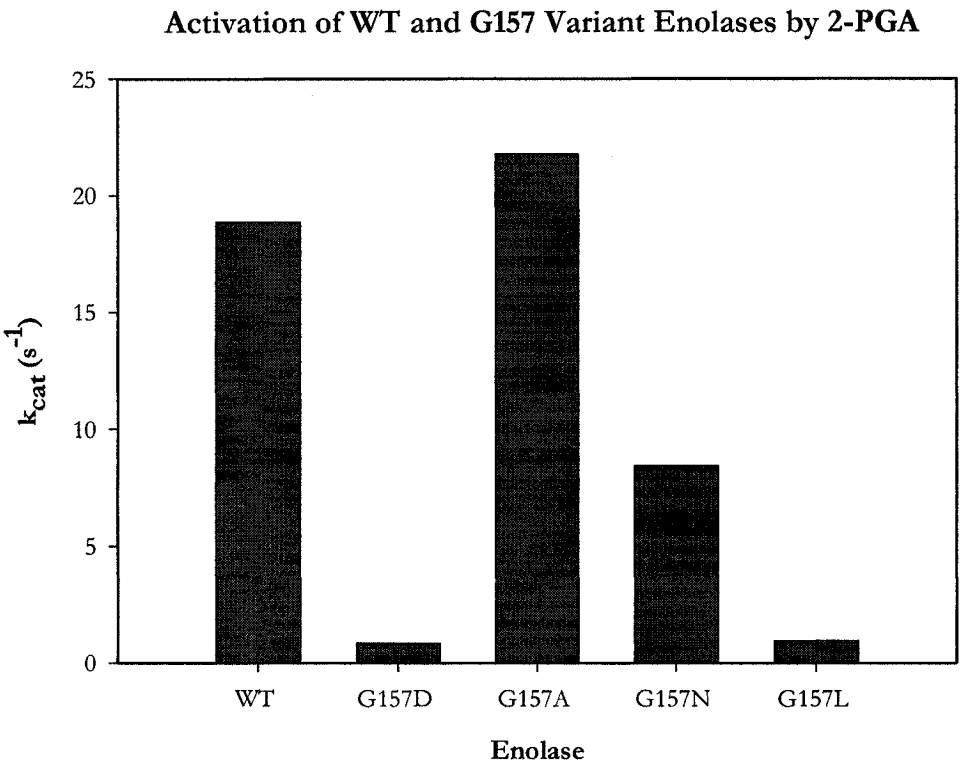

Figure 38. Comparison of k_{cat} of the wild-type and G157 variant enolases on the dependency of 2-PGA at saturating [Mn^{2+}].

III.6.3 Kinetic Isotope Effect

Kinetic parameters determined for the G157 variant enolases all suggest an altered K_M for the Mg^{2+} but a comparable K_M for Mn^{2+} and 2-PGA, with depressed k_{cat}s and catalytic efficiencies. A deeper view into the effects on the catalytic properties that the G157D and G157N substitutions have on enolase was examined using kinetic isotope effect. The dehydration of 2-PGA to PEP requires an initial C-2 proton abstraction from 2-PGA. Comparison of the k_{cat} determined at saturating levels of either H-2-PGA or D-2-PGA elucidates whether the C-2 hydrogen bond breaking has been slowed down in the G157D variant. The kinetic isotope effect of the G157D and G157N was compared to that of the

Reproduced with permission of the copyright owner. Further reproduction prohibited without permission.

wild-type. The isotopic substitution of the 2-PGA was prepared as described in section II.7. Table 15 lists the kinetic parameters obtained by varying the concentration of the metal cofactor, Mg^{2+}, at saturating levels of the deuterated 2-PGA. The K_M for Mg^{2+} has decreased for the wild-type and G157N and remained relatively constant for the G157D enolase. The k_{cat} has decreased for the wild-type and the two G157 variants examined when compared with using the non-deuterated 2-PGA. Figure 39, A-C, exhibits the kinetic fits of the wild-type, G157D, and G157N proteins. The kinetic isotope effect of the G157D protein is comparable to that of the wild-type protein, 2.6 compared to 2.5 respectively. The KIE for G157N enolase, on the other hand, is 1.9 (Table 16).

Enolase	K_M (D-PGA) (μM)	k_{cat} (D-PGA) (s^{-1})	K_M (H-PGA) (μM)	k_{cat} (H-PGA) (s^{-1})	KIE
Wild-type	29.2 ± 1.4	24.1 ± 0.18	34.9 ± 2.9	59.8 ± 1.1	2.5 ± $5.0x10^{-2}$
G157D	1290.0 ± 1.0	0.248 ± $4.5x10^{-5}$	962.1 ± 2.2	0.640 ± $3.7x10^{-4}$	2.6 ± $1.6x10^{-3}$
G157N	1061.4 ± 151.5	7.89 ± 0.23	3761.7 ± 73.7	14.8 ± $7.2x10^{-2}$	1.9 ± $1.7x10^{-3}$

Table 16. Kinetic parameters of the wild-type and G157 variant enolases by varying [Mg^{2+}] at saturating levels of D-2-PGA.

Reproduced with permission of the copyright owner. Further reproduction prohibited without permission.

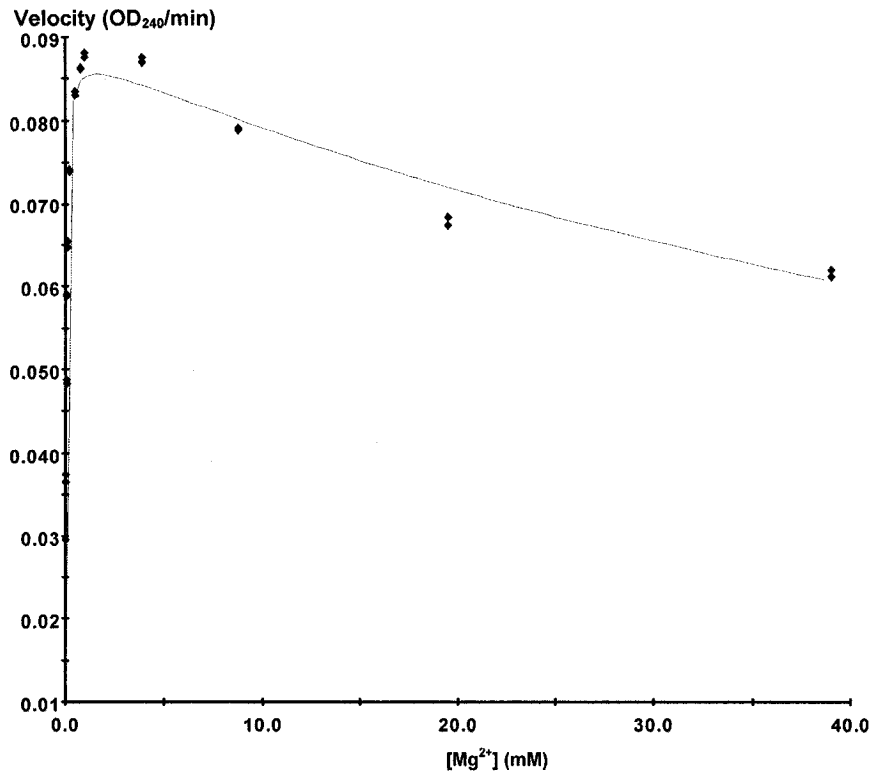

(A)

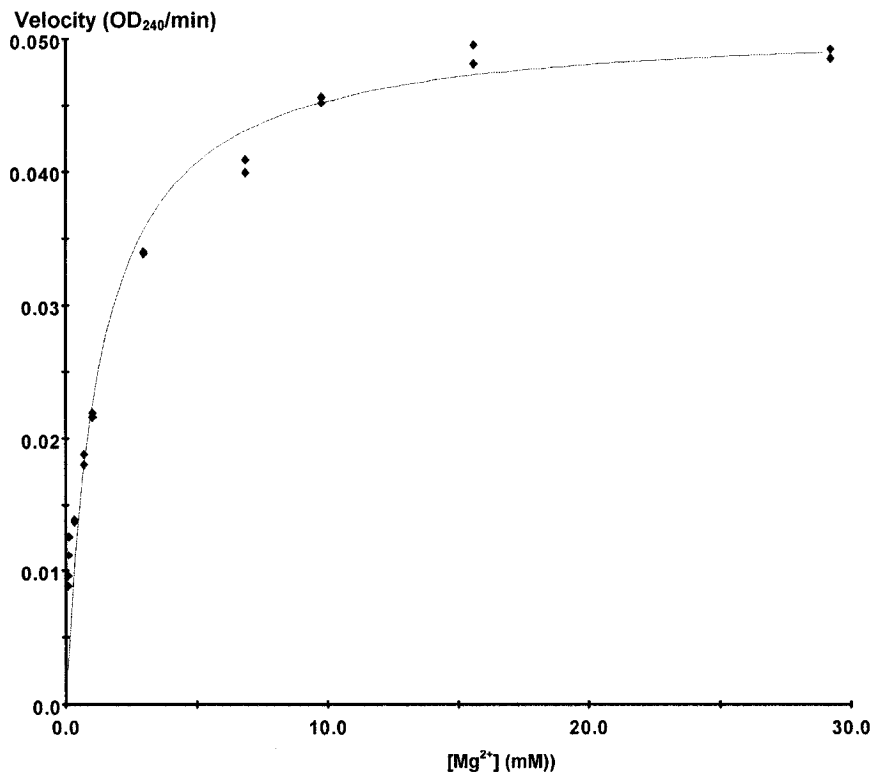

(B)

Reproduced with permission of the copyright owner. Further reproduction prohibited without permission.

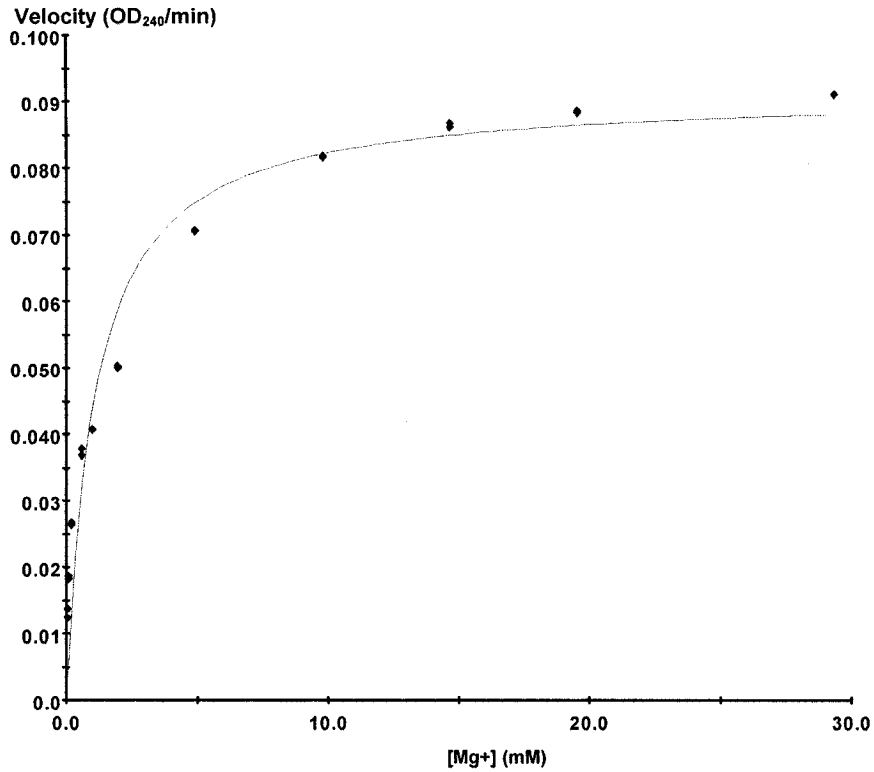

(C)

Figure 39. (A) Wild-type; **(B)** G157D; **(C)** G157N enolase kinetics at increasing [Mg^{2+}] and saturating [D-2-PGA]

Reproduced with permission of the copyright owner. Further reproduction prohibited without permission.

III.7 Measurement of Titration of the First Metal Binding Site through Fluorescence Spectroscopy

The K_d for the first metal binding site was investigated for the wild-type and G157D enolases. Apo enzyme was prepared as described in section II.4. A final concentration of 0.1 mg/mL was obtained by diluting the protein in chelexed Mes/Tris buffer. Titration of the apo-enolases with Mg^{2+} was done as described in section II.22 and monitored by the fluorescence change produced by subsequent addition of Mg^{2+}. The K_d was determined by fitting the data to the ligand binding - low K_d kinetic model. Figure 40 exhibits the fits of the wild-type and G157D proteins. The change in fluorescence intensity for the metal binding to G157D is less than that of the wild-type. This may suggest differences in the local environments of the aromatic amino acid residues for the G157D enzyme as compared to the wild-type enzyme upon binding of the first Mg^{2+}. The K_d determined for the first metal binding site (Table 17) was comparable between the wild-type and G157D enolases indicating the binding of the first metal has not been affected in the variant.

Enolase	K_d (μM)
WT	73.2 ± 6.9
G157D	72.9 ± 5.8

Table 17. Binding constant of Mg^{2+} for the first metal binding site of wild-type and G157D enolase.

Reproduced with permission of the copyright owner. Further reproduction prohibited without permission.

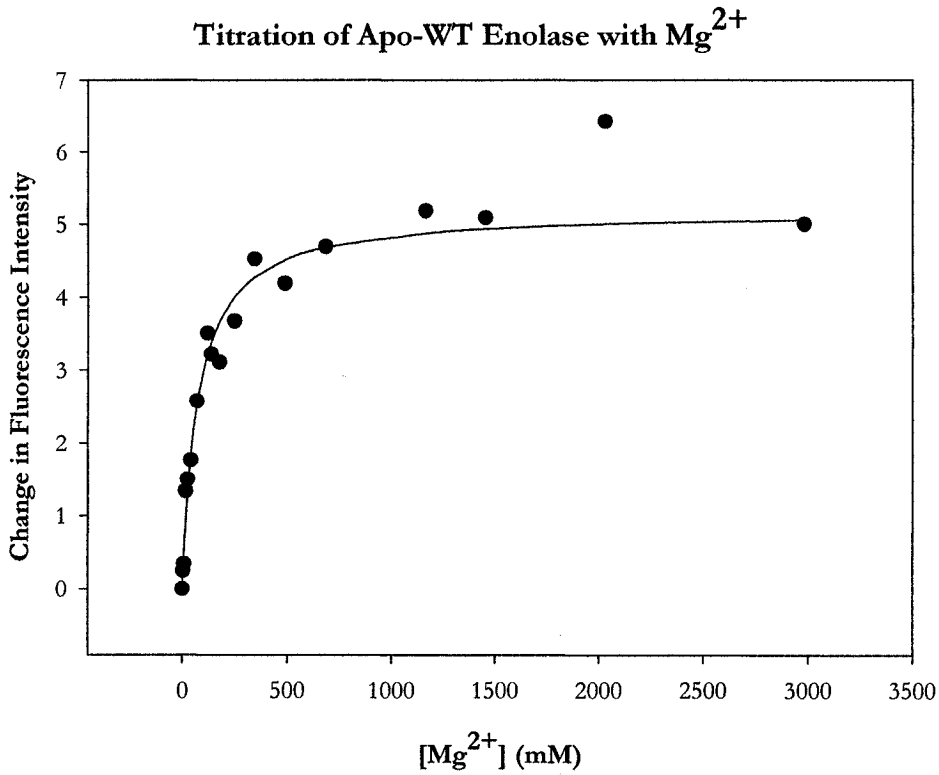

(A)

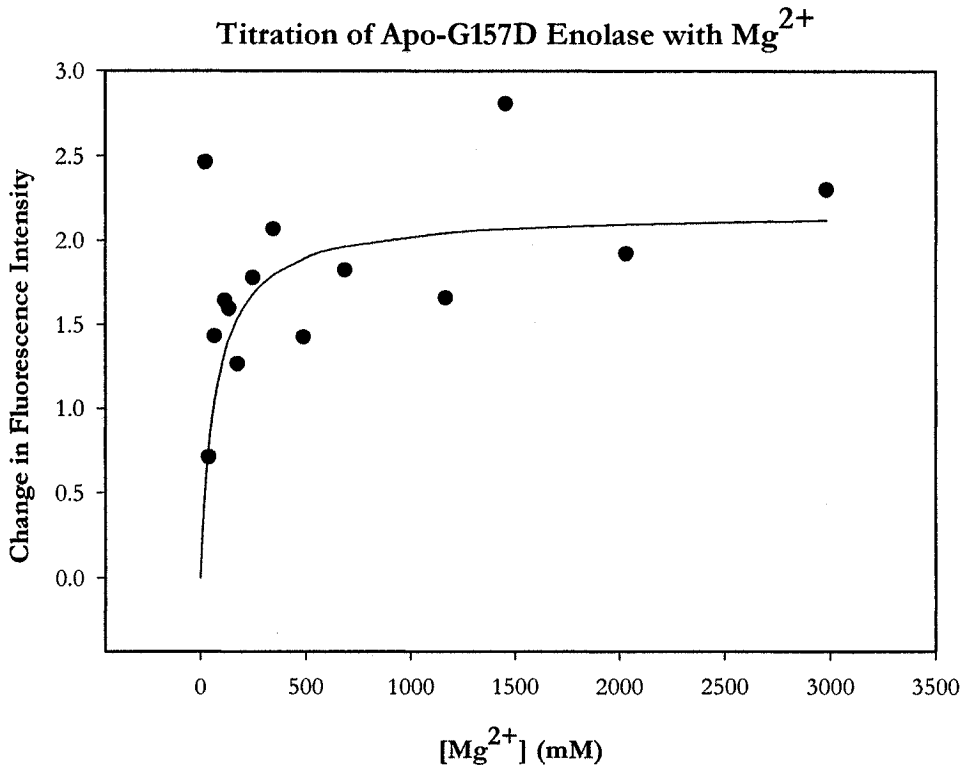

(B)

Figure 40. Titration curve of apo- **(A)** Wild-type and **(B)** G157D with Mg^{2+}.

Reproduced with permission of the copyright owner. Further reproduction prohibited without permission.

III.8 Isothermal Titration Calorimetry

The interactions between either the wild-type or G157D enolase and the metal ligand, PGA/PEP, or the substrate analogue phosphonoacetohydroxamate have been determined using isothermal titration calorimetry. The experiments involve the monitoring of heat change upon titrating the enzyme with the ligand and or substrate in the ITC chamber. The raw data were integrated and the total cumulative heat was plotted against the total ligand concentration using the MicroCal Origin software. All results were fit to either the one binding site or two binding site model. The better fit between the two, determined by the standard errors produced, was chosen to determine the thermodynamic parameters of the enzyme-ligand interaction.

The calorimetric titration of wild-type and G157D enolases with phosphonoacetohydroxamate was performed in Mes/Tris buffer with 1 mM Mn^{2+}. PhAH is a tight binding inhibitor of enolase, which does not produce catalysis upon binding. Therefore, the heat change evolved in the titration PhAH to the enolases is solely attributed to their interactions. The high association constant indicates the tight interaction of the PhAH to the enolases (Table 18). Figure 41 illustrates the enthalpy change per mol of PhAH injected.

Reproduced with permission of the copyright owner. Further reproduction prohibited without permission.

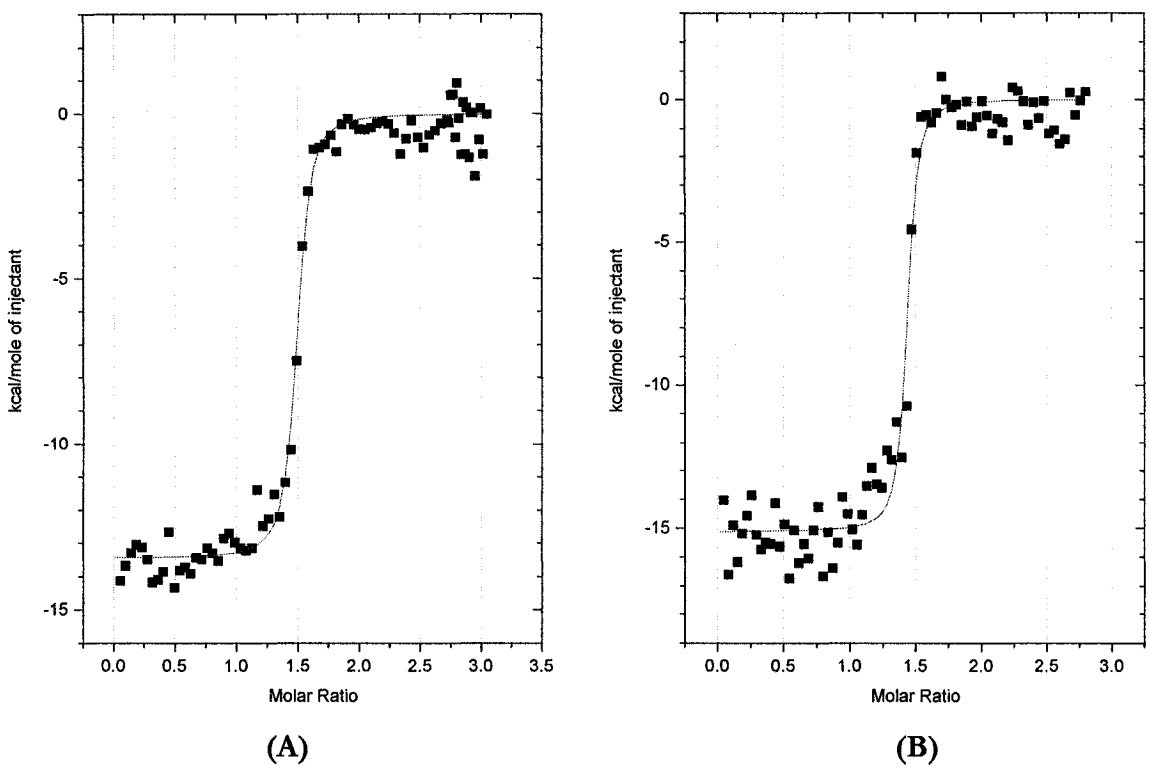

Figure 41. Enthalpy per mol of phosphonoacetohydroxamate injected versus concentration of phosphonoacetohydroxamate injected for **(A)** wild-type enolase and **(B)** G157D enolases.

Enolase	n	ΔS (cal/K)	ΔH (kcal/mol)	K (M^{-1})
WT	$1.5 \pm 7.0 \times 10^{-3}$	-9.9	-13.5 ± 0.1	$4.9 \times 10^{7} \pm 1.1 \times 10^{7}$
G157D	$1.4 \pm 7.5 \times 10^{-3}$	-14.7	-15.1 ± 0.2	$7.4 \times 10^{7} \pm 2.4 \times 10^{7}$

Table 18. Thermodynamic parameters of the association of PhAH to wild-type and G157D enolases.

Reproduced with permission of the copyright owner. Further reproduction prohibited without permission.

The interaction of $MnCl_2$ at the second metal binding site of wild-type and G157D enolases was probed by titrating in $MnCl_2$. The enolases were passed through chelex quickly to chelate excess metal that is not bound to the first metal binding site. An equilibrium mixture of PGA/PEP was added to the enzyme solution before titration. At equilibrium ratio of substrate/product, the heat change due to catalysis upon addition of Mn^{2+} is minimized. The change in enthalpy may be attributed mainly to the binding of Mn^{2+}. Figure 42 is the plot of the calorimetric titration of Mn^{2+} to the wild-type and G157D enolases. The thermodynamic parameters for the interaction are shown in Table 19. The stoichiometry of binding and enthalpy change are comparable between the two enolases.

The enthalpy change per mole of PGA/PEP versus the concentration of PGA/PEP injected into either wild-type or G157D enolase is shown in Figure 43. The titration of the equilibrium mixture of substrate/product yielded similar association constants and stoichiometric ratio (Table 20).

Reproduced with permission of the copyright owner. Further reproduction prohibited without permission.

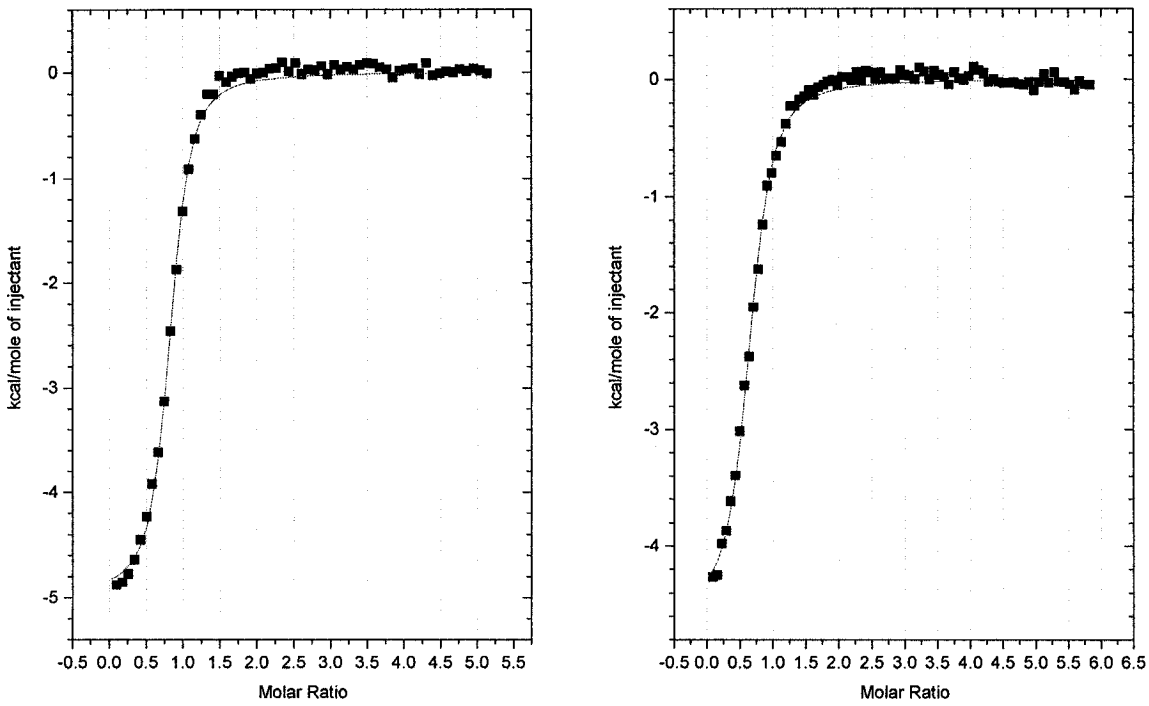

(A) (B)

Figure 42. Enthalpy per mol of $MnCl_2$ injected versus concentration of $MnCl_2$ injected for **(A)** wild-type enolase and **(B)** G157D enolases.

Enolase	n	ΔS (cal/K)	ΔH (kcal/mol)	K (M^{-1})
WT	$0.8 \pm 5.4x10^{-3}$	9.206	-5.0 ± 0.05	$4.5x10^5 \pm 3.3x10^4$
G157D	$0.7 \pm 6.3x10^{-3}$	8.921	-4.6 ± 0.06	$2.1x10^5 \pm 1.4x10^4$

Table 19. Thermodynamic parameters of the association of $MnCl_2$ to wild-type and G157D enolases.

Reproduced with permission of the copyright owner. Further reproduction prohibited without permission.

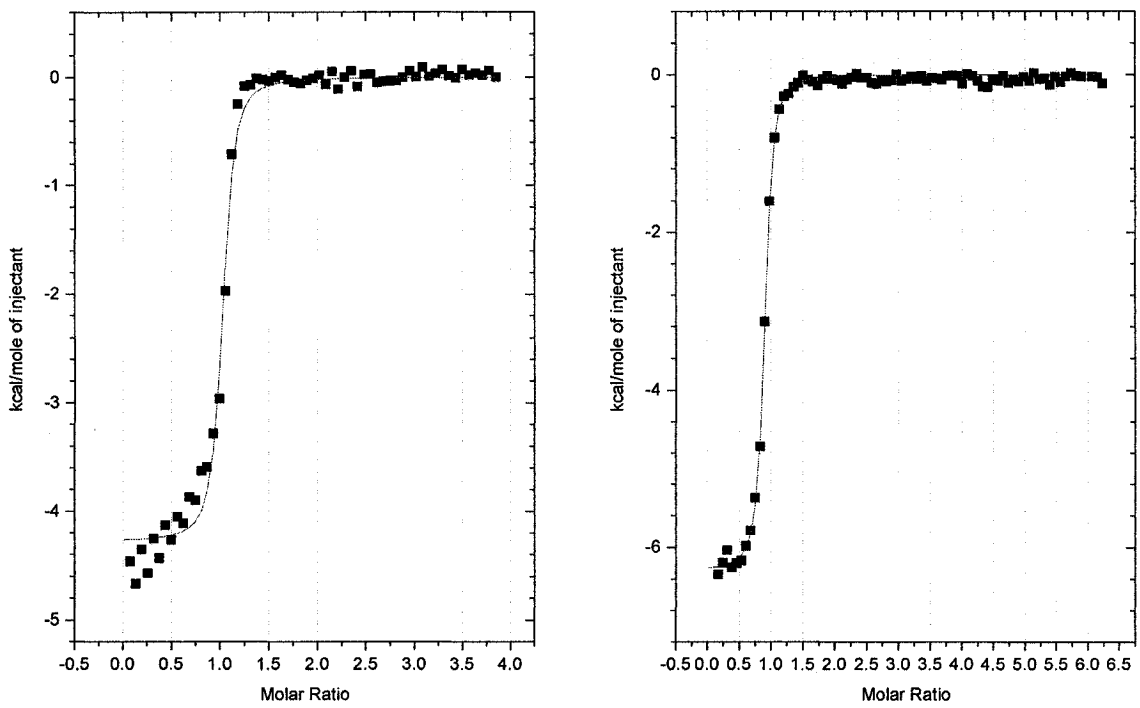

(A) (B)

Figure 43. Enthalpy per mol of PGA/PEP injected versus concentration of PGA/PEP injected for **(A)** wild-type enolase and **(B)** G157D enolases.

Enolase	n	ΔS (cal/K)	ΔH (kcal/mol)	K (M^{-1})
WT	$1.0 \pm 6.0 \times 10^{-3}$	14.8	-4.3 ± 0.04	$2.3 \times 10^{6} \pm 4.2 \times 10^{5}$
G157D	$0.9 \pm 2.2 \times 10^{-3}$	8.8	-6.3 ± 0.03	$3.0 \times 10^{6} \pm 2.5 \times 10^{5}$

Table 20. Thermodynamic parameters of the association of PGA/PEP to wild-type and G157D enolases.

Reproduced with permission of the copyright owner. Further reproduction prohibited without permission.

Chapter IV: Discussion

IV.1 Research Intention Revisited

Enolase catalyzes the dehydration of 2-phosphoglycerate to phosphoenolpyruvate, one of the terminal steps of glycolysis. In 2001, the discovery of the deficiency of β-enolase in humans has led to the identification of a new inborn error of distal glycolysis. The muscle-specific enolase deficiency was categorized as a glycogen storage myopathy that is termed glycogenosis type XIII disorder. Comi et al. (2001) reported on the clinical, biochemical and genetic features of the disorder from the patient. Such features include no increase in venous lactate level upon exercise, isolated muscle enolase deficiency, negative immunohistochemical staining with specific antibodies for β-enolase, reduced β-enolase protein by Western blot analysis of muscle tissue, and evidence of two heterozygous missense mutations affecting highly conserved amino acid residues. The focus of this thesis was on the mutation changing G156 to an aspartate. The G156D amino acid change is located in close proximity to His158. These amino acids are G157 and His159 in the yeast enolase numbering system. Both these amino acids are conserved among the yeast, *E. coli*, rabbit muscle, lobster, and *Homo sapiens* enolases (Figure 1). The analogue of the G157D variant was produced in yeast enolase in order to study the role of G157 and the effects of the G157D mutation on the protein structure, stability, and activity. With this, we hope to get some insights into the effects of the mutation in human ββ-enolase. In addition, the G157A, G157N, and G157L variant yeast enolases were also generated to investigate whether the reduced activity is due to the size and/or the charge of the amino acid at this position.

Reproduced with permission of the copyright owner. Further reproduction prohibited without permission.

IV.2 Structural Characterization of Wild-type and G157 Variant Enolases

Far- and near-UV CD, fluorescence and analytical ultracentrifugation were used to show that the G157D, G157A, G157N, and G157L enolases are correctly folded. Such optical spectroscopic techniques are useful tools to characterize the protein conformation and/or conformational changes. Proteins absorb light mainly through the peptide groups and aromatic amino acids, and emit radiation in the UV range of the spectrum (Schmid, 1997). The structural contents of yeast enolase facilitate its characterization using optical spectroscopic techniques. Yeast enolase is a large protein structured from a mixture of α-helices and β-sheets (I.4.2 and I.4.3), and it contains 5 tryptophans, 9 tyrosines, and 16 phenylalanines that give rise to characteristic signals. All G157 variants showed identical secondary structural folding patterns relative to the wild-type protein when comparing the respective peptide-bond CD spectra (Figure 21) which were practically superimposable. As well, the tertiary structures of the G157 variants showed similar tertiary structural characteristics as observed in the aromatic-UV CD and fluorescence spectra. The aromatic-UV CD spectrum is sensitive to the environmental polarity of the immobilized aromatic amino acids within the protein and is therefore highly significant of the native state of a protein (Schmid, 1997). The G157 variant aromatic-UV CD spectra (Figure 22) showed similar peak patterns to the wild-type spectrum with slight differences in the peak intensities. In particular, minor decreases in the signal based on tryptophan residues were observed along with trivial increases in signals based on phenylalanine residues. These differences may arise from slight changes in the environment of the aromatic chromophores within the variant proteins. If so, the aromatic residues may become either more or less mobile, affecting their signal intensities and those of neighbouring amino acids.

Reproduced with permission of the copyright owner. Further reproduction prohibited without permission.

Fluorescence spectroscopy was also used to obtain information about the tertiary structures of the proteins. Fluorescence emission also arises from the aromatic amino acids that reside within the protein. The fluorescence spectroscopy of the G157 variant proteins shows similar spectra to that of the wild-type protein (Figure 23). The respective spectra show slight differences in fluorescence intensity with no shift in λ_{max} emission of 335 nm. Fluorescence spectroscopy is sensitive to concentration of samples prepared and variations may arise when samples contain minor contaminants. As the G157 variant spectra show no shift in λ_{max} emission, the difference in the intensity may simply be due to the differences in the sample concentrations measured. Alternatively, as observed by slight differences in the aromatic-UV CD spectra, the arrangement of the tryptophan residues may have been altered in such a way that neighbouring aromatic amino acids are brought either closer or further away without perturbing their solvent accessibility. This may cause greater or reduced amounts of energy transfer from the other chromophores to tryptophan, leading to difference in fluorescence intensity.

Analytical ultracentrifugation is a useful technique to obtain information about the shape and conformation of a protein. The sedimentation coefficients obtained from the sedimentation velocities of the protein sample are useful for monitoring changes in the conformation of protein. Sedimentation velocity measurements confirmed that the G157 variants retain their dimeric structure with no significant dissociation. The $S_{w,20}$ of the G157 variant enolases were comparable to that of the wild-type (Table 10). At two concentrations of the proteins, 10.6 μM and 1.06 μM, no measurable differences in the $S_{w,20}$ were observed within the wild-type, G157A, G157N, and G157L enolases. For the G157D variant, slight difference in $S_{w,20}$ at the two different concentrations seems to point to approximately 3% dissociation. However, the experiments must be repeated in order to confirm this. As the

Reproduced with permission of the copyright owner. Further reproduction prohibited without permission.

concentration of the protein affects the subunit association/dissociation (Ralston, 1993), the similarity of the $S_{20,w}$ at high and low concentrations of protein point to the fact that the substitutions at G157 do not cause substantial dissociation. The results indicate that there is no appreciable dissociation of the G157 variant enolases, which retain their dimeric quaternary structure.

From all spectra obtained for the G157 variant enolases as compared to that of the wild-type enzyme, it may be concluded that they are all correctly folded, that is, any structural changes are minimal. Improper folding of the variant enzymes is not expected since G157 is not part of the core of the protein and is not directly involved in domain or subunit interface formation. G157 is located in a highly mobile loop connecting secondary structural elements. Therefore, it seems unlikely that the global structures of the variants will be significantly perturbed due to the mutation. In addition to the evidence from the spectral characterizations of the G157 variant proteins, the variant enzymes behave similarly to the wild-type enzyme in the purification procedure, which further supports the proper folding of the variant proteins.

IV.3 Conformational Stability

The stability of the enzymes may be a factor that limits their proper functioning. How has the substitution of G157 with the various amino acid residues affected the stability of enolase? Thermal-induced denaturation of the G157 variant proteins show lower T_m values compared to that of the wild-type (Figure 24, Table 11). When proteins are exposed to increasing temperature, there is subsequent loss of solubility and enzymatic activity. Proteins are composed of polypeptide chains with unique tertiary structures in the native state. The structures are stabilized by many factors, including electrostatic and hydrophobic

Reproduced with permission of the copyright owner. Further reproduction prohibited without permission.

interactions. As the temperature increases, many interactions in the protein molecule are weakened. Thus, the protein melting point temperature is indicative of the thermal stability of the protein. The G157D, G157N, and G157L variant enolases have similar T_m values of 49.5-49.9°C. They are about 5°C lower than the wild-type protein. The G157A variant has a slightly higher T_m than that of the other variants. It is nonetheless considerably lower than the wild-type protein by 4°C. It is of considerable interest that the small perturbation for substituting a glycine residue by an alanine would lead to a loss of thermal stability of the protein similar to that resulting for the other larger and bulkier amino acid substitutions. A closer examination into the crystal structure of apo-enolase (Stec & Lebioda, 1990) shows that certain interactions within the local environments of the mutation site may be affected. G157 is located in the highly mobile Loop 2 that connects strand 1 to 2 (Table 2). The loop protrudes from the barrel structure of the C-terminal domain (Section I.4.3), described as a classical bulge by Stec and Lebioda. Hydrogen bonds formed between neighbouring water molecules stabilize the bugle architecture. The architecture of Loop 2 places the side chains of Val153 and Leu154 to the exterior of the protein, allowing proper positioning of the side chains of Asn152 and Asn155 to H-bond to each other (Figure 44). Hence, substituting Gly157 with even a slightly bigger amino acid may disturb the 3-D arrangement of Loop 2, weakening or disrupting these hydrogen bonds.

Reproduced with permission of the copyright owner. Further reproduction prohibited without permission.

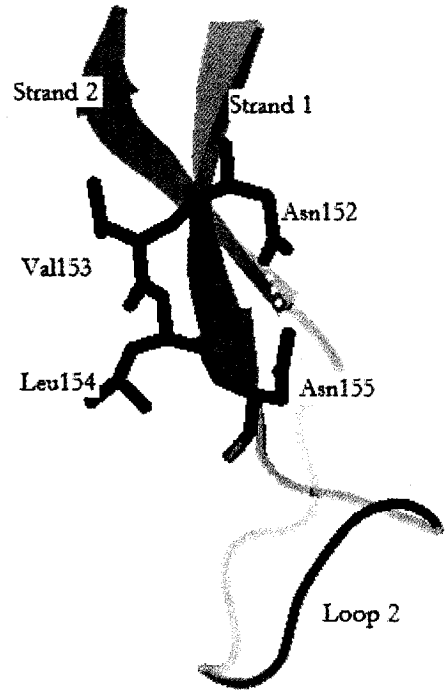

Figure 44. Loop 2 (Classical bulge) of enolase connecting Strands 1 and 2 (pdb: 3ENL). The side chains of Val153 and Leu154 point to the exterior of the protein, placing the side chains Asn152 and Asn155 to the interior of the protein. Dotted yellow line represents the hydrogen bond between the side chains of Asn152 and Asn155. The image was generated using PyMol.

Urea denaturation of G157D and wild-type enolase shows that the denaturation of G157D occurs more readily than the wild-type. The concentration of urea at which 50% of the CD signals is lost is ~1.3 M for the G157D variant compared to ~1.7 M for the wild-type enolase. Urea denatures proteins by exposing hydrophobic groups to solvent by weakening water-water interactions, thereby diminishing the hydrophobic effect (Bennion & Daggett, 2003). The lower urea concentration required to denature G157D enolase suggests that water and H-bonding interactions surrounding and within the protein are weakened in the variant. This is consistent with the local disruptions of the H-bonding patterns of Loop 2 upon substituting G157 with another amino acid as described in the paragraph above.

Reproduced with permission of the copyright owner. Further reproduction prohibited without permission.

The stability of the G157D variant enolase was also examined by comparing the dissociation constant of the dimeric protein into the monomeric forms using $NaClO_4$.

$$D \rightleftharpoons 2M$$

The dissociation of enolase with $NaClO_4$ showed that G157D enolase is more prone to dissociation than native enolase. The calculated subunit dissociation constant of G157D enolase is 178 μM and that of the wild-type enolase is 46.5 μM. $NaClO_4$ is a chaotropic salt and destabilizes protein structures by disrupting the water structure and promoting hydration of buried surfaces. The three tyrosine residues, Tyr6, Tyr11, and Try130, and Trp56 that are located near the subunit interface give rise to signal differences when the subunits dissociate, making it easy to probe for dissociation of yeast enolase. The range of concentrations used to dissociate enolase without denaturing the protein was obtained from previous studies of dissociation of enolase (Kornblatt et al., 1996). The higher dissociation constant of the G157D enolase indicates less rigid water structuring or weakened H-bonds at the subunit interface.

Thermal and urea denaturation and $NaClO_4$ dissociation of the G157 variant enolase reveal that the conformational stability of the G157D protein is lower than that of the wild-type. Is this lowered conformational stability sufficient to lead to the low content of the ββ-enolase within the patient diagnosed with muscle specific enolase deficiency? Comi et al. (2001) have suggested that the missense mutations in the *ENO3* gene may lead to improper folding and assembling of β-enolase dimer complexes, which may result in increased susceptibility to proteolysis. G157 variant enolases were therefore subjected to limited proteolysis by trypsin. Trypsin is a protease that degrades enzymes by cleaving proteins at

Reproduced with permission of the copyright owner. Further reproduction prohibited without permission.

the carboxyl side of the amino acids lysine and arginine. Most native proteins are relatively resistant to low concentrations of proteases. Under limited proteolysis condition, a low ratio of protease to protein, proteolysis would occur only at the most exposed or disordered region of the polypeptide backbone. Hence, increases in susceptibility to proteolysis are generally the result of changes in the protein structure that increase the accessibility of sites in the protein. The wild-type and G157 variant proteins were subjected to trypsin digestion with a weight ratio of trypsin to protein of 1:100 (Morrice & Carrey, 1997). The wild-type enolase was resistant to trypsin digestion whereas the G157 variants showed degradation by 60 min. The relatively intense SDS-PAGE band of the G157A variant compared to the G157D, G157N, and G157L variants shows that the G157A protein is more resistant to proteolytic cleavage than the others. The size and charge of the amino acid replacing G157 in effect, leads to the greater susceptibility of the protein to trypsin digestion. The increased susceptibility to trypsin digest agrees with Comi et al.'s (2001) hypothesis that the reduced β-enolase protein in the patient may be due to proteolysis of the variant protein.

On the other hand, at lower concentrations of trypsin, 1:1000 ratio of trypsin to protein, there is no substantial cleavage of the wild-type and G157D proteins within 2 hrs of incubation as demonstrated in the SDS-PAGE. This suggests that digestion of the variant enolase depends on the physiological concentration of proteases within the body. In addition, the wild-type monomeric protein (obtained from dissociation of the dimer with $NaClO_4$) was also subjected to 1:1000 ratio of trypsin to protein. Interestingly, the monomeric protein shows a time dependent digestion pattern. As the incubation time increases, the monomeric band of ~46 kD disappears and three bands of ~30 kD-45 kD become more and more apparent. The G157D variant protein does not show appreciable

Reproduced with permission of the copyright owner. Further reproduction prohibited without permission.

digestion at a 1:1000 ratio of trypsin to protein compared to the monomeric wild-type enolase, which is consistent with the fully dimeric structure of the G157D variant enolase.

IV.4 Ligand Binding

The mechanism of enolase catalysis requires a series of steps, including the binding and release of metal ions and substrates. As demonstrated from steady-state kinetics, the depressed activity of the G157 enolases may in fact be due to the lowering in affinity for Mg^{2+} or to a lesser extent, 2-PGA. Which element of binding was affected by the G157 mutation? Brewer and Weber (1965) have demonstrated that upon binding of Mg^{2+} to metal free enolase, there is an observable fluorescence intensity change. This feature is therefore useful for studying the binding of Mg^{2+} to the metal-free enolases. Fluorimetric titrations of the metal-free G157D and wild-type enolases determined that both enolases bind to the first Me^{2+} with approximately the same affinity. The K_d was determined to be 73.2±6.9 μM and 72.9±5.8 μM for the wild-type and G157D enolases, respectively. From this, it may be assumed that the G157D mutation did not affect the binding of the first metal binding site.

The binding constant of the second Me^{2+} site was obtained by titrating the substrate bound enolase with Mn^{2+}. The process was monitored by isothermal titration calorimetry. Isothermal titration calorimetry is a useful technique that measures the interaction enthalpy for bimolecular processes (O'Brien et al., 2001). The heats of each individual addition of ligand to the enzyme are integrated and plotted against the molar ratio of the ligand component. The results are then fitted to appropriate binding models to obtain accurate binding constants. Similar binding constants were obtained for the second Mn^{2+} binding site for both the G157D and wild-type enolases. These results are consistent with the steady-

Reproduced with permission of the copyright owner. Further reproduction prohibited without permission.

state kinetic studies on the G157D enolase with Mn^{2+}, where the K_M for Mn^{2+} is not significantly altered between the wild-type and the G157D variant.

To obtain information concerning the ability of the enzyme with the first Me^{2+} bound to bind to the substrate/inhibitor, isothermal titration calorimetry was used to determine the substrate/inhibitor binding. As discussed previously, the G157D variant enolase may have affected the coordination of His159 to the substrate. However, steady-state kinetics results suggest that the affinity for the substrate has not been significantly altered. It would therefore be interesting to directly measure the binding constant of the G157D enolase to the substrate. The G157D variant and wild-type enolases were first titrated with the strongly-bound enzyme enolase inhibitor PhAH. The interaction of the PhAH to enolase is of binding only as catalysis does not occur. Therefore, PhAH is a good substrate analogue to use in order to obtain accurate measures of the binding constant. The titration of the substrate/product (2-PGA/PEP) into enolase with the first Me^{2+} bound also showed similar binding affinities for the G157D variant and wild-type enolase. The G157D enolase binds the substrate/product (2-PGA/PEP) and substrate analogue PhAH with affinities similar to the native enzyme. Although the association constants for the binding of PGA/PEP are extremely similar for the G157D and the wild-type enolases, there exists a greater difference in the enthalpy change involved in the reaction. ΔH is obtained as a direct measure of the number and strength of interactions formed or broken when the enzyme goes from the free to the ligand bound state. The interpretation of the heat change involved in the binding of PGA/PEP is complicated by possible contributions of catalysis. Although an equilibrium mixture of PGA/PEP was titrated into the enzyme with the first Me^{2+} bound, incomplete removal of the second Me^{2+} by chelex may lead to catalysis occurring. In addition, an increase in ΔH for the binding of PGA/PEP to G157D enolase may also be

Reproduced with permission of the copyright owner. Further reproduction prohibited without permission.

attributed to the increased efforts of the enzyme to bind to substrate/product. That is, perhaps Loop 2 in G157D enolase is swayed from the active sites, and therefore needs to be displaced over a longer distance in order for His159 to come close enough to bind. In essence, kinetic assays and isothermal titration calorimetry experiments show that G157D retains the ability to bind metal ions and substrates.

IV.5 Steady-State Kinetics

All G157 variant proteins exhibit reduced activity, with G157A, G157N, G157L, and G157D variants retaining 78.07%, 8.36%, 0.30% and 0.06% native enolase activity under standard assay conditions respectively. Standard enolase assays include 1 mM $Mg(OAc)_2$ and 1 mM 2-PGA, which are both saturating for native enolase. Detailed kinetic studies were performed to see whether the affinity for the divalent metal cofactor, the substrate 2-PGA, or both has been affected due to the mutation. Results of the kinetic studies show that the increasing size and charge of the amino acid substituting G157 in enolase have relative effects on the activity of the enzyme. In summary, **a)** there is an increase of up to 700-fold in K_M for the G157 variant enolases for Mg^{2+}, relatively little variance in K_M for Mn^{2+}, and an increase of up to 5-fold in K_M for 2-PGA at saturating Mg^{2+} or Mn^{2+} concentrations; **b)** with Mg^{2+} as the divalent cation, there is a significant reduction of k_{cat}, up to ~100-fold, as the size and charge of the amino acid at position 157 increases. Similar but smaller trends in k_{cat} were observed when varying Mn^{2+} (40x), varying 2-PGA at saturating Mg^{2+} (50x) or at saturating Mn^{2+} (25x). k_{cat} was lowest for the G157D variant enolase in all cases; **c)** with either Mg^{2+} or Mn^{2+} as the divalent cation, there is reduction in the catalytic efficiency for the G157D variant, with a decrease of 5 orders of magnitude for Mg^{2+} and a decrease of 3x for Mn^{2+}. The catalytic efficiency is lowest for the G157L variant with either divalent metal

Reproduced with permission of the copyright owner. Further reproduction prohibited without permission.

cation. The catalytic efficiency of the variant enolases was reduced by 3-orders of magnitude for 2-PGA with saturating levels of Mg^{2+} or Mn^{2+}, with the G157D variant being the least catalytically efficient; **d)** there is loss of inhibition by high concentrations of metal for the G157D, G157N, and G157L variant enolases.

In essence, the catalytic activities of the larger and/or charged amino acid substitution for the G157 are the most affected. The G157D and G157L variant proteins have the lowest k_{cat}, and k_{cat}/K_M values with the G157N variant showing intermediate values between the G157D and wild-type enolases. The smaller sized amino acid substitution, alanine, replacing G157 experiences the smallest effects on the catalytic activities. How may the G157 mutation affect the overall catalytic activities of the variant enolases? As k_{cat} is an inherent property of the enzyme, conveying the rate of reaction when all enzyme molecules are present in the enzyme substrate complex (Marangoni, 2003), it takes into account all the rate constants upon formation of the enzyme-substrate complex. Which steps in the reaction mechanism of enolase have been affected by the G157 mutation? The mechanism of enolase is one of Bi-Bi ordered sequential (Poyner et al., 2001). Figure 45 illustrates the steps of reaction involved in the mechanism. k_5 and k_6 includes the loop closure, abstraction of the C-2 H^+, removal of C-3 OH^-, and opening of the loops.

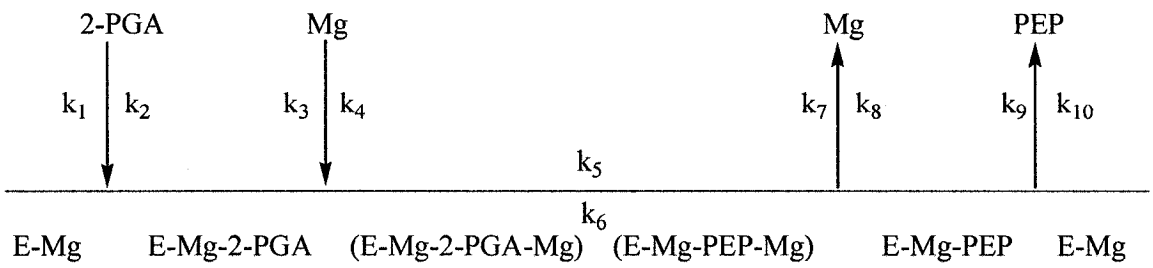

Figure 45. Bi Bi ordered kinetic mechanism of enolase which the second metal ion binds after the substrate and dissociates before the product. E represents enolase.

Reproduced with permission of the copyright owner. Further reproduction prohibited without permission.

Conformational changes that are associated with mobile loops may affect enzyme function (Gunasekaran & Nussinov, 2004). Comparison of the crystal structures of enolase with the substrate bound and unbound reveals a large conformational change in the three highly mobile loops (Figure 10). In particular, His159 moves over a 4 Å distance when the substrate 2-PGA binds, protonating the phosphate of the substrate (Zhang et al., 1997). Zhang et al. (1997) have suggested from the electron density present in the active site that 2-PGA is predominantly bound in the active site when there is a direct H-bond between the substrate and the imidazole side chain of His159, and in the active site where water molecules separate His159 from binding the ligand, PEP is the predominant ligand bound. Therefore, if the G157 mutation has led to improper positioning of Loop 2 as substrate binds, it may weaken the affinity of the enzyme for the substrate. However, this does not seem to be the case, since ITC results indicate similar K_a for wild-type and G157 variant enolase to the substrates. In addition, K_M for 2-PGA at saturating concentrations of Mg^{2+} or Mn^{2+} has not altered significantly for the G157 variant enolases compared to the wild-type. How else may the G157 mutation affect the activity of enolase?

Brewer et al. (2003) have suggested that the role of His159 is not only to H-bond with the substrate, but to polarize the substrate via protonation of the phosphate moiety. Also, the architecture of Loop 2 places the side chains of Val153 and Leu154 to the exterior of the protein, allowing proper positioning of the side chains of Asn152 and Asn155 to H-bond with each other. The two Asn residues are directed towards Glu168, which stabilizes the conformation of the Glu168 side chain (Figure 46). Glu168 plays a significant role in the enolase reaction mechanism.

Reproduced with permission of the copyright owner. Further reproduction prohibited without permission.

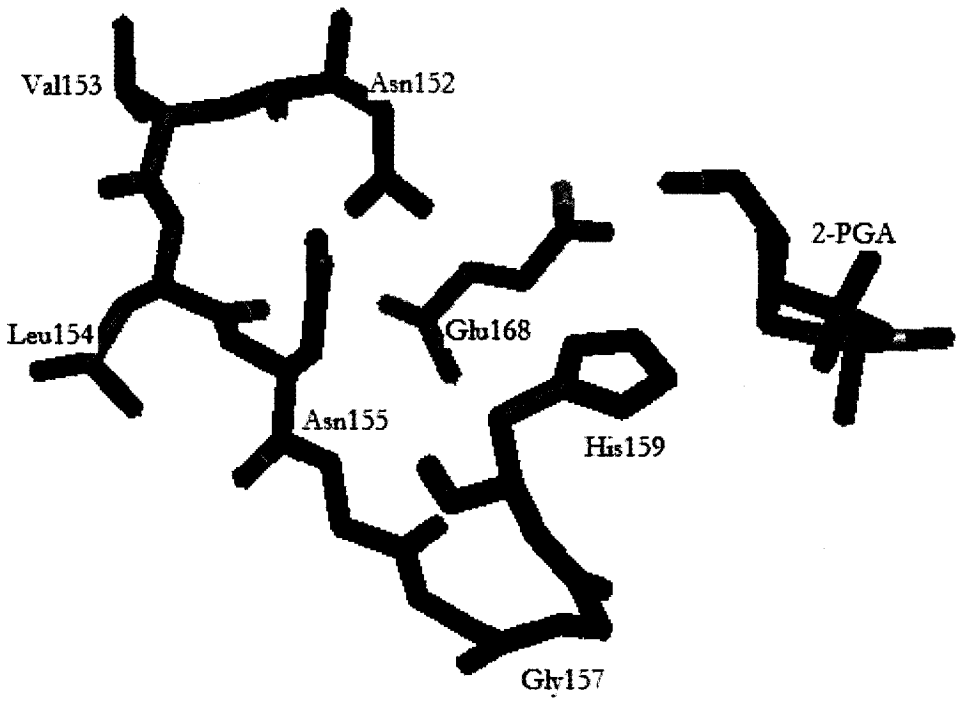

Figure 46. Interaction of Glu168 with 2-PGA (pdb: 2ONE). Asn152 and Asn155 positions Glu168 to interact with 2-PGA. Gly157 forms the hinge site that allows rotation of Loop 2, positioning His159 close enough to interact with the substrate. The figure was generated using PyMol.

Poyner et al. (1996) showed that an E168Q variant enolase showed ~10^{-5}-fold reduction in k_{cat}. They have shown that the E168Q variant enolase retains the ability to catalyze the exchange of the α-proton with solvent D_2O, but however, is severely depressed in the ability to carry out the hydrolysis of (Z)-3-chlorophosphoenolypyruvate to tartronate semialdehyde phosphate (TSP), which mimics the addition of OH^- to C-3 of PEP. In addition, Liu et al. (2000), using both quantum mechanical and molecular mechanical approaches, reveal that G168 plays an important role in the stabilization of the transition state of enolase. In particular, G168 contributes favourably to the forward reaction of the second catalytic step in enolase, by lowering the energy barrier associated with the removal of OH^- from C-3 of 2-PGA. Hence, from both experimental and theoretical point of views,

Reproduced with permission of the copyright owner. Further reproduction prohibited without permission.

Glu168 is crucial for proper functioning of enolase. Relay effects originating from the G157 mutation that may affect the proper coordination of Glu168 could contribute to the low k_{cat} observed for the G157 variant enolases.

Moreover, the closed conformation is induced when 2-phosphoglycerate binds. This positions Gly161 in Loop 2 in one subunit in close proximity to H-bond with the side chain amide oxygen of the Asn207 of the other subunit (Zhang et al. 1997). This interaction helps stabilize the closed conformation of enolase. The closed conformation of the loops is crucial in stabilizing the carbanion intermediate during the reaction (Wedekind et al., 1994). In the introduction (Section I.6.1), it was mentioned that the acidity of the C-2 proton of 2-PGA is relatively weak, with a pK_a of ~28-32. The enzymatic mechanism that facilitates the rapid ionization of this weak C-2 proton must provide a means of stabilization of the resulting intermediate. The two divalent metal ions stabilize the intermediate through coordination to the intermediate (Poyner & Reed, 1992). Gunasekaran et al. (2003) modeled the function of the loop movements in enolase using molecular dynamic simulations. Results using the holo-crystal structure for simulations showed strong interactions between the mobile Loops 1 and 2. The crystal structure of enolase as an asymmetric dimer enolase-2PGA/enolase-PEP (Zhang et al., 1997) shows that Loop 1 moves towards Loops 2 and 3 upon substrate binding. However, Gunasekaran et al. (2003) found that restraining the movement of Loop 2, by mutating the glycine residues that form the hinge sites in Loop 2, Gly156, **Gly157**, Gly161, and Gly162 to alanine residues, causes Loop 1 to shift away from the Loops 2 and 3. Perhaps the movement of Loop 1 is in fact affected in the G157 variant enolases? The movement of Loop 1 is crucial to the enzymatic catalysis of enolase as Ser39 chelates to the second divalent metal as it binds and closes of the active site. Improper positioning of Loop 1 may lead to incomplete closure of the active

Reproduced with permission of the copyright owner. Further reproduction prohibited without permission.

site, and thus affecting enzyme catalysis. Brewer et al. (1998) suggested that the closure of Loop 1 strengthens the electrostatic interactions between the two divalent metals with the substrate and the polar residues within the active site by excluding water. Therefore, incomplete closure of Loop 1 may result in decreased rates of catalysis in enolase. In addition, the ability of Ser39 to coordinate to the second divalent cation may be lost if the closure is not complete, leading to decreases in affinity for the second divalent metal. This is reflected in the S39A variant enolase, where the K_M (termed activation constant in Brewer, 1998) for Mg^{2+} was 1 mM compared to 92 μM for the native enzyme (Brewer et al., 1998). This is comparable to the kinetic results obtained here for the G157 variants, which indicated increased K_M for Mg^{2+}, with the highest K_M for the G157D and G157L variants. In addition, Brewer et al. (1998) have also shown that the K_M for 2-PGA with S39A enolase was increased from 32 μM for the native enolase to 131 μM. This also correlates quite nicely with the kinetic results obtained for the G157D variant, where its K_M for 2-PGA at saturating Mg^{2+} or Mn^{2+} is increased only 3-4x compared to that of the wild-type enzyme. The slightly higher K_M for substrate may be an effect of the higher K_M for Mg^{2+} in the variants.

The proper positioning of His159 also plays a significant role in the inhibition of enolase at high concentrations of divalent metals. Faller et al. (1977) have suggested that inhibition of enolase at high concentrations of Mg^{2+} is due to the existence of a third Mg^{2+} inhibitory binding site. Later, Vinarov and Nowak (1998) suggested that inhibition of native enolase activity was due to a third Mg^{2+} binding site in which the Mg^{2+} is coordinated by His159 and a phosphoryl oxygen of 2-phosphoglycerate. More recently, it was established from the crystal structure of *Trypanosoma brucei* enolase (da Silva Giotto et al., 2003) that His159 (His156 in the *Trypanosoma brucei* numbering system) is one of the ligands to the third

Reproduced with permission of the copyright owner. Further reproduction prohibited without permission.

inhibitory Me^{2+}. It is, therefore, feasible that the lost of inhibition at high concentrations of Me^{2+} for the G157D, G157N, and G157L variants is due to incorrect arrangement of His159 to coordinate to the inhibitory Me^{2+}.

The Gly157 mutation may therefore affect many aspects of the active site arrangement of enolase, thus affecting the enolase mechanism. With the structural characterization and steady-state kinetic results, it may be deduced that reduced activity may in fact be due to the improper positioning of active site residues rather than due to an overall change in the structure of the variant enolase. To reiterate, the positioning of His159 and Glu168, which contribute to the abstraction of the C-2 proton and removal of C-3 hydroxide respectively, may have been disturbed. This prospect is in good agreement with the lowered k_{cat} in the G157 variant enolases, which indicate the catalysis, k_5, k_7, and k_9 (Figure 45), of enolase has been affected. To investigate which step of the catalysis has become rate-limiting, the primary deuterium kinetic isotope effect was examined. Figure 47 illustrates the two-step catalysis of enolase.

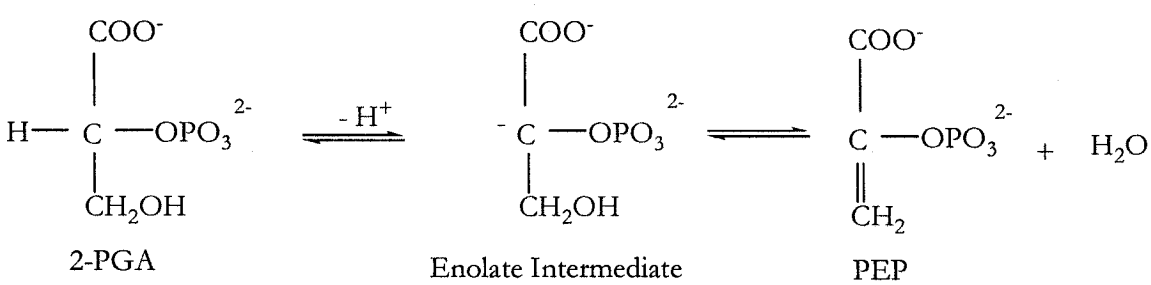

Figure 47. Stepwise reaction of enolase.

Reproduced with permission of the copyright owner. Further reproduction prohibited without permission.

The first step of the reaction involves the chemical breakage of a C-H bond at C-2 of 2-PGA. The rate of reaction upon substitution the C-2 proton with deuterium may elucidate whether the mutation at G157 has affected the rate of removal of the proton. Isotopic substitutions modify the rate of reaction increasing the activation energy for bond cleavage of a heavier atom, which in turn may lower the measured rate for the overall reaction. Similar primary deuterium kinetic isotope effects on k_{cat} for the wild-type and G157D enolases were observed when ^{2}H-2-PGA was used as the substrate. This suggests that the G157D variant did not affect the overall catalysis of enolase and that the proton transfer step is not entirely rate-limiting in the overall reaction. On the other hand, the relatively smaller primary deuterium kinetic isotope effect on k_{cat} was observed with the G157N enolase, suggesting that the abstraction of the hydrogen has not become slower and other steps of the reaction that was fast have slowed down. The magnitude of the KIE can also be strongly influenced by the rates of steps that are not related to the proton transfer. That is, interpretation of the isotope effect for enzyme-catalyzed reactions may be complicated by steady-state factors that can reduce or mask the actual isotopic effect that occurs as a result of the chemical transformation in the transition state (Parkin & Schramm, 1984). For enolase, they may include the release of the second Mg^{2+} and/or PEP from the E'-Mg-PEP-Mg complex. In addition, the positioning of Glu168, contributing to the removal of the C-3 OH^{-}, may have been altered, which may affect the second step of the reaction. Further investigation is required to determine whether the rate of the second step has been affected.

Reproduced with permission of the copyright owner. Further reproduction prohibited without permission.

Conclusion

Characterization of the G157D, G157A, G157N, and G157L variant yeast enolases was performed to elucidate insights into the human disease, muscle-specific enolase deficiency. Site-directed mutagenesis was performed on the wild-type enolase recombinant DNA in order to obtain the desired mutations. Overexpression and purification of the G157 variant enolases were carried out following the same processes as those of the wild-type with the exception of the percentage $NH_4(SO_4)_2$ fractionation of the G157D protein. Achievement of the respective protein products was confirmed by mass spectrometric analyses.

Spectroscopic analysis of the G157 variant enolases showed that they were properly folded. Far-UV CD spectra of the G157 variant enolases are virtually superimposable to that of the wild-type, confirming the correct secondary structural folding of the G157 variant enolases. Near-UV CD spectra of the G157 variant enolases show similar characteristic peaks to those of the wild-type with slight differences in intensities. Fluorescence spectra of the G157 variant enolases also show the same feature λ_{max} emission at 335 nm of the wild-type's with minor differences in the relative intensities. Both near-UV CD and fluorescence spectroscopy point to the proper tertiary assembling of the G157 variant enolases. The sedimentation coefficients of the G157 variant enolases are comparable to that of the wild-type at 10.6 μM and 1.06 μM, indicating no appreciable dissociation of the subunits and that they retain the quaternary dimeric structure of wild-type enolase.

Conformational stability studies of the G157 variant enolases indicate the lowered conformational stability of the variant proteins compared to that of the wild-type. Thermal denaturation of the G157 variant enolases show a decrease of ~4-5°C in the T_m compared to

Reproduced with permission of the copyright owner. Further reproduction prohibited without permission.

that of the wild-type. Urea denaturation of the G157D variant display lower concentration requirement of the denaturant to obtain 50% denaturation compared to the wild-type. $NaClO_4$ dissociation studies indicate the dissociation constant of the two subunits, K_d, is increased ~4-fold for the G157D variant relative to the wild-type. Both urea denaturation and sodium perchlorate dissociation studies indicate weakened H-bonding strength within the G157D variant protein. Limited proteolysis of the G157 variant enolases points to increased susceptibility to trypsin digestion. This indicates an increase in accessibility to trypsin in the G157 variant enolases.

Steady-state kinetics demonstrated an increase in K_M for Mg^{2+}, decrease in k_{cat} and catalytic efficiency, and loss of inhibition at high concentrations of Me^{2+} for the G157 variant enolases. The effects were most prominent for the G157D and G157L variants. KIE studies indicate that the abstraction of the C-2 proton has not become more rate-limiting for the G157D variant protein. Binding studies indicate similar binding constants for the Me^{2+} and substrate/inhibitor for the G157D variant compared to those of the wild-type. Titration of the apo-enolase with Mg^{2+}, monitored by change in fluorescence intensity upon subsequent additions of Mg^{2+}, indicates the binding of the first Mg^{2+} is not affected in the G157D variant. Titration of enolase-Mn^{2+} (wild-type and G157D) with an equilibrium mixture of 2-PGA/PEP or PhAH, indicates similar association constants for both enolases. The association constant obtained for the second Mn^{2+} binding site, by titrating Mn^{2+} into enolase-Mn^{2+}-2-PGA/PEP, is similar for the G157D variant compared to that of the wild-type enolase.

From the results, it may be concluded that G157 is important for the proper positioning of active site residues to coordinate to the substrate and Me^{2+}. The size and charge of the amino acid substituting G157 contributes to the decrease in the G157 variant

Reproduced with permission of the copyright owner. Further reproduction prohibited without permission.

activities. Substitution of the glycine with an alanine, creates the least detrimental effects on the conformational stability and enzymatic activity compared to the other substitutions. The larger substitution of glycine by asparagine gives greater effects on the stability and activity than the glycine to alanine substitution, but smaller effects than the glycine to aspartate or leucine substitutions. The charge of the asparatate residue replacing glycine at position 157 plays a crucial role in the decrease of stability and activity of enolase as aspartate is similar in size to asparagine. The size of the leucine substituting G157 caused a similar extent of decreased conformational stability and enzymatic activity as the G157D variant.

Reproduced with permission of the copyright owner. Further reproduction prohibited without permission.

Future Work

Most binding studies of the G157D enolase have been limited to using Mn^{2+} since it binds more tightly than Mg^{2+} to enolase. As noted from the binding studies and kinetic analyses, the affinity of the G157D enolase for Mn^{2+} is not affected. On the other hand, the K_M for Mg^{2+} has increased by many fold for the G157D enolase compared to that of the wild-type enzyme. It would therefore be useful to try to find the direct binding constant for the second and/or third Mg^{2+} sites. Titration of enolase with the first Mg^{2+} and substrate analogue, PhAH bound, may be monitored by changes in fluorescence. This would allow for the determination of the effects of the G157D mutation on the binding of the physiological metal cofactor of enolase.

Trypsin digestion showed that at low concentrations of trypsin to protein, 1:1000, cleavage of G157D protein was observed. However, at higher concentrations of trypsin to protein, 1:100, practically complete digestion occurred for the G157 variants. Under limited proteolysis conditions, proteolysis would occur only at the most exposed or disordered region of the polypeptide backbone, and increases in susceptibility to proteolysis are generally results of changes in the protein structure that increase the accessibility of sites in the protein. Therefore, it would be informative to determine a good ratio of trypsin to protein where G157D variant is partially digested to give different sized fragments. Analysis of the mixture of these peptides by mass spectrometry may provide information on the accessibility of sites in the G157D protein, and on the changes that occurred as a result of the G157D mutation.

Reproduced with permission of the copyright owner. Further reproduction prohibited without permission.

Another aspect that is worth investigating is the decrease in activity of the G157 variant enolases. As mentioned in the discussion, the rate of abstraction of the α-proton from 2-PGA has become more rate limiting, possibly due to the effects of the G157 mutation on His159. Another amino acid that is postulated to have been affected is the Glu168. Poyner et al. (1996) have shown that the E168Q variant has reduced abilities to catalyze the first step of the reverse reaction of enolase. In order to determine whether the Glu168 has in fact been affected due to the G157D mutation, it would be informative to determine the rate of addition of OH^- to C-3 of PEP in the reverse reaction. The rate of this first step of the reverse reaction may be obtained by monitoring the change in UV signal at 250 nm using (Z)-3-Cl-P-enolpyruvate as the substrate. (Z)-3-Cl-P-enolpyruvate is a PEP analogue that upon hydrolysis, gives the product, TSP (tartronate semialdehyde phosphate), a high affinity inhibitor of enolase (Figure 49). The change in UV signal is due to the enol of TSP. Variant forms of enolase that lead to the inability to catalyze this step would show reduced activity in hydrolysis of (Z)-3-Cl-P-enolpyruvate.

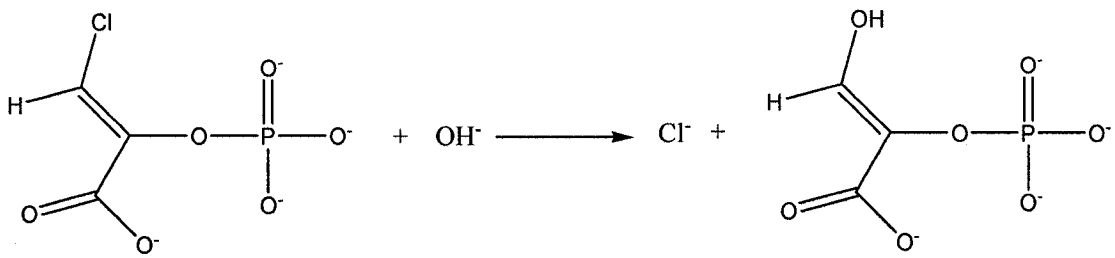

(Z)-3-Cl-P-enolpyruvate

Tartronate semialdehyde phosphate

Figure 49. Hydrolysis of (Z)-3-Cl-P-enolpyruvate to Tartronate semialdehyde phosphate.

Reproduced with permission of the copyright owner. Further reproduction prohibited without permission.

References

Anderson, S. R., Anderson V. E., and Knowles, J. R. (1994) Primary and Secondary Kinetic Isotope Effects as Probes of the Mechanism of Yeast Enolase. *Biochemistry 33*, 10545-10555.

Anderson, V. E., Weiss, P. M., and Cleland, W. W. (1984) Reaction intermediate Analogs for Enolase. *Biochemistry 23*, 2779-2786.

Arakawa, T., and Timasheff, S. N. (1982) Preferential Interactions of Proteins with Salts in Concentrated Solution. *Biochemistry, 21.* 6545-6552.

Babbitt, P. C., Hasson, M. S., Wedekind, J. E., Palmer, D. R. J., Barrett, W. C., Reed, G. H., Rayment, I., Ringe, D., Kenyon, D. L., Gerlt, J. A. (1996) The Enolase Superfamily: A General Strategy for Enzyme-Catalyzed Abstraction of the α-Protons of Carboxylic Acids. *Biochemistry 35*, 16489-16501.

Banner, D. W., Bloomer, A. C., Petsko, G. A., Phillips, D. C., Pogson, C. I., and Wilson, I. A. (1975) Structure of chicken muscle triose phosphate isomerase determined crystallographically at 2.5Å resolution. *Nature 255*, 609-614.

Bennion, B. J., and Daggett, V. (2003) The Molecular Basis for the Chemical Denaturation of Proteins by Urea. *Proc Natl Acad Sci USA 100*, 5142-5147.

Brewer, J. M. (1969) The Interaction of Potassium Chloride and Acetate with Yeast Enolase. *Arch. Biochem. Biophys. 134*, 59-66.

Brewer, J. M. (1976) Stopped-Flow Studies of Changes in Fluorescence of 8-Anilino-1-Naphthalene Sulfonic Acid Caused by Magnesium and Salt Binding to Yeast Enolase. *Eur. J. Biochem. 71*, 425-436.

Brewer, J. M. (1981) Yeast enolase: mechanism of activation by metal ions. *CRC Crit Rev Biochem. 11*, 209-54.

Brewer, J. M., Carreira, L.A., Collins, K. M., Duval, M. C. Cohen, C., and DerVartanian, D. V. (1983) Studies of Activating and Nonactivating Metal Ion Binding to Yeast Enolase. *Journal of Inorganic Biochemistry 19*, 255-267.

Brewer, J. M., Glover, C. V. C., Holland, M. J., and Lebioda, L. (2003) Enzymatic Function of Loop Movement in Enolase: Preparation and Some Properties of H159N, H159A, H159F, and N207A Enolases. *Journal of Protein Chemistry 22*, 353-361.

Reproduced with permission of the copyright owner. Further reproduction prohibited without permission.

Brewer, J. M., Holland, M. J., and Lebioda, L. (2000) The H159A Variant of Yeast Enolase 1 Has Significant Activity. *Biochemical and Biophysical Research Communications 276*, 1199-1202.

Brewer, J. M., and Weber, G. (1965) The Effect of Magnesium on Some Physical Properties of Yeast Enolase. *Journal Biological Chemistry 241*, 2550-2557.

Brewer, J. M., and Weber, G. (1968) The Reversible Dissociation of Yeast Enolase. *Proc. Natl. Acad. Sci. U.S.A. 59,* 216-223.

Brown, C. K., Kulman, P. L., Mattingly, S., Slates, K., Calie, P. J., and Farrar, W. W. (1998) A Model of the Quaternary Structure of Enolases, Based on Structural and Evolutionary Analysis of the Octameric Enolase from *Bacillus subtilis. Journal of Protein Chemistry 17*, 855-866.

Brown, T. A.. ed. (1991) Molecular Biology LabFax. Academic Press Inc and Bios Scientific Publishers Ltd., San Diego, U.S.A.

Capage, M., and Hill, C. W. (1979) Preferential Unequal Recombincation in the GlyS Region of the *Escherichia Coli* Chromosome. *Journal of Molecular Biology 127*, 73-87.

Chai, G., Brewer, J. M., Lovelace, L. L., Aoki, T., Minor, W., and Lebioda, L. (2004) Expression, Purification and the 1.8Å Resolution Crystal Structure of Human Neuron Specific Enolase. *Journal of Molecular Biology 341*, 1015-1021.

Chin, C. C. Q. (1990) The Primary Structure of Rabbit Muscle Enolase. *Journal of Protein Chemistry 9*, 427-432.

Chin, C. C. Q., Brewer, J., and Wold, F. (1981) The Amino Acid Sequence of Yeast Enolase. *The Journal of Biological Chemistry 256*, 1377-1384.

Clarke, A. R. (1996) Analysis of Ligand Binding by Enzymes. In: Engel, E. C., ed. *Enzymology LabFax.* BIOS Scientific Publishers Limited, San Diego, U.S.A.

Cohn, M., Pearson, J. E., O'Connell, E. L., and Rose, I. A. (1970) Nuclear Magnetic Resonance Assignment of the Vinyl Hydrogens of Phosphoenolpyruvate. Sterochemistry of the Enolase Reaction. *J. Amer. Chem. Soc. 92*, 4095-4098.

Comi, G. P., Fortunato, F., Lucchiari, S., Bordoni, A., Prelle, A., Jann, S., Keller, A., Ciscato, P., Galbiati, S., Chiveri, L., Torrente, Y., Scarlato, G., Bresolin, N. (2001) β-Enolase Deficiency, a New Metabolic Myopathy of Distal Glycolysis. *Ann. Neurol. 50*, 202-207.

Dinovo, E. C., and Boyer, P. D. (1971) Isotopic Probes of the Enolase Reaction Mechanism. *Journal Biological Chemistry 246*, 4586-4593.

Duqerroy, S., Carnus, C., and Janin, J. (1995) X-ray Structure and Catalytic Mechanism of Lobster Enolase. *Biochemistry 34*, 12513-12523.

Reproduced with permission of the copyright owner. Further reproduction prohibited without permission.

Ehinger, S., Schubert, W., Bergmann, S., Hammerschmidt, S., and Heinz, D. W. (2004) Plasmin(ogen)-binding α-Enolase from *Streptococcus pneumoniae*: Crystal Structure and Evaluation of Plasmin(ogen)-binding Sites. *Journal of Molecular Biology 343*, 997-1005.

Elliot, J. I., and Brewer, J. M. (1980) Binding of Inhibitory Metals to Yeast Enolase. *Journal of Inorganic Biochemistry 12*, 323-334.

Engel, P.C. (1996) Enzyme LabFax. Bios Scientific publisher, Oxford, UK & Academic Press, San Diego, USA.

Faller, L. D., Baroudy, B. M., Johnson, A. M., and Ewall, R. X. (1977) Magnesium Ion Requirements for Yeast Enolase Activity. *Biochemistry 16*, 3864-3869.

Gawronski, T., and Westhead, E. W. (1969) Equilibrium and Kinetic Studies on the Reversible Dissociation of Yeast Enolase by Neutral Salts. *Biochemistry 8*, 4261-4270.

Gerlt, J. A. (2000) New wine from old barrels. *Nature Struct. Biol. 7*, 171-173.

Gunasekara, K., and Nussinov, R. (2004) Modulating Functional Loop Movements: The Role of Highly Conserved Residues in the Correlated Loop Motions. *ChemBiochem 5*, 224-230.

Gunasekaran, K., Ma, B., and Nussinov, R. (2003) Triggering Loops and Enzyme Function: Identification of Loops that Trigger and Modulate Movements. *J Mol Biol 332*, 143-159.

Hannaert, V., Albert, M. A., Rigden, D. J., da Silva Giotta, M. T., Thiemann, O., Garratt, R. C., Van Roy, J., Opperdoes, F. R., and Michels, P. A. M. (2003). Kinetic Characterization, Structure Modeling Studies and Crystallization of *Trypanosoma brucei* enolase. *Eur. J. Biochem. 270*, 3205-3213.

Henn-Sax, M., Hocker, B., Wilmanns, M., and Sterner, R. (2001) Divergent Evolution of $(\beta\alpha)_8$-Barrel Enzymes. *Biol. Chem. 382*, 1315-1320.

Holland, M. J., Holland, J. P., Thill, G. P., and Jackson, K. A. (1981) The Primary Structures of Two Yeast Enolase Genes. *Journal of Biological Chemistry 256*, 1385-1396.

Holleman, W. H. (1973) The Use of Absorption Optics to Measure Dissociation of Yeast Enolase into Enzymatically Active Monomers. *Biochim Biophys Acta 327*, 176-185.

Joseph, D., Petsko, G. A., and Karplus, M. (1990) Anatomy of a conformational change: hinged "Lid" motion of the triosephosphate isomerase loop. *Science 249*, 1425-1428.

Kaufman, A., and Glusker, J. P. (1994) Coordination of Water to Magnesium Cations. *Inorg. Chem. 33*, 419-427.

Keresztes-Nagy, S., and Orman, R. (1971) Dissociation of Yeast Enolase into Active Monomers. *Biochemistry 10*, 2506-2508.

Reproduced with permission of the copyright owner. Further reproduction prohibited without permission.

Kreig, P., and Melton, D. (1991) Double-Stranded DNA Template Preparation. In: *Promega Protocols and Applications Guide, 2nd Ed.* Promega Corporation, USA.

Kornblatt M. J. (2005) Changing the Metal Ion Selectivity of Rabbit Muscle Enolase by Mutagenesis: Effects of the G37A and G41A Mutations. *Biochim. Biophys. Acta 1748*, 20-25.

Kornblatt, M. J., and Klugerman, A. (1989) Characterization of the Enolase Isozymes of Rabbit Brain: Kinetic Differences between Mammalian and Yeast Enolases. *Biochem. Cell. Biol. 67*, 103-107.

Kornblatt, M. J., and Musil, R. (1990) The Inhibition of Yeast Enolase by Li^+ and Na^+. *Arch. Biochem. Biophys. 277*, 301-305.

Kornblatt, M. J., Al-Ghanim, A., and Kornblatt, J. A. (1996) The Effects of Sodium Perchlorate on Rabbit Muscle Enolase – Spectral Characterization of the Monomer. *Eur. J. Biochem. 236*, 78-84.

Kornblatt, M. J., Lange, R., and Balny, C. (1998) Can Monomers of Yeast Enolase have Enzymatic Activity? *Eur. J. Biochem 251*, 775-780.

Kornblatt, M. J., Lange, R., and Balny, C. (2004) Use of Hydrostatic Pressure to Produce "Native" Monomers of Yeast Enolase. *Eur. J. Biochem. 271*, 3897-3904.

Kühnel, K., and Luisis, B. F. (2001) Crystal Structure of the *Escherichia coli* RNA Degradosome Component Enolase. *J. Mol. Biol. 313*, 583-592.

Larsen, T. M., Wedekind, J., E., Rayment, I., and Reed, G. H. (1996) A Carboxylate Oxygen of the Substrate Bridges the Magnesium Ions at the Active Site of Enolase: Structure of the Yeast Enzyme Complexed with the Equilibrium Mixture of 2-Phosphoglycerate and Phosphoenolpyruvate at 1.8 Å Resolution. *Biochemistry 35*, 4349-4358.

Lebioda, L., and Stec, B. (1991) Mechanism of Enolase: The Crystal Structure of Enolase-Mg^{2+}-2-Phosphoglycerate/Phosphoenolpyruvate Complex at 2.2-Å Resolution. *Biochemistry 30*, 2817-2822.

Lebioda, L., Stec, B., and Brewer, J. M. (1989) The Structure of Yeast Enolase at 2.25-Å Resolution: An 8-Folf β + α-Barrel with a Novel $\beta\beta\alpha\alpha(\beta\alpha)_6$ Topology. *The Journal of Biological Chemistry 264*, 3685-3693.

Lederberg, E. M., and Cohen, S. N. (1974) Transformation of Salmonella Typhimurium by Plasmid Deoxyribonucleic-Acid. *J. Bacteriol. 119*, 1072-1074.

Lee, M. E., and Nowak, T. (1992) Metal Ion Specificity at the Catalytic Site of Yeast Enolase. *Biochemistry 31*, 2172-2180.

Liu, H., Zhang, Y., and Yang, W. (2000) How Is the Active Site of Enolase Organized to Catalyze Two Different Reaction Steps? *J. Am. Chem. Soc. 122*, 6560-6570.

Reproduced with permission of the copyright owner. Further reproduction prohibited without permission.

Marangoni, A. G. (2003) Enzyme Kinetics A Modern Approach. John Wiley & Sons Inc., Hoboken, New Jersey, USA.

McAlister, L., and Holland, M. J. (1982) Targeted Deletion of a Yeast Enolase Structural Gene: Identification and Isolation of Yeast Enolase Isozymes. *The Journal of Biological Chemistry 257*, 7181-7188.

Morrice, N. A., and Carrey, E. A. (1997) Peptide mapping. In: Creighton, T. E., ed. *Protein Structure: A Practical Approach, 2nd Ed.* Oxford University Press Inc., New York, USA.

O'Brien, R., Ladbury, J. E., and Chowdhry, B. Z. (2001) Isothermal Titration Calorimetry of Biomolecules. In: Harding, S. E., and Chowdry, B. Z., eds. *Protein-Ligand Interactions: Hydrodynamics and calorimetry.* Oxford University Press Inc., New York, USA.

Parkin, D. W., and Schramm, V. L. (1984) Effects of Allosteric Activation on the Primary and Secondary Kinetic Isotope Effects for Three AMP Nucleosides. *Journal of Biological Chemistry 259*, 9418-9425.

Pawluk, A., Scopes, R. K., Griffiths-Smiths, K. (1986) Isolation and Properties of the Glycolytic Enzymes from *Zymomomas mobilis. Biochem. J. 238*, 275-281.

Poyner, R. R., Cleland, W. W., and Reed, G. H. (2001) Role of Metal Ions in Catalysis by Enolase: An Ordered Kinetic Mechanism for a Single Substrate Enzyme. *Biochemistry 40*, 8009-8017.

Poyner, R. R., Laughlin, T., Sowa, G. A., and Reed, G. H. (1996) Toward Identification of Acid/Base Catalysis in the Active Site of Enolase: Comparison of the Properties of K345A, E168Q, and E211Q Variants. *Biochemistry 35*, 1692-1699.

Quin, J., Chai, G., Brewer, J. M., Lovelace, L. L., and Lebioda, L. (2006) Fluoride Inhibition of Enolase: Crystal Structure and Thermodynamics. *Biochemistry 45*, 793-800.

Ralston, G. (1993) Introduction to analytical ultracentrifugation. Beckman Instruments Inc.

Sambrook, J., Fritsch, E. F., and Maniatis, T., (1989) Molecular Cloning: A Laboratory Manual. Cold Spring Harbour Laboratory Press, U.S.A., Vol. 3.

Schurig, H., Rutkat, K., Rachel, R., and Jaenicke, R. (1995) Octameric Enolase from the Hyperthermophilic Bacterium *Thermotoga maritima*: Purification, Characterization, and Image Processing. *Protein Sci. 4*, 228-236.

Schmid, F. X. (1997) Optical Spectroscopy to Characterize Protein Conformation and Conformational Changes. In: Creighton, T. E., ed. *Protein Structure: A Practical Approach, 2nd Ed.* Oxford University Press Inc., New York, USA.

Segil, N., Shrutkowski, A., Dworkin, M. B., and Dworkin-Rastl, E. (1988) Enolase Isoenzymes in Adult and Developing *Xenopus laevis* and Characterization of a Cloned Enolase Sequence. *Biochem. J.* 251, 31-39.

Reproduced with permission of the copyright owner. Further reproduction prohibited without permission.

Sims, P. A., and Reed, G. H. (2004) Method for the Enzymatic Synthesis of 2-phospho-D-glycerate from Adenosine 5'-Triphosphate and D-glycerate via D-glycerate-2-kinase. *Journal of Molecular Catalysis B: Enzymatic 32*, 77-81.

Singh, R. P., and Setlow, P. (1978) Enolase from Spores and Cells of *Bacillus megaterium*: Two-Step Purification of the Enzyme and Some of Its Properties. *Journal of Bacteriology 134*, 353-355.

Stec, B., and Lebioda, L. (1990) Refined Structure of Yeast Apo-enolase at 2.25Å Resolution. *J. Mol. Biol. 211*, 235-248.

Stubbes, J., and Abeles, R. H. (1980) Mechanism of Action of Enolase: Effect of the β-hydroxy Group on the Rate of Dissociation of the α-Carbon-Hydrogen Bond. *Biochemistry 19*, 5505-5512.

Stryer, L. (1995) *Biochemistry*, 4^{rth} Ed., W.H. Freeman and Company, United States of America.

Trepanier, D., Wong, C., and Kornblatt, M. J. (1990) The Salt-Induced Dissociation and Inactivation of a Mammalian Enolase: Evidence for the Formation of Active Monomers. *Archives of Biochemistry and Biophysics 238*, 271-277.

Tsujino, S., Nonaka, I., DiMauro, S. (2000) Glycogen Storage Myopathies. *Neurol. Clin. 18*, 125-150.

Vinarov, D. A., and Nowak, T. (1998) pH Dependence of the Reaction Catalyzed by Yeast Mg-Enolase. *Biochemistry 37*, 15238-15246.

Vinarov, D. A., and Nowak, T. (1999) Role of His159 in Yeast Enolase Catalysis. Biochemistry 38, 12138-12149.

Warburg, O., and Christian, W. (1942) Isolation and crystallization of enolase. *Biochem.Z 310*, 384-421.

Wedekind, J. E., Poyner, R. R., Reed, G. H., and Rayment I. (1994) Chelation of Serine 39 to Mg^{2+} Latches a Gate at the Active Site of Enolase: Structure of the Bis(Mg^{2+}) Complex of Yeast Enolase and the Intermediate Analog Phosphonoacetohydrxamate at 2.1-Å Resolution. *Biochemistry 33*, 9333-9342.

Wedekind, J. E., Reed, G. H., and Rayment, I. (1995) Octahedral Coordination at the High-Affinity Metal Site in Enolase: Crystallographic Analysis of the Mg^{II}-Enzyme Complex from Yeast at 1.9Å Resolution. *Biochemistry 34*, 4325-4330.

Wold, F. (1971) Enolase. In: Boyer, P. D. ed. *The Enzyme*, 3rd Ed. *(Vol. 5)*, Academic Press, New York, USA.

Wold, F., and Ballou, C. E. (1957) Studies on the Enzyme Enolase. II. Kinetic Studies. *J. Biol. Chem.* 227, 313-328.

Reproduced with permission of the copyright owner. Further reproduction prohibited without permission.

Zhang, E., Brewer, J. M., Minor, W., Carreira, L. A., and Lebioda, L. (1997) Mechanism of Enolase: The Crystal Structure of Asymmetric Dimer Enolase-2-Phospho-D-glycerate/Enolase-Phosphoenolpyruvate at 2.0Å Resolution. *Biochemistry 36*, 12526-12534.

Reproduced with permission of the copyright owner. Further reproduction prohibited without permission.